Optically stimulated luminescence techniques in retrospective dosimetry using single grains of quartz extracted from unheated materials

Thomsen, Kristina Jørkov

Publication date:
2004

Document Version
Publisher's PDF, also known as Version of record

Risø-PhD-1(EN)

Optically Stimulated Luminescence Techniques in Retrospective Dosimetry using Single Grains of Quartz extracted from Unheated Materials

Kristina Jørkov Thomsen

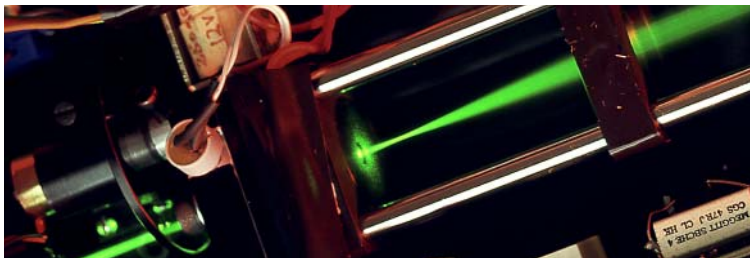

Risø National Laboratory
Roskilde
Denmark
February 2004

Optically Stimulated Luminescence Techniques in Retrospective Dosimetry using Single Grains of Quartz extracted from Unheated Materials

Kristina Jørkov Thomsen

Risø National Laboratory, Roskilde, Denmark
February 2004

Author: Kristina Jørkov Thomsen
Title: Optically Stimulated Luminescence Techniques in Retrospective Dosimetry using Single Grains of Quartz extracted from Unheated Materials
Department: Radiation Research Department

This thesis is submitted in partial fulfilment of the requirements for the Ph.D. degree at the University of Copenhagen, Denmark

Abstract (max. 2000 char.):

This work investigates the possibility of applying optically stimulated luminescence (OSL) in retrospective dose determinations using unheated materials. It focuses on identifying materials suitable for use in assessment of doses absorbed as a consequence of radiation accidents (i.e. accident dosimetry). Special attention has been paid to quartz extracted from unheated building materials such as concrete and mortar. The single-aliquot regeneration-dose (SAR) protocol has been used to determine absorbed doses in small aliquots as well as single grains of quartz. It is shown that OSL measurements of single grains of quartz extracted from poorly-bleached building materials can provide useful information on radiation accident doses, even when the luminescence sensitivity is low. Sources of variance in well-bleached single grain dose distributions have been investigated in detail and it is concluded that the observed variability in the data is consistent with the sum (in quadrature) of a component, which depends on the number of photons detected from each grain, and a fixed component independent of light level. Dose depth profiles through laboratory irradiated concrete bricks have successfully been measured and minimum detection limits of less than 100 mGy are derived. Measurements of thermal transfer in single grains of poorly-bleached quartz show that thermal transfer is variable on a grain-to-grain basis and that it can be a source of variance in single-grain dose distributions. Furthermore, the potential of using common household and workplace chemicals, such as table salt, washing powder and water softener, in retrospective dosimetry has been investigated. It is concluded that such materials should be considered as retrospective dosimeters in the event of a radiation accident

Risø-PhD-1(EN)
February 2004

ISSN 0106-2840
ISBN 87-550-3307-5(internet)

Contract no.:

Group's own reg. no.:

Sponsorship:
Danish Research Academy and Risø National Laboratory, Denmark

Cover :
Top: single grain OSL laser
Left: single grain OSL discs
Right: single grain OSL discs

Pages: 176
Tables: 8
References: 134

Risø National Laboratory
Information Service Department
P.O.Box 49
DK-4000 Roskilde
Denmark
Telephone +45 46774004
bibl@risoe.dk
Fax +45 46774013
www.risoe.dk

Contents

Abbreviations

B	Background dose
CW-OSL	Continuous Wave Optically Stimulated Luminescence
D_a	Transient/accident dose
D_e	Equivalent dose
D_w	Weighted mean dose
EPR	Electron Paramagnetic Resonance
H_2O_2	Hydrogen peroxide
HCl	Hydrochloric acid
HF	Hydrofluoric acid
IEU	Internal-External Uncertainties approach
IR-OSL	Infrared Optically Stimulated Luminescence
LED	Light Emitting Diode
LM-OSL	Linearly Modulated Optically Stimulated Luminescence
MCNP	Monte Carlo N-Particle
OSL	Optically Stimulated Luminescence
PMT	Photomultiplier Tube
POSL	Pulsed Optically Stimulated Luminescence
PP	Probability Plot
RBP	Rapidly Bleaching Peak
RSD	Relative Standard Deviation
SAR	Single Aliquot Regenerated-dose protocol
SBP	Slowly Bleaching Peak
TL	Thermoluminescence
TT	Thermal Transfer

List of Figures

List of Tables

1 Introduction

In the event of a radiation accident, prompt assessment of the dose levels received by radiation workers and by the general population is important. Since radiation accidents by definition are unexpected, routine measurements of the relevant quantities are often insufficient to provide estimates of doses to the relevant population. The objective of this work is to investigate the potential of applying optically stimulated luminescence (OSL) in retrospective dose reconstruction using unheated materials. Most of the effort has concentrated on using single grains of quartz extracted from unheated building materials, such as concrete and mortar, as retrospective dosimeters.

The application of OSL techniques to ceramics for the retrospective assessment of accident radiation doses was first suggested by Bøtter-Jensen (1995), and has since been applied in accident dosimetry with great success (e.g. Banerjee et al., 1999, 2000); these studies have all been carried out using heated materials. Unfortunately, heated materials are not always available, especially in industrial or office environments, where unheated building materials such as concrete and mortar are more widely used. Using these materials is challenging, since they most certainly will not have been adequately zeroed in the last zeroing event (e.g. at the time of manufacture) and because they usually have a very low luminescence sensitivity compared to heated materials. Incomplete zeroing necessitates that measurements are performed on small aliquots or single grains to identify those grains that were adequately zeroed at the time of manufacture.

One way to investigate the incompleteness of the zeroing process in unheated building materials is to measure and examine the distribution of apparent doses in representative modern analogues (i.e. recently manufactured material). If a significant proportion of the grains yield a dose consistent with zero, the essential requirement for using these types of materials is met. The next step is to determine if an accident dose superimposed on the natural distribution of doses can be assessed accurately. This can be investigated by

administering a known dose to the modern analogues in the laboratory and then by attempting to retrieve this dose from the observed dose distribution. This approach has been tested in two separate studies in this work using quartz extracted from two different modern concrete samples (see Chapters 5 and 7).

The fundamental idea behind determining the dose absorbed in individual grains is that it will allow the identification and rejection of poorly-zeroed grains from the population used to estimate the true dose. However, this selection process requires that poorly-zeroed grains can be distinguished from well-zeroed grains. In order to do so the characteristics of a well-zeroed distribution must be established. Most of the single grain studies published so far have generally contained few individual single grain dose estimates, primarily because of the extensive measurement time involved in determining absorbed doses in single grains of quartz. Part of this work attempts to measure a sufficient number of single grains to be able to establish the sources of variability in well-zeroed single-grain dose distributions (see Chapter 6).

A different approach to investigate the suitability of unheated materials is to measure samples which have not received any accident dose and where the manufacturing date is well-known. The environmental dose-rate relevant to the sample can be determined separately and by multiplying this estimate of dose-rate with the time elapsed since manufacture an independent estimate of the true dose can be obtained. If this independent estimate of the true dose is consistent with the dose retrieved from the measured dose distribution, it is likely that a superimposed accident dose could have been determined accurately. This approach has been tested using quartz extracted from three mortar samples taken from a building constructed in 1964 (see Chapter 8).

Most attention in this work has been focused on using quartz as retrospective dosimeters. However, there are other unheated crystalline materials found in the household and workplace environment (e.g. common salt, washing powder and water softener) which may also potentially act as retrospective dosimeters. Such chemicals are usually held in light-tight packaging and are likely to have been recently manufactured. The thermoluminescent and optically stimulated luminescent characteristics of seven different common chemicals have been surveyed (see Chapter 9).

Outline

The thesis outline is as follows. Chapter 2 introduces the basic concepts of retrospective dosimetry based on luminescence methods. Retrospective accident dosimetry is introduced and a short list of available methods and their applicability is presented. This is followed by a brief description of the use of luminescence in retrospective accident dose determinations and an illustration of the difference between using heated and unheated materials as dosimeters.

In Chapter 3 the basic concepts in luminescence are introduced including the band model, thermoluminescence (TL), OSL, resetting of the OSL signal and the dose estimation protocol.

Chapter 4 describes the important characteristic features of the measurement apparatus (the Risø TL/OSL reader equipped with a single grain OSL attachment) used for the OSL studies in this work. The reproducibility of the light sources (the blue LEDs and the green laser) is investigated and the overall reproducibility of the single grain OSL attachment determined.

The work presented in Chapter 5 is based on the paper: *Retrospective dosimetry using unheated quartz: a feasibility study,* published in Radiation Protection Dosimetry (Thomsen et al., 2002b). This study investigates the feasibility of using single grains of quartz extracted from a poorly-bleached modern "premix" concrete in retrospective accident dosimetry. A simulated concrete brick constructed using the premix concrete was irradiated in the laboratory and the dose depth profile measured.

The work presented in Chapter 6 is based on the paper: *Sources of variability in OSL dose measurements using single grains of quartz*, in press in Radiation Measurements (Thomsen et al., 2003b). In this chapter the sources of variability in well-zeroed single grain dose distributions are investigated using a sedimentary quartz sample thermally zeroed and irradiated in the laboratory. It is shown that the observed variability in the data is consistent with the sum of a component which depends on the number of photons detected from each grain, and a fixed component independent of light level.

The work presented in Chapter 7 is based on the paper: *Variation with depth of dose distributions in single grains of quartz extracted from an irradiated concrete block* published in Radiation Measurements (Thomsen et al., 2003a). In this chapter the dose distributions from single grains of quartz extracted from two industrially produced concrete blocks are presented. The natural dose distribution was measured using one block, whereas the other block was irradiated in the laboratory before the apparent distribution of doses were measured. A standard statistical criterion is used to determine the dose absorbed as a result of the laboratory irradiation.

The work presented in Chapter 8 is based on the paper: *Thermal transfer and apparent dose distributions in poorly-bleached mortar samples: results from single grains and small aliquots of quartz*, published in Radiation Measurements (Jain et al., 2003b). This chapter reports on small-aliquot as well as single-grain dose distributions obtained from quartz extracted from three different types of mortar sampled from a building constructed in 1964. It presents thermal transfer measurements on single grains of quartz and grain size dependence of bleaching. Four different methods are used for determining the background dose in the samples.

The work presented in Chapter 9 is based on the paper: *Household and workplace chemicals as retrospective luminescence dosemeters*, published in Radiation Protection Dosimetry (Thomsen et al., 2002a). In this chapter the suitability of using seven different common household and workplace chemicals in accident dosimetry is investigated. These materials are likely to have a negligible background dose owing to their recent manufacture and are often stored in light-tight packaging making them potential candidates as retrospective dosimeters. The OSL sensitivity, background dose, fading characteristics and minimum detection limits are presented.

2 Retrospective dosimetry

Retrospective dosimetry based on luminescence methods can be divided into two main categories: 1) archaeological and geological dating and 2) accident dosimetry. In dating applications the goal is to determine the dose absorbed by natural materials resulting from exposure to naturally occurring radio nuclides in the environment. The weak flux of ionising radiation is derived from the radioactive decay of elements (primarily from the Thorium and Uranium series and Potassium-40) contained within the material. Additionally, a usually small contribution is derived from the flux of cosmic rays. If the dose rate in the media is known (or can be determined separately) and is assumed to be constant throughout time, the absorbed dose can be converted into an age, since the size of the absorbed dose is proportional to the age of the sample. In accident dosimetry the goal is to reconstruct doses absorbed as a consequence of a radiation accident. The accident dose will be superimposed on the background dose; i.e. the dose determined in dating applications. The techniques used in accident dosimetry and dating applications are identical.

Luminescent materials are crystalline and able to store part of the energy imparted to the material by the interaction with ionising radiation. Minerals such as quartz and feldspar are commonly used in luminescence techniques. When ionising radiation interacts with an insulating crystal (e.g. quartz) a redistribution of charge within the crystal takes place. Some part of the redistributed charge becomes trapped at defects in the crystal lattice. This redistribution of charge continues for the duration of the radiation exposure and the amount of trapped charge is related to the total radiation exposure - at least as long as saturation effects are unimportant. Charge trapped in the OSL trap in quartz is stable for long periods of time ($\sim 10^8$ years, Murray and Wintle, 1999) at ambient temperature, but the trapped charge may be released when the crystal is exposed to light or heat. A fraction of the released charges will recombine, which results in the emission of a light flux called luminescence. If heating is applied to release the trapped charges,

the luminescence is called thermoluminescence (TL); if light exposure is the releasing agent the light emission is called optically stimulated luminescence (OSL). The size of the luminescence signal induced in nature, also referred to as the natural luminescence, is related to the amount of trapped charge and thus to the absorbed dose. The natural luminescence signal can be expressed as an absorbed dose by calibrating the sample in the laboratory. This calibration is achieved by giving the sample a known radiation dose (usually done by exposing it to a calibrated beta emitting source) and measuring the induced signal. The dose given in the laboratory that induces an OSL signal identical to the natural OSL signal is known as the equivalent dose and is here denoted D_e.

2.1 Luminescence dating

Optically stimulated luminescence was first used in the dating of quartz from sedimentary samples by Huntley et al. (1985). OSL dating makes use of the fact that the luminescence signal induced in the material by the interaction with ionising radiation can be reset (zeroed) by heating the sample to sufficiently high temperatures (e.g. above 500 °C) or by exposure to daylight. The age obtained in dating applications is the time that has elapsed since the material was last zeroed. In the dating of heated materials such as pottery the last zeroing event took place when the material was fired. In the geological dating of sediments the last zeroing event occurred when the sediment was exposed to daylight, i.e. during transportation and deposition. After deposition the constituent grains in the sediment are buried underneath additional sediment and further light exposure is thus blocked. The grains are exposed to ionising radiation and the luminescence signal starts to rebuild.

One of the prime factors controlling the accuracy with which D_e can be determined is the efficiency of the zeroing process; in unheated materials, the zeroing of the luminescence signal is by exposure to daylight. It has been shown that exposure to full sunlight for a few seconds may reduce the OSL signal from quartz by approximately 50% (Godfrey-Smith et al., 1988). However, the material may have contained a strong latent luminescence signal prior to the zeroing event and the light exposure may have been too short in duration, too dim or too restricted in spectrum because of filtering (Berger and Luternauer, 1987) to completely (or at least adequately) zero the luminescence signal in all grains before burial. In terms of dating, such incomplete zeroing can lead to an overestimation of the age of the sample, since luminescence measurements cannot distinguish between the signal induced before and after the burial. Thus, although the OSL signal can be reset

quickly, this does not necessarily mean that OSL signals in all grains were reset completely at the time of burial. Zeroing (or bleaching) in the natural environment is thus likely to be heterogeneous owing to grain-to-grain variations in bleachability, light-absorbent coatings and duration of exposure to day-light (Aitken, 1998). Thus, some grains may have their latent luminescence signal zeroed before burial, whereas others may be incompletely zeroed (i.e. they still carry a luminescence signal at the time of burial).

In conventional OSL techniques evaluation of the equivalent doses is made using multiple-aliquot protocols originally developed for TL (reviewed by Wintle, 1997). In these protocols measurement of many tens of aliquots (each consisting of several thousand grains) is required to obtain a single estimate of the equivalent dose. The signal measured from a multiple-grain aliquot is an average of the signals from all grains in the aliquot. An implicit assumption in the multiple-aliquot protocols is that the individual aliquots have identical luminescence characteristics. Identical luminescence characteristics can only be assumed if the sample is completely homogeneous or if a sufficient number of grains are used in each aliquot to average out any variations. For materials in which all grains had their latent luminescence signal adequately zeroed at burial (e.g. aeolian sediments), multiple-aliquot procedures may be justified. However, in other situations the presence of a few very bright grains not completely zeroed at burial in an otherwise well-zeroed sample can lead to a significant overestimate of the true burial dose (Duller et al., 1995).

Not until 1997, with the development of the first single-aliquot additive-dose protocol (Murray et al., 1997) and the single-aliquot regenerative (SAR) protocol for quartz (Murray and Roberts, 1998; Murray and Wintle, 2000) could estimation of the equivalent dose be made on a single quartz aliquot (which may consist of a single grain). This has two main advantages: 1) the precision of the equivalent dose estimate is improved, and 2) the distribution of doses within a sample can be examined explicitly by measuring aliquots containing only few grains or even a single grain (Murray and Olley, 2002). If multiple-grain aliquots of incompletely zeroed materials are measured, grain-to-grain variations in individual doses are averaged within aliquots, resulting in an overestimation of the true burial dose. By reducing the number of grains in each aliquot the probability of measuring some aliquots containing only well-zeroed grains is increased. Thus, by using small aliquots (< 100 grains) a distribution of apparent doses can be measured. The best estimate of the burial dose is provided by the aliquots containing only grains that were well-zeroed at burial. Thus, the lower dose estimates in the distribution of apparent doses are more likely to give the true burial dose. Olley et al. (1998) measured an incompletely zeroed modern river sand using small aliquots con-

taining $60 - 100$ grains each and found that only 5% of the aliquots gave an equivalent dose consistent with zero. Murray et al. (1995) and Olley et al. (1998, 1999) argued that the lowest 5 or 10% of the apparent doses measured using small aliquots provided the best estimate of the true burial dose in their samples. Lepper et al. (2000) suggested a method where the equivalent dose distribution is deconvoluted to remove scatter resulting from experimental uncertainties in order to determine the *leading edge* of the distribution, assumed to provide the best estimate of the burial dose. Fuchs and Lang (2000) suggested a method in which individual dose estimates are sorted in increasing order and the arithmetic mean and standard deviation calculated for $n = 2, 3, 4 \ldots$ etc., beginning with the smallest value. When the calculated relative standard deviation just exceeds 4% (thought to be the precision of the method, i.e. the observed relative standard deviation for quartz grains artificially bleached and irradiated in the laboratory), the process is stopped, and the mean value of the included results are assumed to provide the best estimate of the burial dose.

All three methods attempt to identify aliquots containing grains that were well-zeroed at burial. A more direct approach is to estimate equivalent doses from individual grains. So far only a few studies using single grains have been reported (Lamothe et al., 1994; Murray et al., 1997; Roberts et al., 1999; Olley et al., 1999; Duller et al., 2000; Henshilwood et al., 2002), but these have shown that single grain analyses provide a means to obtain a distribution of equivalent doses. These studies have also shown that the luminescence sensitivity (brightness) of individual grains from the same sample is highly variable and that the proportion of bright grains varies considerably from sample to sample. Duller et al. (2000) present single grain data of quartz extracted from a coastal aeolian sand from Southern Africa, where more than 95% of the total OSL signal originated from less than 5% of the measured grains (i.e. if 100 single grains were measured and the cumulative light sum calculated, then five of the grains would contribute $\sim 95\%$ to the cumulative light signal). In an aeolian quartz sand from Australia Duller et al. (2000) found that 70% of the OSL signal originated from $\sim 20\%$ of the measured grains. Thus, the OSL signals from the majority of single grains of unheated quartz tend to be weak, indicating that many grains must be measured to obtain a satisfactory dose distribution.

As discussed above it is expected that obtaining satisfactory distributions of apparent doses in quartz from unheated materials is challenging because of poor luminescence sensitivity in these materials, i.e. it is necessary to measure many grains. One way of performing measurements on single grains is

by hand-picking individual grains and measuring them independently. However, the SAR protocol requires that a number of repeated irradiations, heat treatments and light stimulations are performed on each grain, making the measurement of many separate single grains very time consuming. However, using the recently developed Risø single grain OSL attachment (Duller et al., 1999, 2000; Bøtter-Jensen et al., 2000a, 2003) the measurement time required for each grain is reduced significantly (by a factor of $\sim$ 100) making measurement of a large number of grains feasible in a reasonable time.

2.2 Accident dosimetry

A radiation accident is an unintended or unexpected event occurring with a radiation source, or during a practice involving ionising radiation, which may result in significant human exposure and/or material damage (IAEA and WHO, 1998; IAEA, 1999). In the event of a radiation accident (nuclear accident or other radiological emergency) prompt assessment of the dose levels received by the population and radiation workers is important. Such radiation accidents may include releases of radioactive materials from industrial facilities and military program activities or overexposure of individuals due to improper use and disposal of radiation sources (ICRU Report 68, 2002). In the period 1944-2000, 417 radiation accidents have led to significant overexposure of at least one person, i.e. the absorbed dose to the whole body exceeded 0.25 Gy, or 6 Gy to skin, or 0.75 Gy to any other organ (Turai and Veress, 2001). These radiation accidents have resulted in an overexposure of about 3,000 individuals causing 127 registered fatalities in 57 years (Orise, 2000). This number does not include: the tens of thousands of individuals exposed as a consequence of the detonation of nuclear weapons over Hiroshima and Nagasaki; the 30,000 individuals living in communities located in the Techa River basin, near the southern Ural Mountains, exposed to elevated levels of radiation as a result of past plutonium production, the 19,000 workers at the Mayak facilities (the largest production site for weapon-grade plutonium in the Soviet Union) located near the city of Chelyabinsk, who received radiation exposures that exceeded those of nuclear workers in other countries; nor the liquidators (cleanup workers) and local population in the Chernobyl area, who received significant radiation doses during the Chernobyl accident (Pierce et al., 1996; Karaoglou and Chadwick, 1998).

Since accidental release of ionising radiation or radioactive material into the environment is by definition unexpected, the measurements of the relevant quantities (e.g. radioactive contamination and dose rates) are often insufficient to provide satisfactory information on the full extent of the sit-

uation, and this has complicated - and in some instances even prevented - proper dose assessment of the exposed individuals or critical groups. Nonetheless, retrospective assessment of radiation exposure is of fundamental importance to the analysis of the radiation risk and is an essential part of many radio-epidemiological studies. A particular sub-class of retrospective dose assessment is called dose reconstruction, which is the retrospective assessment of dose due to past human exposure when conventional dosimetric data are unavailable or inadequate. The radiation measurements performed to support dose reconstruction are collectively described as retrospective dosimetry (ICRU Report 68, 2002).

2.2.1 Available methods

Dose reconstruction can involve various physical and biological measurement methods as well as numerical analyses of radioactivity data records. The type of method used will depend on whether doses to individuals or to population groups are to be assessed. Dose reconstruction based on dose measurements performed for individuals include methods that evaluate the absorbed doses by examination of teeth, blood and radionuclide activity in the body. The most appropriate method depends on the purpose of the given study and the relevant pathways (external or internal) for the irradiation and the availability of data records. For external exposures appropriate methods are usually based on persistent effects, such as free radicals or electrons trapped at defect sites in minerals, neutron activation products or changes in blood constituents. For internal exposures measurements of radionuclides in the human body can be used. A summary of some of the methods commonly used for dose reconstruction is given below.

Biological methods:

- ***Chromosome aberrations***: biological method employing scoring of dicentric chromosome aberrations in metaphases prepared from human lymphocytes (Edwards, 1997). It is the preferred method in dose reconstruction within some weeks after acute, uniform whole-body exposures. The dicentric aberrations are unstable and will thus be eliminated from the peripheral blood. If longer time has passed since the radiation event, a method termed Fluorescence In Situ Hybridisation (FISH) can be applied. In FISH (also known as chromosome painting) composite chromosome-specific DNA probes are used to identify reciprocal translocations and insertions in the DNA, which are classified as

stable aberrations (Bauchinger, 1998). However, the use of this method for doses < 500 mGy is not yet definitive.

- ***Micronuclei***: biological method in which micronuclei are scored in peripheral lymphocytes. The main advantage of this method is that a quick estimate of the absorbed dose is possible (Nakamura and Miyazawa, 1997).

- ***Radionuclides in the human body***: Radioactive contamination of the environment will result in ingestion and inhalation of radionuclides by contaminated drinking water, foodstuff and air. Radionuclide activities in the body can be estimated by measuring the intensity of gamma, x-rays and bremsstrahlung leaving the human body or by measuring the activities in urine, faeces or exhaled air.

Physical methods:

- ***EPR of enamel***: Electron Paramagnetic Resonance (EPR) is a physical method based on the measurement of stable radiation induced radicals in tooth enamel (or other calcified tissue) in the human body (Wieser et al., 2000).

- ***Luminescence of ceramics***: physical method based on thermoluminescence (Bailiff, 1997) and optically stimulated luminescence (Bøtter-Jensen and McKeever, 1996) dosimetry. These methods are based on measurements of the luminescent emission from minerals such as quartz and feldspar. The methods enable measurement of integrated absorbed doses a long time after the radiation event. Additional modelling and photon transport calculations (Bailiff and Stepanenko, 1996) are required in order to assess doses absorbed by individuals.

- ***Radionuclides in the environment***: Measurements of radioactive contamination of the environment.

Dose modelling (i.e. Monte Carlo simulations) based on measurements obtained from dose rate meters such as GM-counters that were active at the time of the accident has also been used (Meckbach and Chumak, 1996). The appropriateness of each method is given in Table 2.1 (ICRU Report 68, 2002)

2.2.2 Luminescence in accident dosimetry

Solid state luminescence dosimetry techniques can be used to determine accumulated absorbed doses in environmental media (e.g. building materials).

Measurement of	Type of exposure			
	External	Internal		
	gamma	alpha	beta	gamma
EPR of enamel	1	-	2	1
Chromosome aberrations	2	-	-	2
Micronuclei	3	-	-	3
Luminescence of ceramics	3	-	-	-
Radionuclides in human body	-	1	1	1
Radionuclides in environment	3	3	3	3

Table 2.1: Fields of applicability of methods of dose reconstruction. **1**: possibility of determining individual protracted exposures that have occurred a long time previously with doses down to 100 mGy. **2**: limitations, e.g. large uncertainties, problems with longer times after exposure or high detection limits. **3**: possibility of determining doses to population groups. The first four methods are applicable even if no detectable amount of radioactivity has remained after the exposure event (From ICRU Report 68, 2002).

Luminescence methods are particularly suited to determining doses to population groups caused by external gamma exposures. In order to transform an absorbed dose measured by luminescence methods into doses to individuals or population groups additional modelling is required.

Thermoluminescence was first used in the retrospective dose assessment of the cumulative absorbed dose caused by gamma irradiation from the atomic bomb at Hiroshima (Higashimura et al., 1963). Luminescence techniques have since been applied in retrospective dosimetry to reconstruct doses at Hiroshima and Nagasaki (Roesch, 1987; Haskell, 1993), in populated areas in the vicinity of the Nevada Test Site (Haskell et al., 1994), at the Chernobyl power plant (Hütt et al., 1993), in the area surrounding the Chernobyl power plant (Bøtter-Jensen, 1995), in populated areas near the Semipalatinsk nuclear test site in Kazakhstan (Takada et al., 1997), and in the vicinity of the Techa River valley polluted by the Mayak Facility in Russia (Bougrov et al., 1998). Luminescence techniques have been applied to various types of clay-based ceramic materials such as bricks (Banerjee et al., 1999, 2000), glazed and unglazed tiles, roof tiles, interior floor tiles, flower pots and porcelain fittings (e.g. sanitary ware, Poolton et al., 1995; Bøtter-Jensen et al., 1996) and exterior fittings (lamp holders and electrical power line insulators) from houses in the affected area (see Figure 2.1). Using house bricks in retrospective assessment of radiation accident doses is of great value, since it en-

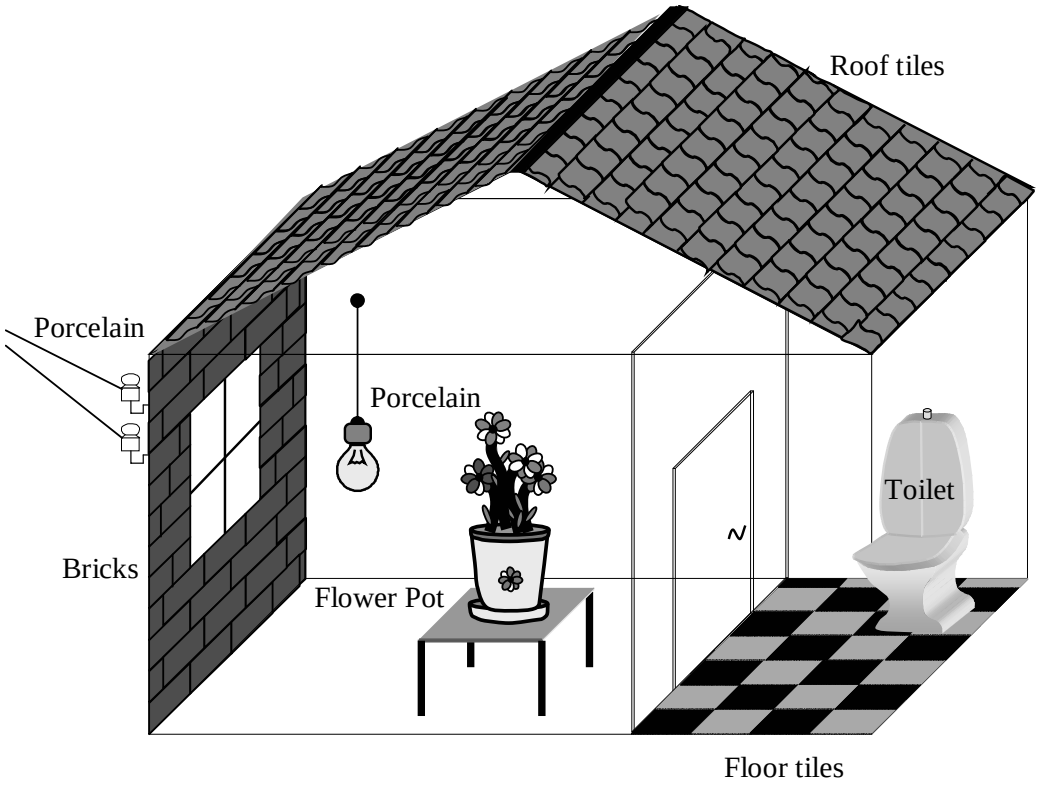

Figure 2.1: Schematic drawing showing various ceramic materials that have been used in retrospective dose determinations.

ables measurement of dose-depth profiles into the brick-material. Dose-depth profiles give information about the average energy of the incident photon radiation. Luminescence dose measurements on quartz extracted from such materials have shown that doses as low as 10 mGy can be determined accurately (Bøtter-Jensen, 2000).

The absorbed dose D_e in minerals after a radiation accident consist of two components:

1. a background dose component B received by the material since manufacture (or last zeroing event) primarily derived from naturally occurring radioactive nuclides in the surrounding media. In dating applications this dose is known as the geological dose and is the dose of interest.

2. a transient dose component D_a resulting from the radiation accident superimposed on the background dose.

In accident dosimetry the goal is to determine this transient dose, which is given by $D_a = D_e - B$. The precision with which D_a can be determined is usually limited by the uncertainties in the estimation of the background dose. The background dose-rate may be estimated using high-resolution gamma or alpha spectrometry or $Al_2O_3:C$ dosimeters (Bøtter-Jensen et al., 1999a). In assessment of B, homogeneity in both radioactive content and in absorption coefficients is assumed. It is further assumed that the dose-rate has remained constant since the last zeroing event and that the time of this event is well known. For coarse-grain samples (grain size $> 100\,\mu$m) the annual dose-rate is given by

$$kD_\beta + D_\gamma + D_c \tag{2.1}$$

where D_β, D_γ and D_c are the beta, gamma and cosmic annual dose-rates and k is a numerical factor that incorporates attenuation of the beta contribution. For coarse-grain samples, the external contribution from alpha radiation is made negligible by chemical removal of the outer rind of the grains (Aitken, 1998).

Using heated materials it is possible to to resolve a transient dose of approximately 18 mGy (3σ) on top of a background dose of 100 mGy (Banerjee et al., 1999). The measured accident dose can be related to dose in air at an external reference location by use of conversion factors derived from computational modelling (Bailiff and Stepanenko, 1996). The basic concepts and experimental techniques used in luminescence accident dosimetry are the same as those being employed in the luminescence dating of archaeological artifacts and geological deposits (Aitken, 1985, 1998).

Heated and unheated materials

Most attempts to apply retrospective dosimetry using luminescence methods to building materials have made use of heated materials. One of the major advantages of using materials that in the past have been heated to (usually) more than 500 °C is that any prior luminescence signal is completely zeroed. Thus, the time period the luminescence signal accumulated in is well-defined. If, for instance, a brick collected from a 70 year old house is sampled (and quartz and/or feldspar extracted), all mineral grains from the brick will contain a background dose corresponding to 70 years of radiation exposure as well as any additional radiation accident dose. Figure 2.2a shows an example of a dose distribution obtained from a heated quartz sample. This sample is a sedimentary quartz that was heated and then irradiated to a dose of approximately 7.4 Gy in the laboratory using a ^{137}Cs point source. The measured doses range between 6.88 ± 0.13 Gy and 7.89 ± 0.11 Gy and the average is 7.37 ± 0.02 Gy ($n = 84$).

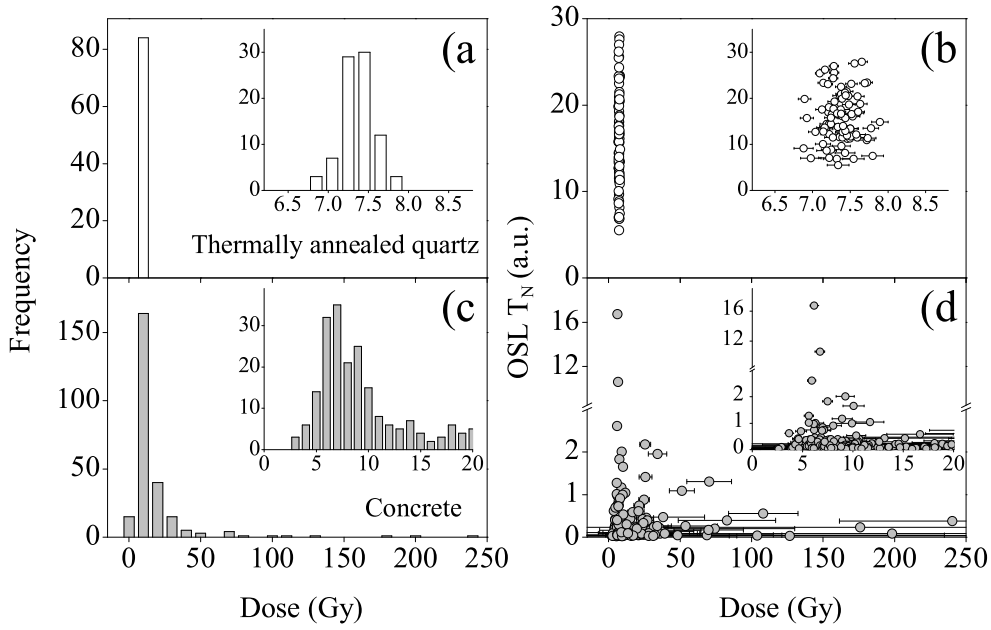

Figure 2.2: Illustration of the difference between using heated and unheated materials in luminescence retrospective dosimetry. **a)** Sedimentary quartz sample that was heated and irradiated using a ^{137}Cs point source to a dose of approximately 7.4 Gy in the laboratory. The dose estimates were obtained using small aliquots each containing $\sim$ 65 grains and the SAR protocol (Murray and Wintle, 2000). **b)** Same data as displayed in a), but now the OSL signal obtained by irradiating the sample to a fixed dose is plotted as a function of the estimated dose. Thus, increasing values on the y-axis represent increasing precision. **c)** Doses measured in small aliquots of unheated quartz containing $\sim$ 65 grains. The quartz was extracted from a concrete sample given a dose of approximately 4.8 Gy. **d)** Same data as displayed in c), but presented as in b).

In unheated materials, however, the time period in which the luminescence signal has accumulated is not as well-defined as it is for heated materials. Sand for building material is quarried from geological deposits, which may have received natural doses of more than 100 Gy, depending on the age of the deposit. During quarrying, refining and construction, the sand will be exposed to light, but generally this exposure is not sufficient to completely (or at least adequately) zero the latent luminescence signal in all the grains. Thus, some grains will have their luminescence signal completely zeroed at the time of manufacture, but the bulk of grains will only be partially zeroed (incompletely bleached), i.e. they will still record an absorbed dose. As a result, grains of quartz extracted from unheated materials such as concrete

will often show a wide distribution of doses. This is illustrated in Figure 2.2c, where quartz grains extracted from a modern concrete sample have been given a dose of 4.85 Gy (on top of the natural dose distribution) in the laboratory using a ^{137}Cs point source. The measured doses range between 3 ± 4 Gy and 240 ± 80 Gy and the average is 17.1 ± 1.7 Gy ($n = 253$). The challenge in using such materials as retrospective dosimeters is to identify those grains that had their luminescence signals zeroed at the event of interest. In a heterogeneous dose distribution, the grains giving the lowest estimates of absorbed dose are likely to be best bleached, but whether these grains were in fact adequately zeroed at the time of manufacture is difficult to determine. This complicates the estimation of the radiation accident dose superimposed on the natural dose distribution. Another challenge in using unheated materials is the sensitivity of the material to ionising radiation, which is often very low compared to the sensitivity of heated materials. Low sensitivity materials require a large number of grains to be measured to obtain a suitable dose distribution and many of these grains (usually the majority) will not have been completely zeroed at the time of manufacture.

3 Basic Concepts in Luminescence

3.1 Luminescence

Luminescence is a generic term for the electromagnetic radiation (usually in the form of visible light) emitted as a consequence of an atomic or molecular non-thermal excitation. Thus, luminescence is often described as cold light to distinguish it from incandescent light emission, which occurs when a material is excited thermally. Luminescent materials are able to absorb energy, store part of it and convert it into light; these materials usually have a crystalline structure.

Luminescence can broadly be categorised as either fluorescence or phosphorescence. The two types of luminescence are distinguished by the atomic mechanisms whereby the light is emitted (see Figure 3.1).

Fluorescence: the light emission resulting from the relaxation of an electron from an excited state to the ground state (possibly through a meta stable state from which transition to the ground state is allowed). The delay between the absorption of energy resulting in the excited state and the emission is determined by the life time of the excited state. The life time can be as short as picoseconds and as long as milliseconds in special cases. Photoluminescence, cathodoluminescence, chemiluminescence, bioluminescence and triboluminescence are all examples of different fluorescence processes with different means of excitation (i.e. photons, electrons, chemical energy, biochemical and mechanical energy, respectively)

Phosphorescence: the relaxation back to the ground state is delayed by a transition from the excited state into a meta stable state from which relaxation to the ground state is not permitted. These meta stable

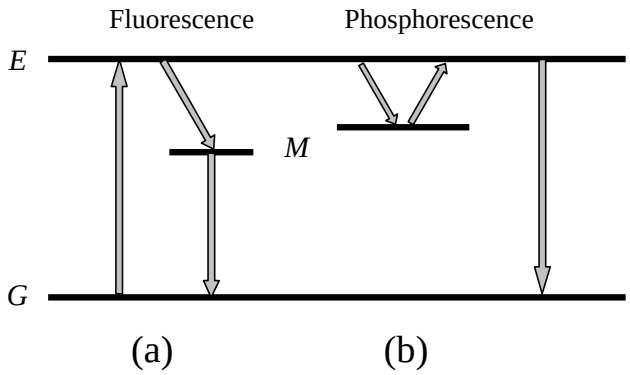

Figure 3.1: A schematic energy level diagram showing (a) the excitation and relaxation of an electron in fluorescence and (b) the excitation, trapping, detrapping and relaxation of an electron in phosphorescence. G represents the ground state, E represents an excited state and M a meta stable state

states function as electron traps, and energy must be supplied to detrap (release) the electrons back to the excited state from where they can relax to the ground state (McKinlay, 1981). The return to the ground state is thus delayed for a finite period of time; the length of which depends on the life time of the electron in the meta stable state.

In phosphorescence the energy difference between the excited state and the meta stable state is generally so small that detrapping occurs by lattice vibrations at ambient temperature, i.e. no external supply of energy is required. However, in TL and OSL the energy difference between the excited state and the meta stable state is so large that external energy must be applied to detrap the electrons. In TL the luminescence emission is accelerated by thermal stimulation whereas in OSL the luminescence emission is accelerated by optical stimulation.

3.2 Band model

An electron orbiting an atom is only allowed to exist in certain discrete energy levels. Energy values between these discrete levels are forbidden for an electron in a free atom. Atoms bound together in a solid have a marked effect upon each other. The forces that bind the atoms together greatly modify the behaviour of the other electrons. One consequence of the close proximity of atoms is to cause the individual energy levels of an atom to break up and form bands of allowed energy states. These energy bands in the solid are

separated (as before) by energy bands forbidden to the electrons.

The two outermost bands in a solid are called the valence band and the conduction band and the two bands of allowed energy states are separated by an intervening forbidden energy gap, which is referred to as the band gap (see Figure 3.2 p. 21). The valence band is the lower band of allowed states. It is labelled by E_v, representing the highest energy state in the valence band. Since electrons will tend to fill the lowest available energy states first, the valence band is nearly completely filled with electrons. The conduction band is the upper band of allowed states. The lowest possible energy state in the conduction band is given by E_c. Electrons in the conduction band are not attached to any single atom and therefore free to move about the crystal under the influence of any external electrical field. The band gap energy $E_g(= E_c - E_v)$ is the energy required to break a bond in the crystal. When a bond is broken, the electron has absorbed sufficient energy to leave the valence band and be promoted to the conduction band. Crystalline materials can be classified according to the width of the band gap. If the width of the band gap is large ($\sim$ 3 to 10 eV) the material is classified as an insulator (poor conductor), if the width is negligible or non-existing (i.e. the valence and conduction bands overlap) the material is classified as a conductor. Semi-conductor materials are intermediate between an insulator and a conductor. Thus, in an insulator the conduction band will contain only very few electrons, since the thermal energy of an individual electron is not large enough to promote it from the valence band to the conduction band. Luminescent materials are classified as insulators. In crystalline silicon dioxide (i.e. quartz) the width of the band gap is approximately 9 eV, thus making it a good insulator.

In a perfect insulator crystal lattice the probability for an electron making a transition from the valence band to the conduction band without the aid of external forces is negligible. When ionising radiation interacts with matter energy is deposited. This energy deposition can lead to an electron gaining sufficient energy ($\geq E_g$) to make the transition from the valence band to the conduction band. When the electron is promoted a hole is created in the valence band. The electrons in the valence band are now able to move by shuffling into the space left by the promoted electron. Thus, whenever an electron is promoted from the valence band to the conduction band an electron-hole pair is created. The excited electron will often only reside in the conduction band $\leq$ 10 ns (an average life time), before it loses its excitation energy and drops back down to the valence band, where it recombines with a hole. In the recombination process the energy is released as light (radiative recombination) or heat (non-radiative recombination). However, within

a crystalline solid, the crystal structure is not perfect. The structure contains various types of defects, the most common of which is a class of defects termed point defects. The different types of defects can be classified as intrinsic or extrinsic.

Intrinsic: unoccupied sites (vacancies) and occupied sites that in a perfect crystal would be unoccupied (interstitials).

Extrinsic: impurities at sites that in a perfect crystal would be occupied (substitutional impurities) or unoccupied (interstitial impurities).

Impurities refer to the random placement of foreign atoms into the crystal. Point defects can extend over several atomic spacings. The existence of defects results in the creation of allowed energy states in the otherwise forbidden band gap. A crystal defect is classified as a trap centre if the defect is able to capture a charge carrier (electron or hole) and re-emit it back to the band it came from. A crystal defect where charge carriers of opposite sign can be captured, resulting in an electron-hole recombination is classified as a recombination centre (Larsen, 1999). The structural defects in the crystal lattice create localised charge deficits, which are able to temporarily capture a conduction band electron attempting to return to the valence band. The captured electron remains trapped (and thereby immobilised) at the defect E_t until thermal excitation returns the electron to the conduction band.
The probability p per unit time for an electron leaving its trapping state is given by the Boltzmann factor:

$$p = s \exp\left(-\Delta E/kT\right) \tag{3.1}$$

where $\Delta E = E_c - E_t$ is the energy depth of the trap compared to the conduction band, k is Boltzmann's constant, T is the absolute temperature and s is the frequency factor (also known as the *attempt to escape frequency factor*), which is the product of the electron's oscillation frequency and the coefficient of reflection (Becker, 1973). The time an electron spends trapped depends on the energy depth of the trap compared to the conduction band ΔE (transitions from the trap to the valence band are not allowed), the temperature T and the frequency factor s. Thus, for a given trap type (constant s) and constant temperature the stability of a given trap is greater the further away from the lowest state of the conduction band it is located. In order for a trap to be of dosimetric interest it must have an adequate depth to prevent trapped electrons from being shaken free by lattice vibrations, i.e. the half life of the captured electrons in the trap must be at least of the order of weeks.

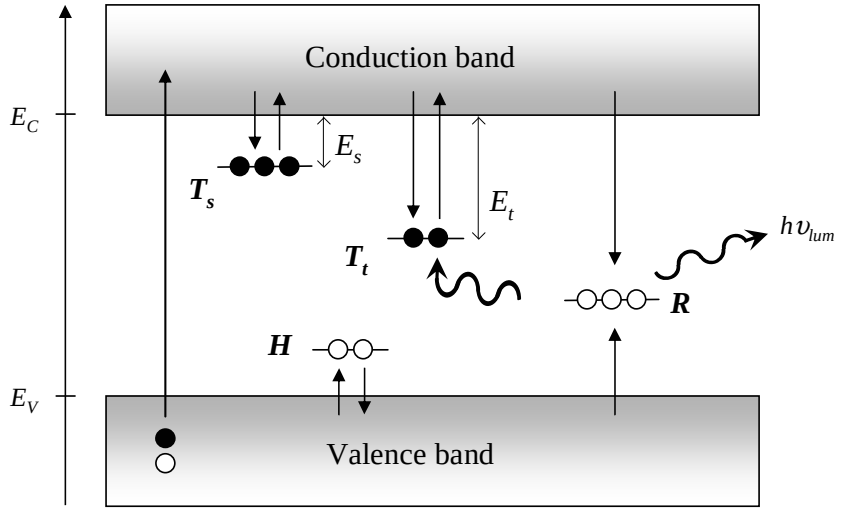

Figure 3.2: Simple band model illustrating TL and OSL processes. Ionisation results in the creation of an electron-hole pair. These electrons and holes become trapped at defects T and H. The trap T_s represents a shallow (unstable) trap from where the probability of thermal eviction is large. Storage of electrons is represented by the trap T_t, where the probability of thermal eviction (without external stimulation) is negligible. Thus, this is the trapping level of interest in dosimetry. By stimulating the sample either thermally (TL) or optically (OSL) electrons may gain sufficient energy to escape the trap and be released into the conduction band. Some of these released electrons find their way to radiative recombination centres (R), where they recombine with trapped holes and luminescence is emitted.

3.3 Thermoluminescence

At low doses the number of trapped electrons is proportional to the absorbed dose in the material. Thus, if the trapped charge can be released and the resulting recombination light measured, assessment of the absorbed dose is possible. By increasing the temperature of the crystal the probability of eviction increases. At a certain temperature range trapped electrons in a given trap type gain sufficient energy to overcome the potential barrier of the trap and the electrons are released into the conduction band. The detrapped electrons diffuse around the crystal and a fraction of electrons will find their way to a recombination centre, where recombination with a hole will take place (see Figure 3.2). The diffusion time is very short and recombination can be regarded as instantaneous (Aitken, 1998). A fraction of all electron-hole recombination events take place without any light emission (non-radiative). The size of this fraction can vary between 0 and 1, depending on factors such as crystal temperature and type of impurity (Horowitz, 1984).

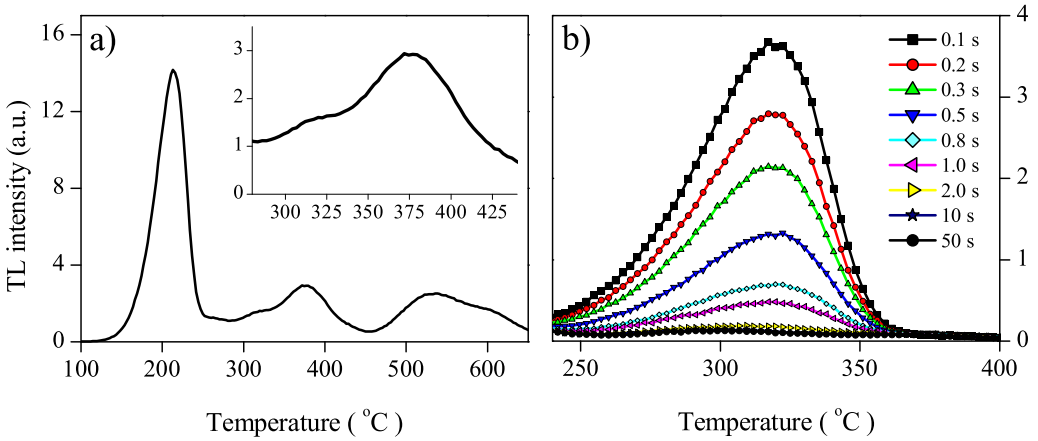

Figure 3.3: **a)** Example of a quartz TL glow-curve (Pers. comm. M. Jain). The quartz was extracted from a brick from a radioactive waste storage building (Jain et al., 2002), thermally emptied and irradiated in the laboratory. Before measuring the induced TL signal the sample was preheated to 160 °C. The strong peak at $\sim$ 220 °C is considered to be unstable for dosimetry applications. The inset shows the 325 °C and 375 °C peaks (RBP and SBP respectively) in quartz; the former appearing as a "shoulder" on the latter. **b)** Illustration of the effect of exposure to light (blue LED's) on the RBP (Pers. comm. M. Jain). About 2 s of exposure (photon energy fluence rate of approximately 50 mW/cm^2) is sufficient to deplete the trap. The sample is an Australian quartz (WIDG8), which was dosed and preheated to 260 °C prior to measurement.

If the intensity of the emitted luminescence (recombination light) is measured and plotted against temperature, the result is called a glow-curve. As the temperature is increased the probability of detrapping increases. The intensity initially increases, then it reaches a maximum value as the rate of detrapping peaks, and then it drops to zero again. The drop in luminescent intensity is caused by depletion of the trap. Since any real material will contain a number of different trap types situated at various energy levels a glow-curve may consist of a number of glow-peaks, each corresponding to different trapping levels. The lifetime of electrons in deep traps (ΔE large) is longer than the lifetime of electrons in shallow traps (ΔE small). Traps giving rise to glow-peaks with a maximum intensity occurring at temperatures $<$ 200 °C are generally considered unstable at environmental temperatures and therefore of no dosimetric interest. In order for a trap to be considered useful in dosimetry applications its glow-peak is usually situated at 200 °C or higher. In quartz some of the most common glow-peaks occur at 110 °C, 160 °C, 220 °C, 325 °C and 375 °C (see Figure 3.3). The peaks at 325 °C and 375 °C are known as the rapidly bleaching peak (RBP) and the slowly bleach-

ing peak (SBP) respectively (Franklin and Hornyak, 1990), since the 325 °C peak is bleached by optical stimulation more rapidly than the 375 °C peak. The rapidity of the bleaching of the RBP is illustrated in Figure 3.3b. The RBP is particularly important in OSL.

A complication in TL measurements is thermal quenching (Wintle, 1975). When the sample temperature is increased the efficiency of the luminescence often decreases. In quartz this drop in efficiency can be explained by the probability for non-radiative recombinations increasing as the temperature is increased (Mott and Gurney, 1948).

3.4 Optically stimulated luminescence

Optically stimulated luminescence relies on the same basic concepts as TL, but in OSL the stimulation energy is supplied by photons instead of heat. Thus, the physical principles of OSL are closely related to those of TL. However, it is not clear that the same defect centres are involved in both processes in any one material (McKeever, 2001). OSL has several advantages over TL. When dealing with unheated materials (i.e. materials zeroed by light exposure) the most important of these advantages are that in OSL only the trapping levels most sensitive to light are sampled; that is the charge population most effectively zeroed. In many samples, it is believed that 99% of the initial OSL signal originates from the 325 °C TL peak in quartz (Murray and Wintle, 1999). Another advantage of OSL over TL is that stimulation can be performed at room temperature (although some advantages may be obtained at slightly elevated temperatures), which means that thermal quenching is not made worse by heating.

OSL is applied in three main areas of dosimetry: 1) personal dosimetry, 2) environmental dosimetry and 3) retrospective dosimetry. OSL has also found application in the detection of artificial irradiation of foodstuff (Sanderson et al., 1998) and techniques are currently being developed for applications in radiation medicine, where an optical fibre OSL dosimeter measures the dose received by patients during radiotherapy or diagnostic radiology (Huston et al., 2002; Polf, 2002; Andersen et al., 2003).

3.4.1 Stimulation modes

In OSL the sample is stimulated with light of a specific wavelength, while the luminescence emission is measured at a different (usually shorter) wavelength. There are a number of different stimulation modes available: 1) continuous

wave-OSL (CW-OSL), 2) linearly modulated OSL (LM-OSL) and 3) pulsed OSL (POSL).

Continuous wave-OSL (CW-OSL)

In most OSL applications the measurements have been performed in the CW-OSL mode, where the sample is stimulated with constant light intensity and the luminescence emission is monitored during the stimulation (illumination). In this mode filters are required to discriminate between stimulation and emission light and to prevent scattered stimulation light from reaching the detector. The luminescence signal is observed to decrease with stimulation time as the OSL traps are being depleted. The OSL is usually monitored from the instant the light source is switched on and usually until the signal reaches a constant background level, resulting in the so-called OSL decay curve (see Figure 3.4). Various types of light sources have been in use in the past decade, some of which are: IR LEDs (Infrared light emitting diodes Hütt et al., 1993), filtered incandescent broad band lamps (Bøtter-Jensen and Duller, 1992; Bøtter-Jensen and Murray, 1999), green LEDs (Galloway, 1993, 1994), blue LEDs (Bøtter-Jensen, 1997) and green lasers (Duller et al., 1999).

Linearly modulated OSL (LM-OSL)

In the LM-OSL mode (Bulur, 1996) the intensity I of the stimulation light is not kept constant as in CW-OSL, but linearly increased with time from 0 to some value of the intensity I. Varying the stimulation power can be considered analogous to linearly increasing the temperature in TL. Initially the rate of release of trapped electrons is small, since the stimulation power is low. The OSL signal then increases with stimulation power until a maximum is reached. Hereafter the intensity of the OSL signal decreases non-linearly as a consequence of depletion in the concentration of trapped charge. The emitted OSL as a function of stimulation time is thus shaped like a peak. The position of the peak (in units of time) depends on the rate of linear increase in intensity of the stimulation light and the photoionisation cross-section of the trap being emptied. For a given ramp rate and stimulation wavelength, traps with different photoionisation cross-section values appear at different times and the method enables distinction between OSL originating from different traps. Figure 3.5 shows an example of a LM-OSL curve from a Danish quartz sample. LM-OSL curves are deconvolved by fitting exponential components to the data. The LM-OSL curve shown in Figure 3.5 is fitted adequately by 6 exponential components.

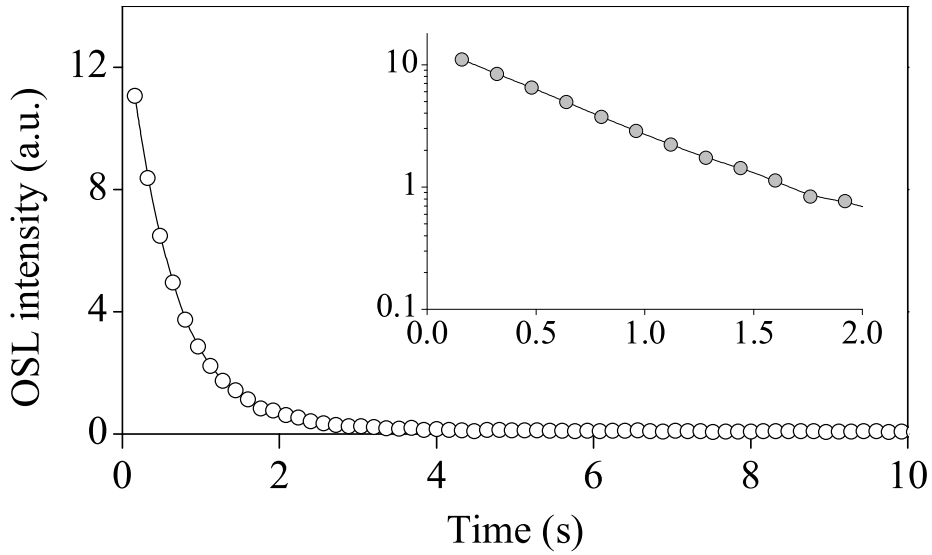

Figure 3.4: A CW-OSL decay curve obtained from a sedimentary aeolian quartz sample (lab code: 010414). The sample was stimulated using blue LEDs and the luminescence detected through 7.5 mm Hoya U-340 filters. Inset: same data as the graph but shown on a log scale. The initial part of the decay in this sample can be fitted adequately by a simple decaying exponential function. Note the logarithmic scale.

Pulsed OSL (POSL)

In pulsed OSL (McKeever et al., 1996) the stimulation light is pulsed and the OSL is only measured between pulses. Since the emitted luminescence is measured when the stimulation light is off, the need for optical filters to discriminate between emission and stimulation light is decreased. In POSL the discrimination between the emission and stimulation light is achieved by time resolution rather than wavelength resolution as in CW-OSL and LM-OSL. The POSL technique has not been used in this work and is not described further.

3.4.2 OSL model

When the sample is stimulated with constant light intensity (CW-mode), it is expected that the luminescence signal will decay with stimulation time due to detrapping of captured electrons and subsequent radiative recombination between electrons and holes at a radiative recombination centre. In the following the General One-Trap (GOT, Levy, 1985) model will be developed. This model includes a single type of electron trap T, a single type of radia-

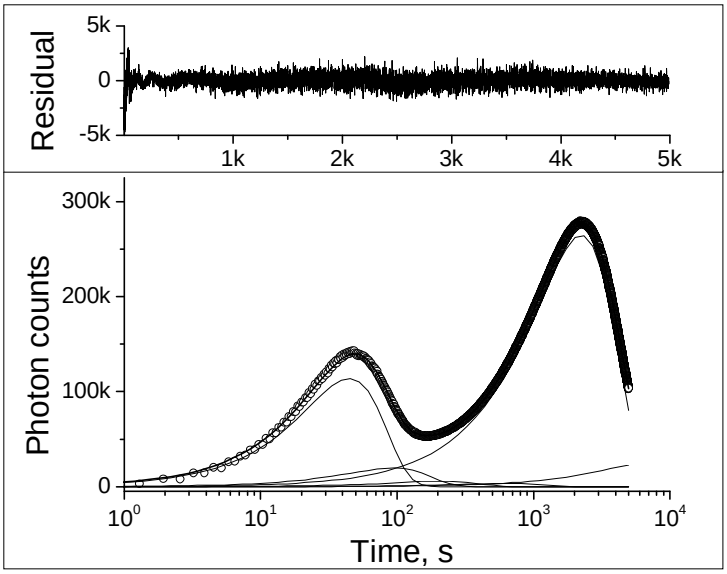

Figure 3.5: An example of a LM-OSL curve from a sensitised (heated to 700 °C) and irradiated quartz sample from Denmark. The sample was stimulated using blue LEDs and the luminescence detected through 7.5 mm Hoya U-340 filters. The LM-OSL consists of 6 exponential components. The upper graph shows the difference (residual) between the data and the fitted values. From Jain et al. (2003a).

tive recombination centre R and the conduction band (see Figure 3.6). Only electrons are considered in the trapping and recombination processes and all charge transport take place via the conduction band. Every transition to the recombination centre R is assumed to result in radiative recombination.

The probability per unit time of an electron leaving its trapping state is proportional to the photon fluence rate ϕ (photons $\cdot\, \mathrm{m}^{-2} \cdot \mathrm{s}^{-1}$) of the stimulation light (assumed to be constant). Thus,

$$p = \sigma(\lambda)\, \phi \tag{3.2}$$

where $\sigma(\lambda)$ is the photoionisation cross-section (m^2) for the release of charge from a trap. $\sigma(\lambda)$ depends strongly on the wavelength of the stimulation light, but for simplicity the stimulation light is assumed to be monochromatic. The detrapping rate of electrons from the trap T during external light stimulation is thus

$$\frac{\mathrm{d}n_u}{\mathrm{d}t} = -pn \tag{3.3}$$

where p is given by Equation 3.2 and n is the concentration of trapped electrons.

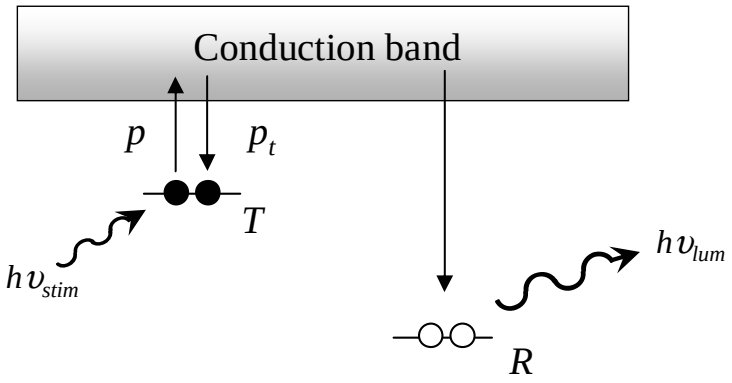

Figure 3.6: Enegy level diagram of the simple General One-Trap (GOT) model. An electron captured in the trap T is optically excited into the conduction band. The released electron will either be retrapped in T or recombine in the radiative recombination centre R, whereby a photon is emitted.

The rate at which electrons get trapped (or retrapped) in the trap T is proportional to the concentration of electrons in the conduction band and the concentration of available trapping sites in the trap T, i.e.:

$$\frac{\mathrm{d}n_d}{\mathrm{d}t} = p_t n_c (N - n) \tag{3.4}$$

where p_t is the trapping probability, n_c is the concentration of electrons in the conduction band, N is the concentration of electron traps and n is the concentration of trapped electrons.
The recombination rate (i.e. the transition rate of electrons from the conduction band to the recombination centre R) is proportional to the concentration of electrons n_c in the conduction band and to the concentration of holes h in the recombination centre R, that is

$$\frac{\mathrm{d}h}{\mathrm{d}t} = -p_r n_c h \tag{3.5}$$

where p_r is the probability for recombination.
The following rate equations describe the traffic of electrons between the conduction band and the centres:

$$\frac{\mathrm{d}n_c}{\mathrm{d}t} = -\frac{\mathrm{d}n_u}{\mathrm{d}t} - \frac{\mathrm{d}n_d}{\mathrm{d}t} - \frac{\mathrm{d}h}{\mathrm{d}t} = pn - p_t n_c (N - n) - p_r n_c h \tag{3.6}$$

$$\frac{\mathrm{d}n}{\mathrm{d}t} = \frac{\mathrm{d}n_u}{\mathrm{d}t} + \frac{\mathrm{d}n_d}{\mathrm{d}t} = -pn + p_t n_c (N - n) \tag{3.7}$$

$$\frac{\mathrm{d}h}{\mathrm{d}t} = -p_r n_c h \tag{3.8}$$

If it is further assumed that all holes created in the initial ionisation process are trapped in recombination centres, then

$$n + n_c = h \qquad \text{thus} \qquad \left|\frac{\mathrm{d}n_c}{\mathrm{d}t}\right| = -\left|\frac{\mathrm{d}n}{\mathrm{d}t}\right| + \left|\frac{\mathrm{d}h}{\mathrm{d}t}\right| \tag{3.9}$$

The expression in Equation 3.9 is known as the charge neutrality condition. In this model the intensity I_{OSL} (photons/s) of the OSL signal is equal to the rate at which recombination occurs, i.e.

$$I_{OSL}(t) = -\mathrm{d}h/\mathrm{d}t = -\mathrm{d}n_c/\mathrm{d}t - \mathrm{d}n/\mathrm{d}t \approx -\mathrm{d}n/\mathrm{d}t \tag{3.10}$$

where a state of quasi-equilibrium has been assumed, i.e. $n_c \ll n$ (concentration of electrons in the conduction band is much smaller than the concentration of trapped electrons) and $|\mathrm{d}n_c/\mathrm{d}t| \ll |\mathrm{d}n/\mathrm{d}t|$ (the rate of change of the electron concentration in the conduction band is much smaller than the rate of change of the trapped electron concentration). By using the implicit approximation $\mathrm{d}n_c/\mathrm{d}t \approx 0$ to find an expression for n_c and inserting it into Equation 3.10 the following equation for the OSL intensity $I_{OSL}(t)$ can be derived

$$I_{OSL}(t) \approx pn\left(1 - \frac{p_t(N-n)}{p_r h + p_t(N-n)}\right) \tag{3.11}$$

This equation is referred to as the General One-Trap (GOT) equation for OSL. A similar expression can be derived for TL.

CW-OSL decay curve

If retrapping is assumed to be negligible, i.e. $p_r h \gg p_t(N-n)$ The GOT Equation (3.11) reduces to a first order differential equation

$$I_{OSL}(t) = -\frac{\mathrm{d}n}{\mathrm{d}t} = pn \tag{3.12}$$

Integration of Equation 3.12 gives the first-order solution

$$I_{OSL}(t) = I_0 \exp(-t/\tau) \tag{3.13}$$

where I_0 is the initial intensity of the OSL signal at $t = 0$ and τ is the characteristic decay time given by $(\sigma(\lambda)\,\phi)^{-1}$, where ϕ is the photon fluence rate of the stimulation light.

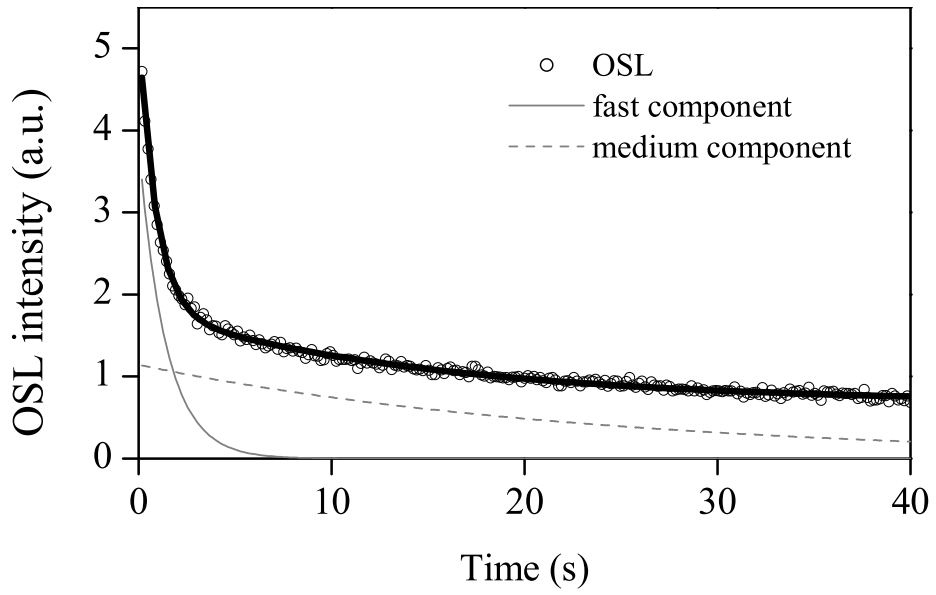

Figure 3.7: A CW-OSL decay curve obtained from a sedimentary aeolian quartz sample (lab code: 010414). The OSL curve can adequately be described by two decaying exponential functions.

Any material will naturally contain more than just one trap type, and since all traps in the sample are stimulated simultaneously the OSL signal can be considered to be a sum of series of decaying exponentials (i.e. if the first-order solution is applicable), when the material has a distribution of traps sensitive to optical stimulation ($\sigma > 0$). Thus,

$$I_{OSL} = \sum_{i=i}^{m} I_{i0} \exp(-t/\tau_i) \tag{3.14}$$

where m is the number of optical trap types with different cross-sections ($i = 1, 2, \ldots, m$). The OSL curve from quartz is usually said to be composed of three exponential components: a fast, medium and slow component with a characteristic life times of 0.4 s, 10 s and 150 s respectively (measured with blue LEDs giving approximately 50 mW/cm^2 at the sample position at 125 °C; Bøtter-Jensen et al., 2000a).

However, in general the shape of the decay curve is non-exponential. An assumption in deriving Equation 3.13 was that the retrapping probability of the excited electron into the trap T was negligible. By taking retrapping into account a second and general order equation can be derived (see for instance Larsen, 1999) for this simple model. The model of the OSL emission

can be expanded by including additional trapping states that are optically inactive ($\sigma = 0$) and act as competing traps (Polf, 2002). However, the shape of the decay curve is dependent on different parameters such as sample, absorbed dose, stimulation wavelength and sample temperature. No model-based analytical function describe the overall shape of the CW-OSL decay curve, but numerical solutions of differential equations used to describe the charge transfer processes occurring on the basis of simple models can be predicted (McKeever, 2001).

3.5 Resetting or zeroing the OSL signal

For a small dose the integrated OSL signal is proportional to the dose absorbed by the material. The absorbed dose is imparted to the material by exposure to the weak natural environmental background radiation and/or man-made radiation sources. The OSL signal can be zeroed by heat or exposure to light. Assessment of the integrated radiation dose in retrospective dosimetry is dependent on the efficiency with which any latent OSL signal has been zeroed in the past. Subsequent to the zeroing event the OSL signal starts to rebuild (see Figure 3.8). In dating applications the date refers to the time lapsed since the material was last zeroed (i.e. the burial time). Thus, in dating applications the unknown is the burial time. In accident dosimetry there are two unknowns: the accident dose and the burial time. This can be circumvented by using samples where the time lapsed since the last zeroing event is known; preferably by using samples recently zeroed.

3.5.1 Thermal zeroing

The OSL signal can be zeroed by heating. In Figure 3.9a 510 independent dose estimates are shown from a sedimentary quartz sample heated to 850 degrees (and held for one hour). The dose distribution is symmetrical and narrow (i.e. small absolute standard deviation; ~ 63 mGy) and the average dose is 10 ± 3 mGy $(n = 510)$. Thus, heating a sample to more than 500 degrees is a very efficient way of zeroing a sample. Another advantage of using heated samples is that heating to high temperatures increases the sensitivity to ionising radiation, i.e. the size of the induced OSL signal per unit absorbed dose is increased. Generally, the precision of the dose estimates is improved (because of a smaller contribution from counting statistics) and the number of grains giving a detectable light signal (i.e. the recovery) is increased compared to before the heating. As an example, in this sample 600 grains were measured and 510 of these gave detectable light signals in the laboratory irradiations,

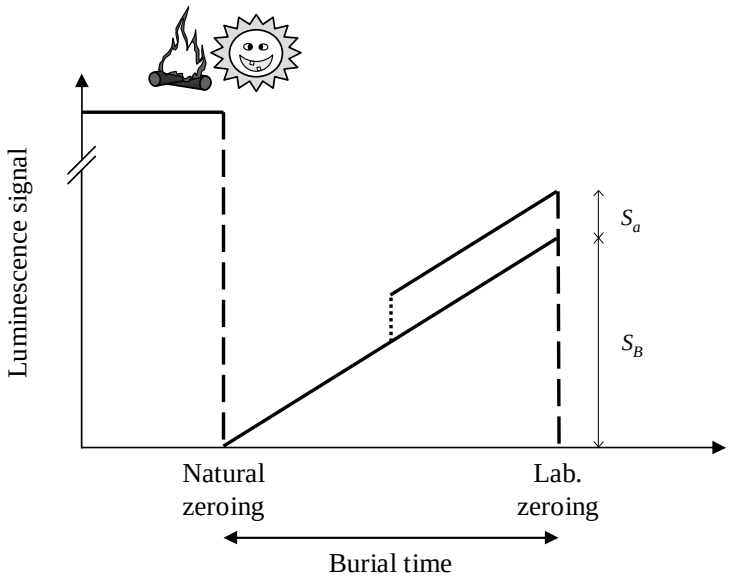

Figure 3.8: Schematic diagram of the zeroing process (based on Figure 1.1 in Aitken, 1998). The luminescence signal can be zeroed thermally or optically. The dose estimated in luminescence techniques is the dose imparted to the material since the last zeroing event took place. In heated materials (e.g. pottery and bricks) the last zeroing event occurred, when the material was heated to high temperatures, whereas for unheated materials it took place when the material was last exposed to daylight (e.g. during erosion, transport and deposition). After the zeroing event the luminescence signal starts to rebuild. The material is then sampled (in darkness) and brought into the laboratory, where the luminescence signal is measured using either TL or OSL. S_B denotes the luminescence signal induced by exposure to the natural environmental background radiation, and S_a denotes the additional luminescence signal induced by a radiation accident

thus giving a recovery of 85%. For comparison the recovery for this sample before heating was approximately 1%.

Figure 3.9b shows the single-grain dose distribution of quartz extracted from a sand core inside a Juno bronze statue (sample supplied by Dr. C. Goedicke, Rathgen-Forschungslabor, SMPK, Berlin). The sample had been heated to a high temperature during manufacture at some time in the past. The dose distribution is again symmetrical and narrow with an average dose of 0.17 ± 0.08 Gy ($n = 28$). The statue was believed to have been manufactured in the 16^{th} century, but the dose rate the sample was subjected to since manufacture was estimated (by Dr. Goedicke) to be 1.255 mGy/a, which dates the last heating to about 1860.

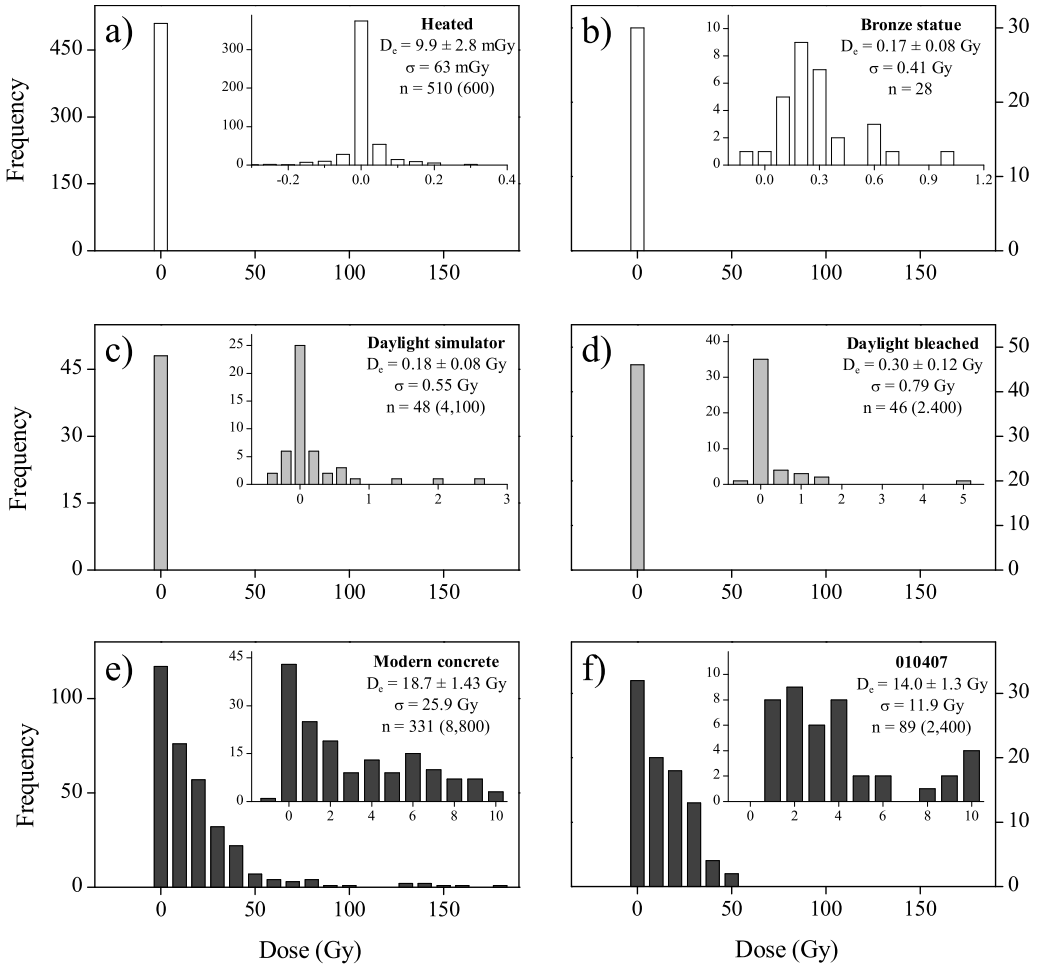

Figure 3.9: Examples of heated and unheated dose distributions presented as dose histograms. Insets show enlargements of the individual distributions. The equivalent dose D_e is the simple arithmetic mean of the individual dose estimates, the given uncertainty is the standard uncertainty, i.e. the standard deviation σ divided by the square root of the number n of included individual dose estimates. The number in parenthesis is the total number of aliquots measured. **a)** Single-grain dose distribution from a sedimentary quartz sample thermally zeroed in the laboratory. **b)** Single-grain quartz dose distribution from a heated historic artifact (bronze statue). **c)** Single-grain dose distribution of unheated quartz extracted from a modern concrete sample, that was bleached in a daylight simulator in the laboratory for one hour prior to measurement. **d)** Single-grain dose distribution of quartz extracted from an unheated, modern concrete sample, that was bleached in the windowsill for two hours prior to measurement. **e)** Single-grain dose distribution of unheated quartz extracted from a modern concrete sample. **f)** Single-grain dose distribution of unheated quartz extracted (lab code: 010407) from a sand layer in a prehistoric stone wall.

3.5.2 Optical zeroing

The OSL signal can also be zeroed by exposure to (day)light. This is illustrated in Figure 3.9c, where quartz – extracted from a modern concrete sample containing a wide range of doses (see Figure 3.9e) – prior to measurement was bleached in the laboratory for one hour using a daylight simulator. The distribution is near symmetrical and has an average dose of 0.18 ± 0.08 Gy ($n = 48$). The individual estimates of uncertainty on the 48 dose estimates are based purely on counting statistics. 52% of the dose estimates fall within 1σ of zero, 77% within 2σ and 94% within 3σ. Clearly, not all the dose estimates are consistent with zero. One possible explanation for the non-zero grains in Figure 3.9c is thermal transfer. It is standard practice to preheat the sample (generally to 200 – 300 °C) prior to OSL measurement. This is done to allow a direct comparison of the natural OSL signal with that induced by subsequent laboratory irradiation (see section 3.6.2). By preheating the sample it is possible to transfer charge trapped in light-insensitive traps into the OSL traps and thereby induce an OSL signal.

The dose distribution presented in Figure 3.9d was obtained from quartz grains extracted from another modern concrete sample (the natural dose distribution obtained using small aliquots is shown in Figure 5.3 on page 79). These grains were first bleached in the laboratory using the green laser in the single grain OSL attachment (the grains mounted in the special single-grain sample discs; see section 4.5) and then given a beta dose of approximately 100 Gy. The grains were then placed in a windowsill for two hours to investigate if exposure to daylight (on a typical cloudy day in May in Denmark) could sufficiently zero a latent luminescence signal of 100 Gy in this sample. The majority of grains were completely zeroed, but again some grains did record a dose not consistent with zero (54% of the dose estimates fall within 1σ of zero, 83% within 2σ and 89% within 3σ).

Godfrey-Smith et al. (1988) showed that the OSL signal may be reduced by approximately 50% in quartz by exposure to full sun-light for a few seconds. Optical dating has successfully dated aeolian and coastal dune sediments (Huntley et al., 1985; Stokes and Rhodes, 1989; Berger, 1995; Duller, 1996), which typically received prolonged exposure to sun-light before deposition. However, even though the OSL signal is zeroed rapidly, it is not always completely zeroed at the time of deposition. In some environments (e.g. fluvial and colluvial) the sediments are less likely to be adequately zeroed by exposure to sunlight for various reasons, such as the duration of light exposure (e.g. rapid deposition or large latent OSL signal), significantly reduced light intensities and restricted (filtered) light spectrum (Berger and Luternauer, 1987; Wallinga, 2001). Samples in which the zeroing was not complete

are usually referred to as incompletely zeroed, partially bleached or poorly-bleached. Duller (1994) classified such poorly bleached samples as Type A or Type B. In Type A sediments all grains were equally but incompletely zeroed at the time of deposition (i.e. no grain-to-grain variations). Type B sediments contain a mixture of grains exposed to daylight at deposition for very different periods of time (i.e. grain-to-grain variations). Thus, some of the grains may have been exposed to sufficient daylight to zero the latent OSL signals, whereas others still carry an OSL signal at burial. The materials used in this work (except for household and workplace chemicals, Chapter 9) can all be classified as Type B.

In conventional OSL techniques, the equivalent dose estimates are made on subsamples (aliquots) – each typically containing several thousand grains. Thus, attempts to determine the absorbed dose in incompletely zeroed materials are likely to produce an overestimate of the true burial dose (e.g. Li, 1994; Rhodes and Pownall, 1994; Berger, 1995; Murray et al., 1995; Olley et al., 1998). It is therefore important to assess whether a given sample is incompletely zeroed; an indication of this is the degree of scatter observed in the individual dose estimates. This has been demonstrated in previous studies (e.g. Li, 1994; Duller, 1994, 1995; Clarke, 1996; Clarke et al., 1999). However, if large aliquots (several thousand grains) are used, grain-to-grain variations in equivalent doses are averaged within aliquots, so that scatter in the equivalent dose estimates as a consequence of incomplete zeroing will only occur if the OSL signal is dominated by a small number of bright grains with different equivalent doses or only a small portion of the grains were incompletely zeroed (Wallinga, 2001). Absence of scatter in the equivalent dose estimates is not a guarantee that the sample was well-zeroed at deposition. Li (1994) and Wallinga (2001) showed that the inter-aliquot scatter is dependent on the number of grains in each aliquot. By reducing the number of grains in each aliquot, the scatter in equivalent doses becomes more pronounced and incomplete zeroing more easily identified. The best estimate of the burial dose is provided by the grains that were most completely zeroed at burial and can thus be derived from the grains giving the smallest equivalent doses. By reducing the number of grains in each individual aliquot the probability of measuring an aliquot only containing well-zeroed grains is increased. Olley et al. (1998) suggested that the lowest measured doses in small aliquots containing between 60 and 100 grains is likely to closely approximate the true burial dose. Olley et al. (1999) used a binomial distribution model to predict the probability of selecting k poorly-bleached grains, i.e.

$$P\{n,k,p\} = \binom{n}{k} p^k (1-p)^{n-k} \tag{3.15}$$

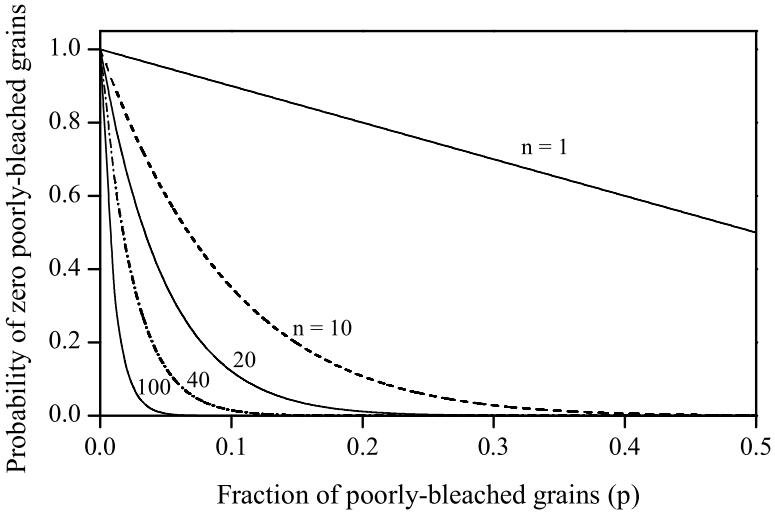

Figure 3.10: Probability of including only well-bleached grains in an aliquot consisting of n grains as a function of the fraction of poorly-bleached grains in the sample. Based on Figure 4 in Olley et al. (1999).

where p is the probability of selecting a poorly-bleached grain (i.e. the fraction of poorly-bleached grains in the sample) and n is the number of grains in each aliquot. When the probability of selecting a poorly-bleached grain is less than 5% (i.e. $p < 0.05$), the predicted distributions are asymmetric (positively skewed). When the probability of selecting a poorly-bleached grain is increased (the fraction of poorly-bleached grains is increased) the distributions become more symmetrical. The authors recognised that natural dose distributions are likely to contain a range of doses instead of just two dose components, but argue that the general forms of the distributions and in particular their leading edges will be similar to those predicted by the binomial distribution (Olley et al., 1999). The probability of selecting only well-bleached grains in an aliquot containing n grains is given by $(1-p)^n$ (i.e. $k = 0$) and is plotted as a function of the fraction of poorly-bleached grains in Figure 3.10. In an aliquot consisting of 100 "active" grains (i.e. all grains contribute to the OSL signal) the probability of selecting only well-bleached grains is approximately 1%, when the fraction of poorly-bleached grains in the sample is $> 4.5\%$. By reducing the number of grains in each aliquot to a single grain, the probability of selecting only well-bleached grains is increased until it eventually equals the fraction of well-bleached grains in the sample, when $n = 1$.

A basic assumption in luminescence techniques is that the dose-rate is constant with respect to time and uniform within a sample. By reducing

the number of grains in an aliquot to a single grain, heterogeneity in external beta dose-rate (i.e. differences in dose-rates on a grain-to-grain scale) might become an important factor. Murray and Roberts (1997) found that the observed spread in their data was significantly larger than expected and attributed it to heterogeneity in external beta dosimetry. However, McFee (1998) and Olley et al. (1999) argued that the effect of beta dose heterogeneity is small in their samples.

Figure 3.9e shows a single-grain dose distribution of unheated quartz extracted from a modern concrete block. The block had recently been manufactured and was presumably exposed to light during this process. However the dose distribution is broad and highly asymmetric, indicating that the zeroing was incomplete. In this case using the average dose (18.7 ± 1.4 Gy, $n = 331$) to characterise the dose distribution is meaningless. However, the inset shows that some of the dose estimates are consistent with zero, implying that some of the grains were exposed to sufficient light to have their luminescence signals completely zeroed. In this sample only 331 grains out of the 8,800 measured grains gave detectable light signals, which gives a recovery of 4%.

Figure 3.9f shows a single-grain dose distribution of unheated quartz extracted from a sand layer inside a prehistoric stone wall estimated to have been built 2000 years ago (further details on the sample can be found in Baran et al., 2003). When the stone wall was built it is considered likely that some sediment was attached to the surfaces of the stones. These sediment grains would have been exposed to daylight during construction. Thus it is likely that some grains were completely zeroed at the time of construction. The dose distribution is clearly asymmetric and the doses range between 0.9 ± 0.4 Gy and 51 ± 24 Gy, but there are no grains giving a dose consistent with zero. The dose population centred at approximately 2 Gy probably indicates the best estimate of the true burial dose.

3.6 Dose estimation

The basic assumption enabling assessment of the accumulated dose is that the OSL signal (either the integral or the initial intensity) is uniquely related to the absorbed dose. The absorbed dose is calculated by comparing the natural OSL signal with *artificial* OSL signals induced in the laboratory by administering known doses to the sample. The laboratory dose that would have been required to induce an OSL signal identical to the natural OSL signal is known as the equivalent dose, D_e.

3.6.1 Choice of OSL signal

In regenerative measurement procedures the OSL signal is stimulated until the OSL traps have become depleted and the OSL emission ceases – or nearly so. As mentioned in section 3.4 the quartz signal is generally made up of at least three different contributions: the fast, medium and slow component. The traps contributing to the slow component are only weakly sensitive to optical stimulation and in practice difficult to completely empty optically (i.e. the stimulation times required are impractically long). Given that the photoionisation cross-sections of these traps are small, they were in all likelihood not well-zeroed at burial. Because these traps are difficult to bleach, this contribution is likely to accumulate through the repeated measurement cycles in the SAR protocol (see section 3.6.3). In OSL the main interest is focused on traps most likely to have been well-zeroed at burial, that is the traps contributing to the fast and possibly the medium components. To exclude the contribution from the slow component a background based on the average OSL observed towards the end of the stimulation period is subtracted from the earlier OSL signal. In subtracting this background the contribution from the instrumental background (e.g. including PMT dark counts and filter break through contributions) is also removed. It is this net signal, which is used in OSL analyses (see Figure 3.11). Murray et al. (1997) showed that the initial OSL signal is directly proportional to the integrated OSL signal and Banerjee et al. (2000) found that the smallest statistical uncertainty (for both dim and bright signals) in the net OSL signal is achieved using the initial part of the decay curve. Thus, using the initial OSL signal in analyses has the advantages of including the part of the OSL signal most sensitive to light and an enhanced signal-to-noise ratio.

3.6.2 The regenerative approach

In theory estimation of the natural dose is quite simple. The natural OSL signal is measured and in the process light-sensitive traps are emptied of trapped charge. A laboratory dose D_i is then given to the sample and a regenerated OSL signal measured. This procedure can be repeated any number of times and by varying the regeneration doses, a dose response curve (also known as a growth curve) showing how the OSL signal grows with radiation dose can be constructed. Interpolating the natural OSL signal onto this growth curve gives the laboratory dose (the equivalent dose) required to induce an OSL signal equivalent to the natural OSL signal.

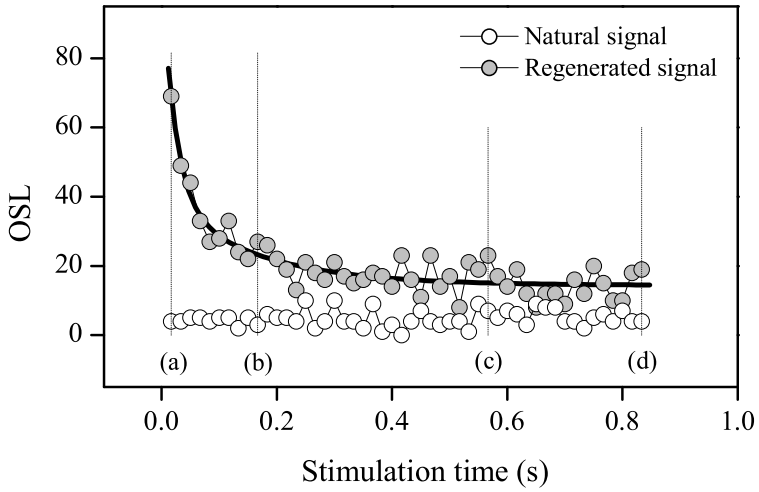

Figure 3.11: OSL single-grain decay curves of a thermally zeroed (heated to 850 °C) quartz grain. The "natural signal" is the OSL signal measured after thermally zeroing the grain (open symbols) and the "regenerated signal" is the OSL signal measured subsequent to administering a dose of 1 Gy to the grain. For each decay curve the net signal is calculated by integrating the initial part of the decay curve (i.e. from a to b) and subtracting the appropriate background (integrated from c to d). Thus, negative values of equivalent doses can be derived when the integrated background happens to be larger than the initial signal (as is the case for the natural signal here).

However, dose estimation is complicated by the fact that the sample needs to be preheated prior to OSL measurement. Godfrey-Smith (1994) observed that the OSL signal from a laboratory irradiated quartz sample decayed substantially over a time period of 68 days at ambient temperature, indicating that the OSL is generated from at least one stable and one unstable trap. Murray and Wintle (1999) carried out isothermal decay experiments on both natural and laboratory irradiated aliquots of a 35,000 year old Australian sedimentary quartz sample. They concluded that a single trap with a life time of $\sim 10^8$ y at ambient temperature explained $\sim 99\%$ of the natural OSL (this trap is believed to correspond to the 325 °C TL trap). However, the laboratory irradiated aliquots contained an additional unstable component, with a life time of ~ 400 y. Franklin et al. (1995) concluded that the quartz TL peaks located at 110 °, 180 °, 220 ° and 325 °C all use the same luminescence centre, which is accessed via the conduction band. Thus, in order to be able to compare natural and regenerated signals the unstable contributions to the observed OSL signal (probably originating from the 110 °, 180 ° and 220 °C TL traps) must be removed. One way of doing this is by preheating the sample, i.e. to heat the sample prior to OSL measurement. It is stan-

Table 3.1: Generalised single-aliquot regeneration sequence. From Murray and Wintle (2000).

Step	Treatment[a]	Observed[d]
1	Give dose, D_i	-
2	Preheat[b] (160–300 °C for 10 s)	-
3	Stimulate[c] at 125 °C	L_i
4	Give test dose, D_t	-
5	Heat to 160 °C	-
6	Stimulate at 125 °C	T_i
7	Return to 1	-

[a] For the natural sample, $i = N$, and $D_N = 0$ Gy.
[b] Aliquot cooled to < 60 °C after heating. In step 5, the TL signal from the test dose can be observed, but it is not made use of in routine applications.
[c] The stimulation time is dependent on the stimulation light intensity.
[d] L_i and T_i are derived from the initial OSL signal minus a background estimated from the last part of the stimulation curve.

dard practice to preheat the samples to a temperature between 160 ° and 300 °C. Unfortunately, heating quartz alters the sensitivity (emitted luminescence per unit dose) of the sample to radiation, which complicates the dose estimation. Changes in sensitivity can be caused by heat treatment, optical stimulation and irradiation, and for many years prevented the use of single-aliquot protocols for quartz. Until 1997 many aliquots (typically 50–100, each of about 10 mg) were required to obtain a single equivalent dose estimate for quartz. The first true single-aliquot regenerative-dose (SAR) protocol able to overcome the problem of sensitivity changes in quartz was described by Murray and Roberts (1998) and improved by Murray and Wintle (2000). In the SAR protocol sensitivity changes are explicitly monitored and corrected by the insertion of a test dose. There are many published descriptions of the SAR protocol and its applications (e.g. Murray and Olley, 1999; Murray and Wintle, 2000; Bailey et al., 2001; Stokes et al., 2001). In the following a brief description of the SAR protocol is presented and a generalised measurement sequence is shown in Table 3.1.

3.6.3 Single-aliquot regenerative-dose (SAR) protocol

The material is given a dose D_N before sampling (i.e. during a radiation accident, or during burial). In the laboratory the sample is preheated to a temperature T_{PH} (usually between 160 ° and 300 °C and held for 10 s). The natural OSL signal L_N is then measured by optical stimulation until the signal has decayed to a negligible level (i.e. until the OSL traps are empty). A small test dose D_t (usually $\sim$ 10% of the natural dose D_N) is then administered to the sample. The sample is subsequently heated to a temperature T_{CH} (typically 160 °C to empty the 110 °C TL trap), cooled immediately and the OSL signal T_N induced by the test dose measured. The second measurement cycle in the SAR protocol is initiated by giving the first regenerative dose D_1 to the sample. After irradiation the sample is heated to the same preheat temperature T_{PH} as in the first measurement cycle and the regenerated signal L_1 measured. The sample is then given another test dose D_t (same as in the first cycle), heated to T_{CH} and the induced OSL signal T_1 measured. In order to build a growth curve the second regenerative cycle is repeated, only changing the size of the regenerative dose D_i. It is the OSL response to the fixed test dose D_t that is used to monitor sensitivity changes occurring in the measurement protocol. If no sensitivity changes took place all values of T_i would be identical, but in practice they are often seen to vary considerably. By dividing the natural and regenerated OSL signals with the subsequent test dose signals (i.e. L_N/T_N and L_i/T_i respectively) a sensitivity corrected measure of the OSL signal is obtained. The regeneration doses are typically chosen such that the sensitivity corrected values $R_i = (L_i/T_i)$ encompass the natural sensitivity corrected value $R_N = (L_N/T_N)$, i.e. 1) $R_1 < R_N$, 2) $R_2 \approx R_N$ and 3) $R_3 > R_N$. A sensitivity corrected growth curve is constructed by plotting values of R as a function of D. The natural dose D_N (or rather its equivalent in the laboratory - the equivalent dose D_e) is then estimated by interpolation of the ratio R_N onto the sensitivity corrected growth curve. If the correction for sensitivity change works properly the corrected OSL ratio R_i should remain constant throughout the measurement cycle for a fixed D_i, i.e. it should be independent of prior dose and thermal treatment. This is tested in the SAR protocol by repeating one of the regeneration cycles, usually the 6$^{\text{th}}$ cycle is a repetition of the 2$^{\text{nd}}$ cycle, i.e. $D_5 = D_1$. If the protocol corrects for sensitivity change, then $R_5 = R_1$ or equivalently $R_5/R_1 = 1$. The ratio R_5/R_1 is called the recycling ratio and should ideally be equal to unity.

If no dose ($D = 0$ Gy) is administered to a sample, no detectable OSL signal should be observed. In practice,however, a detectable recuperated OSL signal is seen (Aitken and Smith, 1988). In the SAR protocol the recuperation

is estimated by inserting a measurement cycle with $D_i = 0$ Gy (usually $i = 4$). The ratio R_4 should ideally be zero, but is in practice finite. One of the prime reasons for preheating is to prevent contamination of the regenerated signals by contributions from thermally unstable but light-sensitive traps. However, preheating can also result in recuperation of the OSL signal after the OSL traps have been emptied optically. Murray and Wintle (2000) suggested that the recuperated signal (at least in part) arises from charge inserted by the test dose into thermally shallow but light-insensitive traps, which are not emptied by heating to T_{CH} (usually 160 °C), but are emptied by heating to T_{PH} (usually 260 °C) and partly retrapped by the OSL trap.
A standard SAR protocol for quartz usually consists of six measurement cycles: 1) natural, 2) $D_1 < D_N$, 3) $D_2 \approx D_N$, 4) $D_3 > D_N$, 5) $D_4 = 0$ and 6) $D_5 = D_1$. OSL measurements are conventionally carried out at 125 °C to prevent retrapping in the trap associated with the 110 °C TL trap (Murray and Wintle, 1998).
The growth curve will often appear linear at low dose levels, but at higher dose levels the luminescence signal saturates, because of a finite number of available charge traps. The growth curve is usually fitted adequately by a single saturating exponential, i.e.

$$I = I_\infty \left(1 - e^{-D/D_0}\right) \tag{3.16}$$

where I is the intensity of the luminescence signal for a dose D, I_∞ is the maximal attainable signal and D_0 is a parameter which characterises the shape of the curve.
If the dose response of the sample can be assumed to be linear, the natural dose can be estimated by simply taking the ratio of the integrated natural and regeneration signal (and multiplying by D_i).

In this work the SAR protocol has been used to measure absorbed doses. Equivalent dose estimates for individual aliquots are obtained by linear interpolation between the two test dose corrected OSL signals bracketing the natural signal. The dose range of interest in this work is from 0 to 10 Gy. The regeneration doses were generally closely spaced (by ~ 2 Gy) to ensure that deviation from linearity was small. Dose estimates outside the regeneration dose range are based on linear extrapolation.

4 Instrumentation

Essential components of an OSL measurement facility are 1) a stimulation light source, 2) a light detection system, 3) an irradiation source and 4) a heater for heating the samples. The measurement equipment used to obtain the results presented in this thesis is a Risø TL/OSL reader (model TL/OSL-DA-15) equipped with a single grain OSL attachment (Bøtter-Jensen et al., 2000a). In this chapter the most essential parts of the system will be outlined, and where necessary characterised.

The Risø TL/OSL measurement system enables measurement of both thermoluminescence and optically stimulated luminescence. The system allows up to 48 samples to be individually heated to any temperature between room temperature and 700 °C, to be individually irradiated by a beta source (^{90}Sr/^{90}Y) mounted on the reader and to be optically stimulated by various light sources *in situ*. The emitted luminescence is measured by a light detection system comprised of a photomultiplier tube and suitable detection filters. A schematic drawing of the system is shown in Figure 4.1.

4.1 The Risø TL/OSL system

Samples are either mounted on 9.7 mm diameter aluminium or stainless steel discs using silicone oil as an adhesive or poured (as loose grains) into sample cups. Samples are loaded onto an exchangeable sample carousel that can accommodate up to 48 samples. The sample carousel is then placed in the sample chamber which can be programmed to be evacuated or have a nitrogen atmosphere maintained by a nitrogen flow. The sample carousel rests on a motor driven turntable, which enables rotation (in steps) of the sample carousel. Rotation is computer controlled and position holes drilled though the carousel in close proximity to the sample positions enable the system to keep track of the position of the carousel using opto-electronics and a stepper

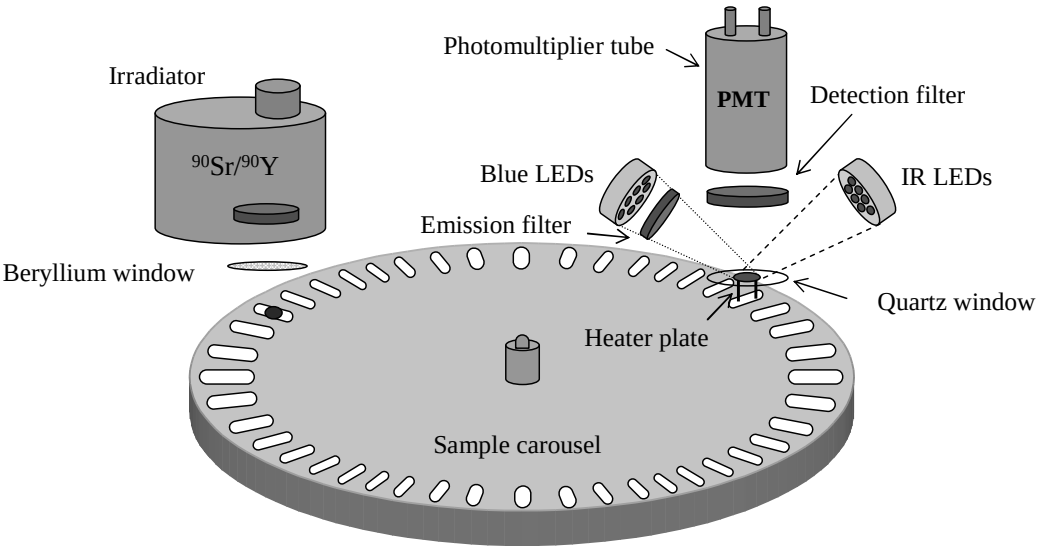

Figure 4.1: Schematic drawing of the Risø TL/OSL luminescence reader

motor. An infrared light emitting diode (LED) is positioned underneath the turntable, which is switched on during rotation. The measurement is initiated by moving a given sample to the measurement position located directly underneath the light detection system. The sample is then lifted through slots in the sample carousel into the measurement position by a lift, which also functions as the heating element. In the measurement position the sample can be stimulated thermally and/or optically. Thermal stimulation is obtained by linearly increasing the temperature of the heater strip and optical stimulation is provided by different light sources focused onto the sample position. The emitted luminescence is measured by the light detection system (see Figure 4.1).

4.2 Light detection system

The essential components of the light detection system are 1) a photomultiplier tube (PMT) and 2) suitable detection filters. The detection filters serve both to shield the PMT from scattered stimulation light and to define the spectral detection window.

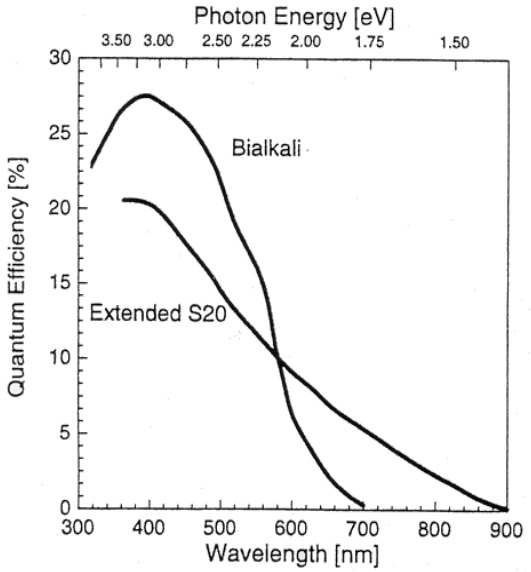

Figure 4.2: The quantum efficiency of the photomultiplier tubes EMI 9235QA PMT (Bialkali) and EMI 9658R PMT (Extended S20) as a function of photon wavelength and energy; (from Bøtter-Jensen, 1997).

4.2.1 Photomultiplier tube

The emitted luminescence is detected by a photomultiplier tube (PMT). The light sensitive component in the PMT is the cathode. This is coated with a photo-emissive substance; CsSb and other bialkali compounds are commonly used for this material. Typically, ten photons in the visible range striking the cathode are converted into one to three electrons. Electrons emitted from the photocathode are accelerated towards a series of dynodes maintained at a positive voltage relative to the photocathode. Electrons with sufficient velocity striking the dynode will eject several secondary electrons from the surface.

The standard PMT in the Risø TL/OSL luminescence reader is a bialkali EMI 9235QA PMT, which has maximum detection efficiency at approximately 400 nm, making it suitable for detection of luminescence from both quartz and feldspar (see emission spectra in Figure 4.3). Figure 4.2 displays the quantum efficiency (i.e. sensitivity) as a function of incident photon wavelength for EMI 9235QA. The response from an S-20 cathode PMT is also shown. The PMT is operated in "photon counting" mode, where each pulse of charge arising at the anode is counted. Many samples are only weakly luminescent making optimisation of light collection important. Thus, it is

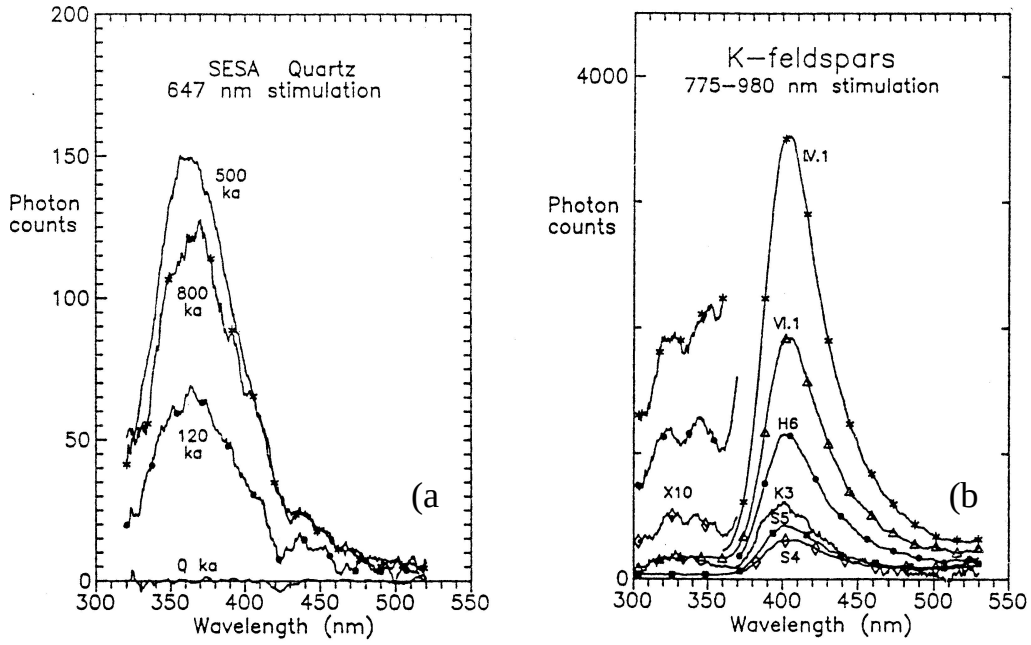

Figure 4.3: Emission spectra of sedimentary quartz and K feldspars (from Huntley et al., 1991). **a)** Emission spectra of several sedimentary quartz samples from South Australia obtained for stimulation using the 647 nm line from a Krypton laser. **b)** Emission spectra of several sedimentary K feldspars using IR diode stimulation.

critical that the distance between the PMT and the sample is as small as possible. As the stimulation sources have to be placed between the sample and the PMT the sample-to-PMT cathode distance in the Risø TL/OSL luminescence reader is 55 mm, giving a detection solid angle of approximately 0.4 steradians.

4.2.2 Detection filters

The intensity of the stimulation light is $\sim 10^{18}$ orders of magnitude larger than the emitted luminescence. In order to be able to measure the emitted luminescence, detection filters must be used to prevent scattered stimulation light from reaching the PMT, and the spectral stimulation and detection windows must be well separated. Quartz has a strong emission centred on 365 nm (near UV) and many types of feldspars have a strong emission centred on 410 nm (violet). In Figure 4.3 emission spectra from several samples of sedimentary quartz and K feldspars are shown. A commonly used detection filter is Hoya U-340 (see Figure 4.5), which has a peak transmission around 340 nm (FWHM = 80 nm).

4.3 Luminescence stimulation system

4.3.1 Heating system

The heating element and lift mechanism is located directly underneath the photomultiplier tube. The heating element has two functions: 1) it heats the sample and 2) it lifts the sample into the measurement position. The heater strip is made of Kanthal (a high resistance alloy) which is shaped with a depression to provide good heat transmission to the sample and to lift it securely and reproducibly into the measurement position. Heating is accomplished by feeding a controlled current through the heating element. Feedback control of the temperature employs an Alumel-Cromel thermocouple mounted underneath the heater strip. Heating is provided by a non-switching continuous full sine wave generator operating at 20 kHz. The heating system is able to heat samples to 700 °C at linear heating rates from 0.1 to 30 K/s. To minimise thermal lag between sample and heater strip heating rates above 5 K/s are usually not employed. The heating strip can be cooled by a nitrogen flow, which also protects the heating system from oxidation at high temperatures.

4.3.2 Optical stimulation system

In OSL, the probability of eviction depends on the rate at which photons arrive at the trap and the sensitivity of that particular trap to photoeviction. The sensitivity of the trap depends strongly on the wavelength of the stimulating light, generally the shorter the wavelength the greater the chance of eviction. However the wavelength of the stimulation light is not the only factor to take into consideration. The wavelength of the emitted luminescence must also be considered. The intensity of the emitted luminescence is many orders of magnitude smaller than the intensity of the stimulation light, so in order to effectively prevent stimulation light from reaching the PMT, the wavelengths of the stimulation light and the luminescence must be well separated or appropriate filters used. In the standard Risø TL/OSL luminescence reader (Bøtter-Jensen et al., 2000a) a choice of two stimulation sources exists: 1) infrared (IR) light emitting diodes (LEDs) and 2) blue LEDs (see Figure 4.4). LEDs are inexpensive, compact, have short response times and the illumination power density can be controlled electronically. The latter offers the possibility of stimulation at different intensities and varying the stimulation intensity as a function of stimulation time. The array of LEDs is equipped with an optical feedback servo-system to ensure the stability of the stimulation power. Stimulation in CW-mode as well as LM-mode is possible.

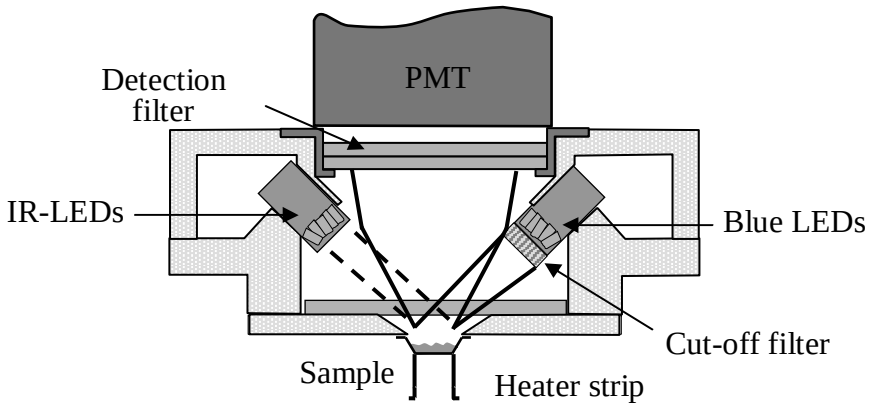

Figure 4.4: Schematic diagram of the combined blue and IR LED OSL unit. The unit contains 28 blue LEDs (in 4 clusters) emitting at 470 nm delivering ∼40 mW/cm^2 at the sample and 21 IR LEDs (in three clusters) emitting at 875 nm delivering ∼135 mW/cm^2 at the sample.

The LEDs are arranged in clusters, which are mounted concentrically in a ring-shaped holder located between the heater element and the photomultiplier tube. The holder is machined so that all individual diodes are focused at the sample. Each cluster contains seven LEDs and the ring-shaped holder can contain up to seven clusters (i.e. a total of 49 LEDs). The distance between the diodes and the sample is approximately 20 mm.

Infrared LEDs

Infrared (IR) stimulation in the region 800–900 nm can stimulate luminescence from most feldspars (but not from quartz at room temperature) probably by a thermal assistance mechanism (Hütt et al., 1988). This has the important advantage that a wider range of wavelengths for the detection window becomes available. The IR LEDs used here emit at 875 nm, which is close to the IR resonance wavelength at 870 nm found in most feldspars (Bøtter-Jensen et al., 2003). The IR LEDs are arranged in 3 clusters each containing seven individual LEDs. The maximum power from the 21 IR LEDs is approximately 135 mW/cm^2 at the sample position (Bøtter-Jensen et al., 2003).

Blue LEDs

The Risø reader is equipped with blue LEDs (NISHIA type NSPB-500s) with a peak emission at 470 nm (FWHM = 20 nm). They have an emission angle

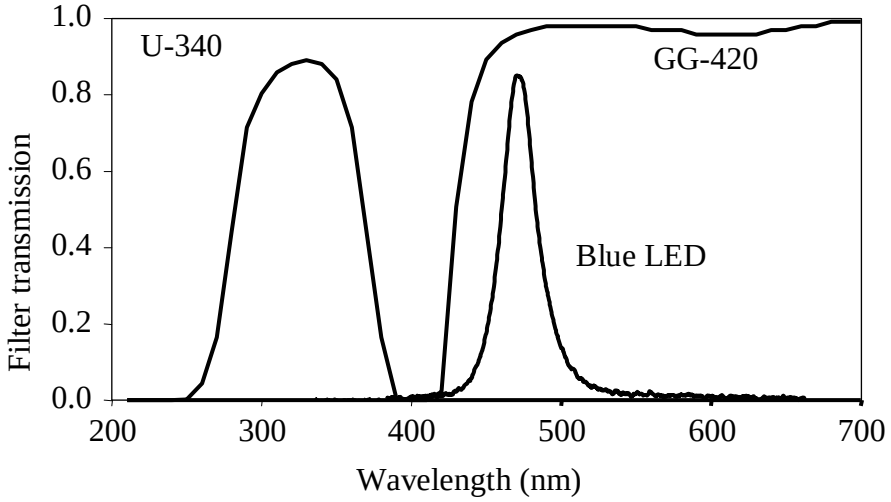

Figure 4.5: The emission spectrum of blue LEDs. Also shown are the transmission curves for the GG-420 green long pass filter (cut-off filter in front of the blue LEDs) and the Hoya U-340 filter (detection filter in front of the PMT); after Bøtter-Jensen et al. (1999b).

of 15 degrees and a power output of ∼2 cd at 20 mA (Bøtter-Jensen et al., 1999b). The energy fluence rate at a distance of 2 cm is 1.9 $\mathrm{mW/cm^2}$. The blue LEDs are usually arranged in 4 clusters each containing seven individual LEDs. The total power from 28 LEDs is > 40 $\mathrm{mW/cm^2}$ at the sample position (Bøtter-Jensen et al., 2003). The advantage of using the stimulation spectrum from the blue LEDs is that the OSL decay will be rapid because of the short wavelength, but the disadvantage is that the spectrum has a significant tail into the detection window (centred on 365 nm). To reduce the intensity of this tail, and thereby minimise the amount of directly scattered blue light reaching the light detection system, a green long pass filter (GG-420) is incorporated in front of each blue LED cluster. The filter effectively attenuates the high energy photons from the blue LEDs at the cost of approximately 5% attenuation of the peak centred on 470 nm. Figure 4.5 displays the measured LED emission spectrum compared with the published transmission curve for the GG-420 filter and the U-340 detection filter.

Cross-talk

On a 48-sample carousel the distance between the centres of adjacent sample positions is 17 mm. The consequence of this close spacing is that optical stimulation of one sample may affect adjacent samples. This phenomenon is referred to as optical cross-talk (or cross-bleaching). In the following the

optical cross-talk is expressed as a percentage of the equivalent stimulation time on the adjacent sample. Bray et al. (2002) measured the optical cross-talk using an array of blue LEDs delivering 18 $\mathrm{mW/cm^2}$ to the sample and estimated it to be 0.014%. Bøtter-Jensen et al. (2000a) measured the optical cross-talk on a similar instrument to be 0.006% using an array of blue LEDs delivering 28 $\mathrm{mW/cm^2}$ to the sample. Although this cross-talk can be significant in highly sensitive samples, the effects can usually be disregarded if care is taken with the measurement sequence design.

4.3.3 Blue LED reproducibility

In the determination of equivalent doses a given sample is repeatedly dosed and illuminated and the induced signals compared to each other (and the natural signal). Thus, it is important to investigate the reproducibly of the stimulation sources. The reproducibility of the blue LEDs was investigated by measuring the intensity of the light reflected from an aluminium disc. The PMT was used to detect the reflected light. The conventional detection filters in front of the PMT were removed and replaced by neutral density filters, which attenuated the reflected light by a factor of $\sim 10^7$. The blue LEDs were then switched on/off 100 times each for a period of 10 s. The measured signal was recorded in 260 consecutive time intervals of equal length known as channels, i.e. the length of one channel was ∼38 ms. The intensity of the reflected light at 90% power was ∼73,000 counts in each channel, giving an expected relative standard deviation of 0.37%. The blue LEDs were switched on in channel 6 and switched off again in channel 255 (i.e. the first 5 and last five channels were dead channels). In Figure 4.6a the data from the 25,000 measurements (performed at 90% power) of the intensity of the reflected light are presented as a histogram. The data have been normalised to the average intensity for convenience. The distribution is clearly normal and has an observed relative standard deviation of 0.47%. The difference between the observed standard deviation and that expected on the basis of Poisson statistics is ∼0.3% ($\sqrt{0.47^2 - 0.37^2}$). It is deduced that switching the LEDs on and off introduces a variability of $\sim 0.3\%$ in the stimulation power.

The same experiment was carried out at different power settings: 1, 10, 20 and 50% and the differences between the observed standard deviation and the expected are 0.7%, 0.2%, 0.1% and 0.1% respectively. Clearly, the light output is not as reproducible at 1% of full power. In Figure 4.6b the normalised intensity of the reflected light is plotted as a function of laser power for the first two channels (channel 6 and 7). At 1% power there is a significant delay before the LEDs reach the average intensity, i.e. at 1%

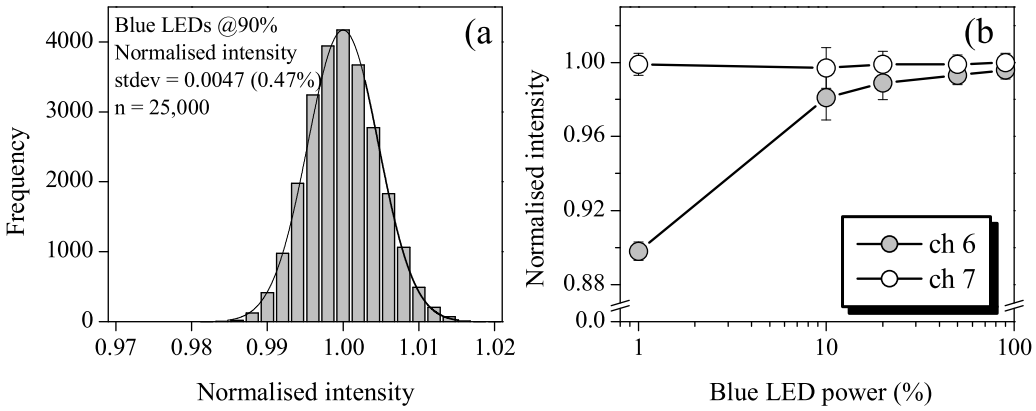

Figure 4.6: Reproducibility of the blue LEDs. **a)** A frequency histogram of the normalised intensity from 25,000 measurements performed at 90% power. **b)** Normalised intensity as a function of the predefined blue LED power level shown for the first two data channels (filled symbols: channel 6; unfilled symbols: channel 7). The values in the first channel are consistently lower than unity, due to the effect of a small rise time. The resolution of this experiment is too poor to determine the average rise time accurately, but it is certainly less than 40 ms.

power the intensity is 0.898 ± 0.005 (the uncertainty is the observed standard deviation) in channel 6. However, the corresponding value in channel 7 is 0.999 ± 0.006, which is consistent with unity. There is clearly a significant *rise time* at 1% power of ≤ 40 ms. If the data points from channel 6 are removed, the difference between the observed standard deviation and the expected standard deviation is reduced from 0.7% to 0.4%, which is comparable to the values found for other power settings.

4.4 Beta irradiator

A detachable beta irradiator is located above the sample carousel and a schematic drawing of the irradiator unit is shown in Figure 4.7. The irradiator normally accommodates a $^{90}Sr/^{90}Y$ beta source, which emits beta particles with a maximum energy of 2.27 MeV. The source strength is usually about 40 mCi, which gives a dose rate in quartz at the sample position of approximately 0.1 Gy/s. The source is mounted into a rotating, stainless steel wheel, which is pneumatically activated; it takes the source 0.11 s to rotate from the closed position to the open position (Markey et al., 1997). This off-set time is constant for all irradiations and is negligible for long radiations. In brief irradiations it can be compensated for by subtracting it from the programmed irradiation time. The source-to-sample distance should be as small

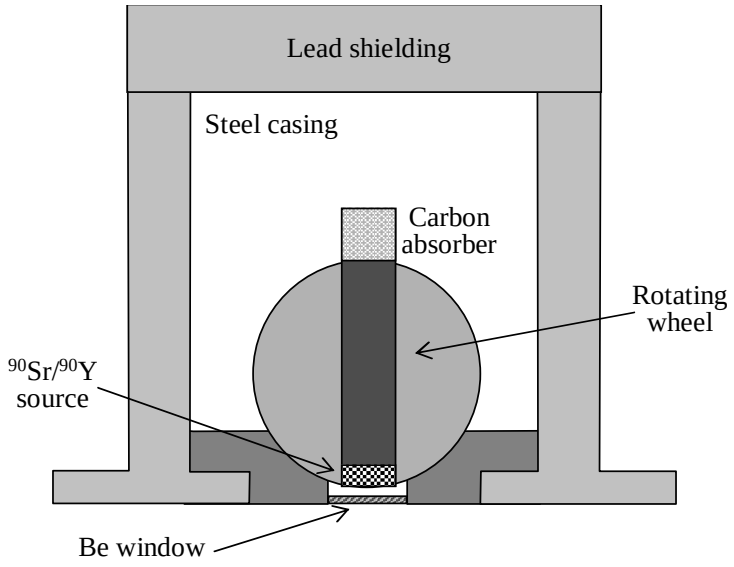

Figure 4.7: Schematic diagram of the cross section of the beta irradiator. The ^{90}Sr/^{90}Y source is placed in a rotating stainless steel wheel, which is pneumatically activated. The source is shown in the *on* (irradiating) position. When the source is *off* the wheel is rotated 180 °, so that the source points directly at the carbon absorber.

as possible to provide the highest possible dose rate at the sample, however any spatial variations in dose rate across the source will be accentuated at small source-to-sample distances, so a compromise is required. The distance between the source and the sample is 5 mm. A 0.125 mm beryllium window is located between the irradiator and the measurement chamber to act as vacuum interface for the measurement chamber.

On a 48 sample carousel the distance between the centres of adjacent sample positions is 17 mm. The consequence of this close spacing is that irradiation of one sample will lead to a dose being absorbed in the adjacent samples. This phenomenon is referred to as irradiation cross-talk. Markey et al. (1997) measured the cross-talk to be 60 μGy/Gy for adjacent samples and 6 μGy/Gy for second nearest neighbours.

4.5 Single grain laser OSL system

This thesis makes considerable use of OSL signals from single grains of quartz. One way of performing such measurements is by hand picking individual grains and mounting them individually, each on a separate sample disc. The

measurement protocol (see section 3.6.3) requires a number of repeated irradiations, heat treatments and light stimulations to be made on each aliquot. In irradiations the sample is exposed to the calibrated beta source. The beta irradiator attached to the conventional Risø TL/OSL luminescence reader is designed to irradiate the entire sample area (9.7 mm diameter), i.e. the irradiation time is the same irrespective of the number of grains present in each aliquot. Depending on the samples, the irradiation time usually dominates the total measurement time. Also, the sample has to be heated to temperatures between 160 and 300 °C prior to OSL read out several times. Again, this will take the same length of time irrespective of the number of grains in the aliquot. The stimulation sources are optimised to illuminate the entire sample area evenly. Less than 0.1% of the optical stimulation energy is made use of if the sample size is reduced to a single sand-sized grain (Duller et al., 1999). The maximum capacity of the conventional Risø reader is 48 samples. In most samples, the OSL signal intensity varies considerably from grain to grain. The proportion of grains giving a detectable luminescence signal is sample dependent, but in most samples, a significant proportion of grains will not give any luminescence signal in response to a laboratory dose. In an unheated mortar sample (Jain et al., 2003b) less than 0.3% of all the grains gave detectable luminescence signals. Thus, measuring individual grains using the standard Risø TL/OSL luminescence reader is a very inefficient use of instrument time. With this in mind Duller et al. (1999) developed a single grain OSL unit attachable to the Risø TL/OSL reader.

The Risø single grain OSL attachment enables routine measurements of sand-sized single grains. The sample is loaded into special aluminium discs, each containing 100 grains in holes of known position on the disc surface. Irradiation and heating can thus be performed simultaneously on all 100 grains, whereas the OSL signal can be measured separately from individual grains by using a focused laser (beam diameter on the sample disc is $< 20\,\mu$m). This laser spot is steered to each of the grain holes in turn and switched on. The focused laser enables a high energy fluence rate and reduces the risk of optical cross-talk by ensuring that the entire spot enters the $300\,\mu$m diameter hole. Only a small part of the grain will be stimulated directly by the laser beam, but internal reflection within the grain hole is assumed to provide a uniform illumination of the grain. The OSL is detected by an EMI 9635QA photomultiplier tube that is shielded from the stimulation light by 4 mm of Hoya U-340 filter. A schematic diagram of the single grain OSL attachment is shown in Figure 4.8.

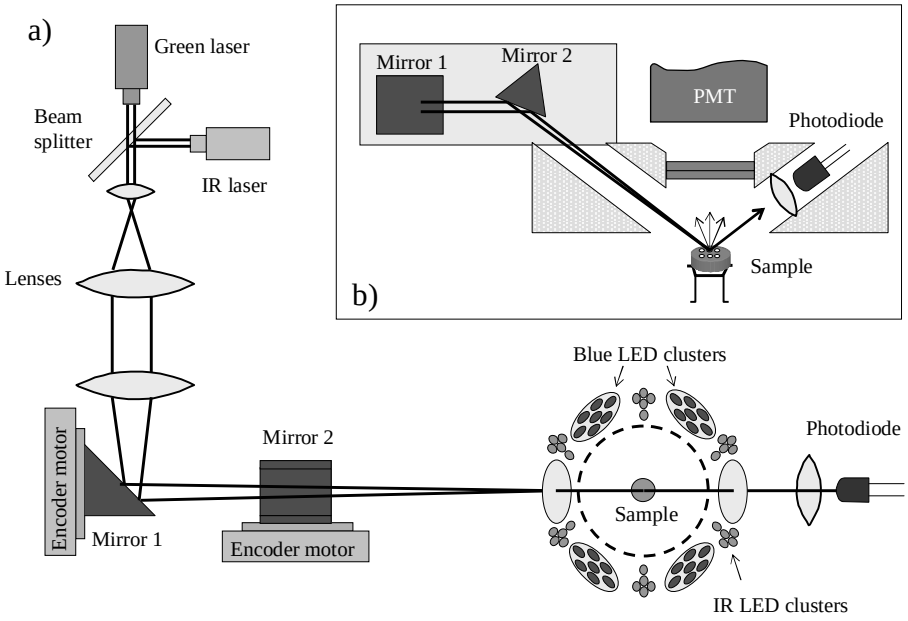

Figure 4.8: Schematic diagram of the single grain OSL attachment (redrawn from Bøtter-Jensen et al., 2000a). Optical stimulation is achieved using a laser beam focused by three lenses. The position of the laser spot on the sample is controlled by moving the two mirrors. **a)** Single grain OSL attachment seen from above. **b)** Cross-section of the single grain OSL attachment

4.5.1 Laser beam

At present two different stimulation sources are available for single grain measurements. One is a 10 mW $Nd:YVO_4$ solid state diode-pumped laser emitting at 532 nm focused to a spot < 20 μm. The maximum energy fluence rate at the sample is estimated to be $50\,W/cm^2$ (Duller et al., 1999). The second is a 150 mW 830 nm IR laser positioned perpendicular to the green laser beam. A beam splitter enables the use of the same optics to focus the IR laser beam onto the sample disc as used for the green laser. The maximum energy fluence rate of the IR laser is estimated to be $500\,W/cm^2$ (Bøtter-Jensen et al., 2003). The power of the laser beams can be electronically controlled to vary between zero and full power, thus enabling linearly modulated OSL measurements on single grains.

Three lenses are used to focus the laser beam, which is approximately Gaussian, with 90% of the power contained within a spot of $< 20\mu$m on the sample disc. The laser spot is steered by two orthogonal mirrors and can be positioned arbitrarily on the sample disc. The mirrors are moved by

two motor driven stages equipped with position encoders. The mirror in the x-direction is placed at an angle of 45 ° to the direction of the laser and the y-mirror at an angle of 22.5 ° to obtain an angle of incidence on the sample disc of 45 °. Ideally the angle of incidence on the sample should be 90 ° to reduce the possibility of scattered light affecting the adjacent grain, but that would greatly increase the distance between the sample and the photomultiplier tube and so decrease the light collection efficiency. Thus, the angle of incidence of 45 ° is a compromise between minimising optical cross-talk and optimising detection efficiency.

4.5.2 Laser reproducibility

A key element in determining the overall reproducibility of the single grain system is the reproducibility of the stimulation light source. In this section the following aspects of the reproducibility of the green laser will be discussed: linearity, shape variations, rise time, and absolute intensity variations.

The reproducibility of the laser was measured using the PMT as the detector, by replacing the detection filters with neutral density filters (see section 4.3.3). The laser was then repeatedly switched on for a period of 0.83 s and the light reflected from an aluminium disc measured. Ideally, the laser beam should hit the same spot on the sample disc every time it is switched on to avoid problems with differences in reflectivity from different parts of the disc. Although, in these experiments, the system moved the laser between the different illuminations the standard deviation of the laser positioning was determined to be $< 1\,\mu$m (see section 4.5.5 on p. 65). The total measurement time in these reproducibility experiments was 1 s and the data was collected in 60 channels (i.e. 1 channel corresponds to approximately 30 ms). The first five and the last five channels collected dark counts, i.e. the laser was not switched on. Most of the single grain data presented in this thesis have been measured using these settings. Ideally, the normalised intensity ought to be zero in the first 5 channels, 1 in channel 6–55 and zero again in channel 56–60.

Laser linearity

The power of the laser beam can be varied electronically between $\sim 3\%$ and 100% (the laser does not *switch on* until the power level exceeds $\sim 3\%$). The linearity of the laser has been tested by measuring the intensity of the reflected light for different power levels ranging from 10 to 90%. At 90% power the number of counts recorded in each channel was approximately 25,000, which gives a predicted relative uncertainty of $\sim$0.6% in each channel. In Figure 4.9 the average measured signal from 100 stimulations (averaged from

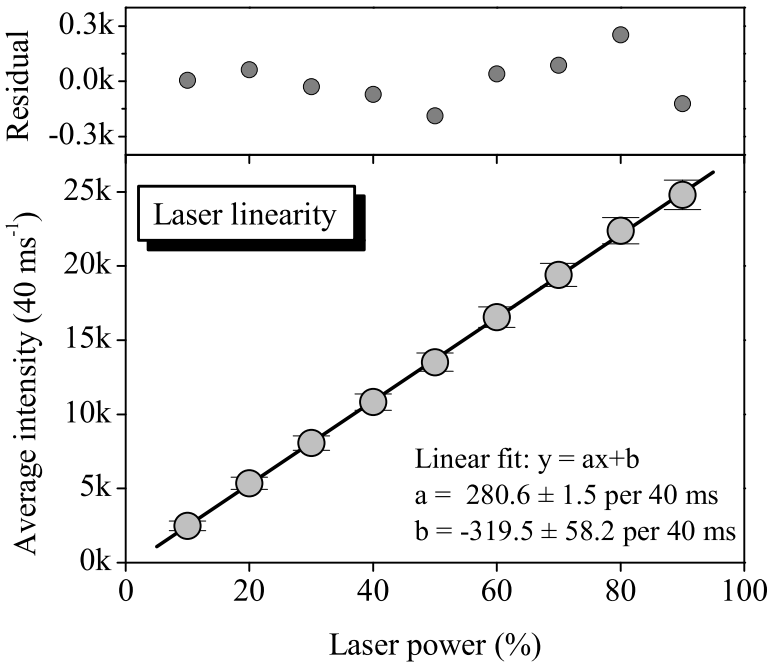

Figure 4.9: Linearity of the green laser. The average intensity of the light measured in channel 6 to 55 from 100 stimulations. The upper graph shows the differences (residuals) between the data and the fitted values.

channel 6 to 55) are plotted against the predefined power level in percent. The uncertainties on the data points are the observed standard deviations. Also shown is a linear fit to the data, which shows that the response of the laser can satisfactorily be described by a straight line.

Laser power shape variations

In Figure 4.10a the normalised average light intensity from 100 stimulations are plotted against channel number (laser power 90%). The laser was switched on in channel 6 and switched off again in channel 55. The data from each stimulation have been normalised to the average count (channel 7-55) measured in the given illumination to eliminate differences in absolute intensity between different illuminations. This allows that variations in the shape of the laser power output can be investigated. The inset is an enlargement of Figure 4.10. Also shown in the inset are the individual data points (unfilled symbols). There is a clear systematic trend in the laser power; the average power does not remain constant throughout the ∼83 ms of stimulation. Initially the laser 'overshoots' the average value by 0.5% and the intensity falls

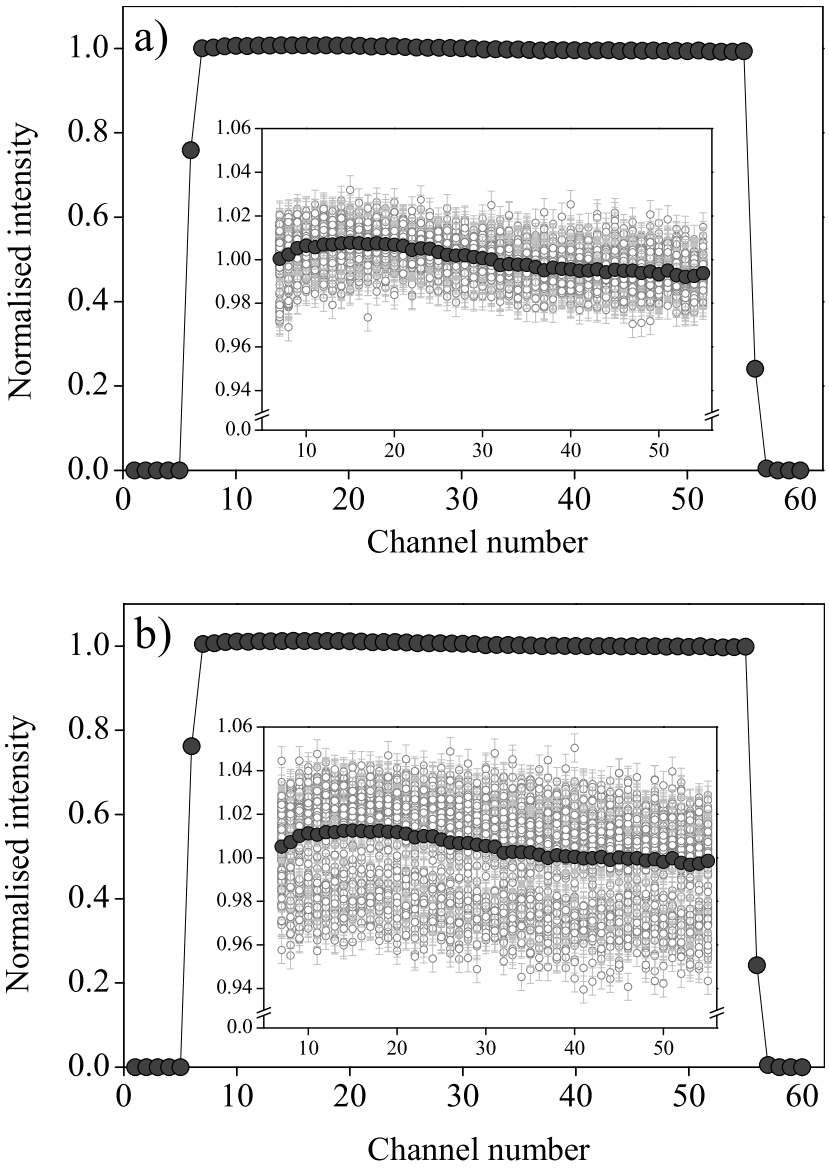

Figure 4.10: Reproducibility of the green laser. The average normalised light intensity as a function channel number. **a)** The data have been normalised to the average intensity of each stimulation (channel 7–55). **b)** The data have been normalised to the average intensity of all measurements (channel 7–55).

to a value of 0.995 at the end of the stimulation period. This systematic effect is assumed to be due to the response of the laser to the feedback control circuit. The relative standard deviation of the individual channels range between 0.64 and 1.25% with an average value of $0.79 \pm 0.08\%$ (the average value σ_{av} is calculated by averaging the variances and the uncertainty is calculated by $\sigma_{av}/\sqrt{2(n-1)}$). From counting statistics the relative standard deviation is expected to be 0.63%. The reproducibility of the laser in any one channel is then calculated as the difference between the observed and the expected standard deviation, which is 0.48% ($\sqrt{0.79^2 - 0.63^2}$). Thus, from one stimulation to another the shape of the intensity curve is constant within an envelope with a standard deviation of $\sim 0.5\%$.

Laser rise time

Ideally, the normalised value in channel 6 in Figure 4.10a should be unity. However, the value is significantly lower than one, implying that the laser has a rise time, i.e. it takes the laser a certain period of time to reach some predefined power, defined here to be the time it takes the laser to reach 50% of the final value. The normalised signal in channel 6 is 0.759 ± 0.007 (0.9%) and in channel 7 it is 1.00 ± 0.01 (1%), where the uncertainties are the standard deviations of the 100 measurements in each channel. This implies that the laser rise time is ≤ 17 ms. The expected relative standard deviation from counting statistics is $\sim 0.6\%$ and the observed relative standard deviation is 0.9%, thus giving a reproducibility of $\sim 0.7\%$, which is slightly higher than the average reproducibility of the laser in the remaining channels. In Figure 4.11 the average normalised light intensity is plotted as a function of channel number for different power settings, and it can be seen that the rise time is longer for a lower power setting. The resolution in these experiments is too poor to determine the rise times precisely, but it is possible to deduce approximate rise times (see Table 4.1).

Laser power (%)	5	10	20	30	40	50	60-90
Approximate rise time (ms)	43	24	17	14	12	12	11

Table 4.1: Approximate laser rise time.

The inset in Figure 4.11 shows the average normalised intensity plotted against laser power in % for channel 6 and 7. The rise time will influence the measured intensity for all power levels in the first channel (channel 6), but the second channel (channel 7) will be unaffected if the predefined power level exceeds 20%.

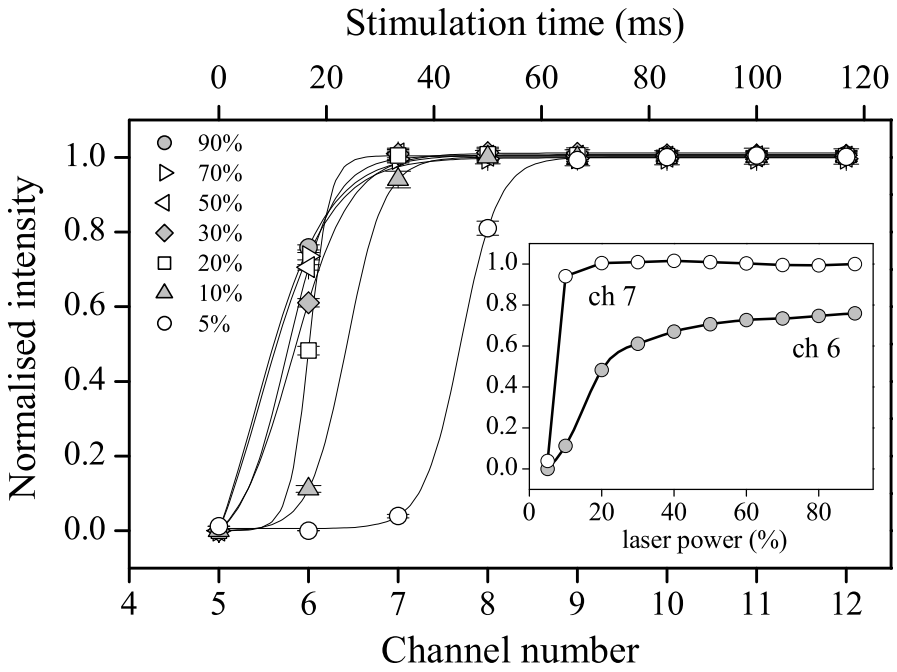

Figure 4.11: Laser rise time. The normalised intensity plotted as a function of channel number and stimulation time. The rise time is increased for decreased power levels. The inset shows the normalised intensity as a function of laser power for channel 6 (filled symbols) and channel 7 (unfilled symbols).

Absolute intensity variations

In the preceding section, measurements from one stimulation were normalised to the average intensity measured in that stimulation to eliminate any scatter in the data caused by absolute variations in intensity (i.e. one stimulation might give an average intensity of 23,000 counts/channel whereas another might give an average of 25,000 counts/channel). In this section the data have been normalised to the average intensity of all measurements in channel 7 to 55 and plotted in Figure 4.10b as a function of channel number. The variation in the shape of the output power is still visible, but the standard deviation of the intensity in each channel has increased; it now lies in the range between 1.8 and 2.2% with an average value of $2.1 \pm 0.2\%$. The expected relative standard deviation is still 0.63%, giving a reproducibility of $\sim$2% (including the variance arising from shape variations as well as differences in absolute intensity from one illumination to another). Thus, the total laser power will fluctuate with a relative standard deviation of 2%.

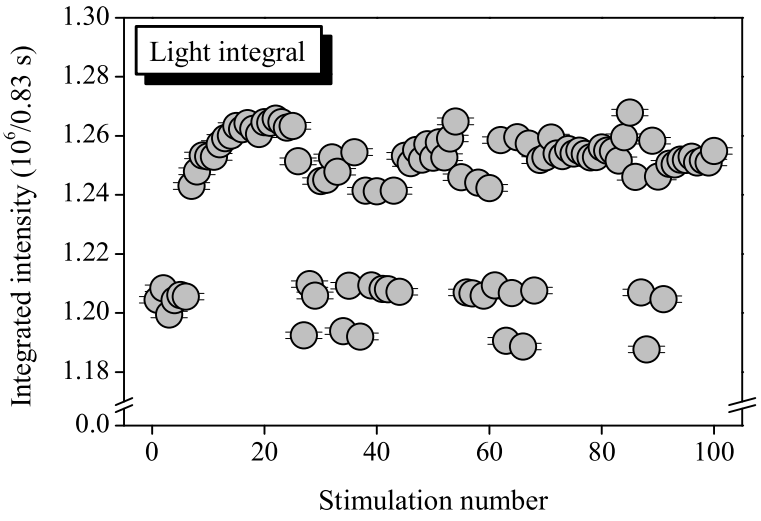

Figure 4.12: Integrated laser intensity. The laser was switched on 100 times and the light reflected from an aluminium disc measured. The integrated light intensity (channel 6–55) is plotted as a function of stimulation number.

In OSL measurements, the emitted light is integrated over some range of channels (usually, the first few channels). Thus, in OSL we are mostly interested in the changes in the total (integrated) power output between different stimulations.

In Figure 4.12 the integrated intensity of the entire stimulation period (channel 6-55) is shown as a function of stimulation number. The variation in integrated intensity is random with respect to stimulation number, but it is interesting that the absolute integrated intensity seems to be varying between two levels; one at $\sim 1.25 \cdot 10^6$ counts/0.83 s and the other at $\sim 1.20 \cdot 10^6$. Currently, this behaviour can not be explained. The variability caused by variations in absolute power has a relative standard deviation of 1.9%

4.5.3 Single grain sample discs

The aluminium sample discs designed for mounting single grains are 1 mm thick and have a diameter of 9.7 mm (i.e. same surface area as the conventional sample discs). The individual grains are placed in 100 holes drilled into the surface of the sample disc. These holes are $300\,\mu$m deep by $300\,\mu$m in diameter and drilled on a 10 by 10 grid with $600\,\mu$m spacing between centres (see Figure 4.13). The 100 sample holes are drilled using a CAD/CAM controlled computerised numerical control system type DMU 50V from DMG,

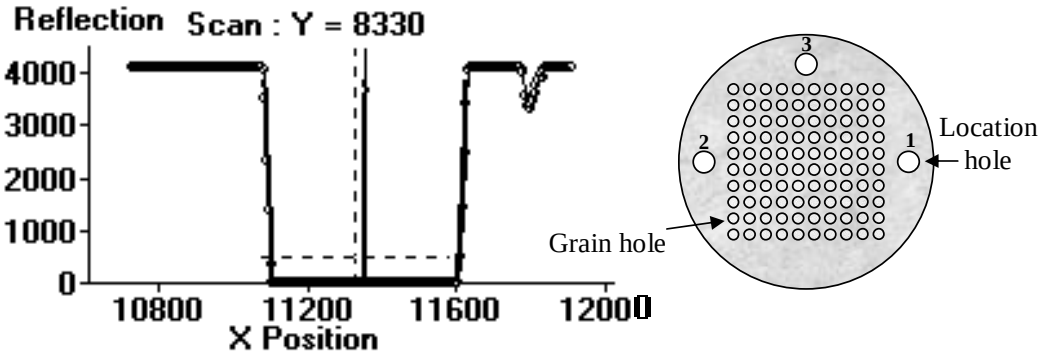

Figure 4.13: Example of a location hole scan. The change in reflectivity as the laser passes over the location hole is clearly seen. The diameter of the location hole is $500\,\mu$m as expected. Also shown is a schematic drawing of a single grain disc.

Germany, which has an accuracy of $1-2\,\mu$m. The holes are drilled automatically one at a time using hardened drills. At the same time three further holes are drilled at the periphery of the disc. These holes (called location holes) have a diameter of $500\,\mu$m and are drilled all the way through the disc. The relative positions between the location holes and the grain holes are well-known, but the relative distance between the holes and the circumference of the disc may vary slightly from disc to disc. The purpose of the location holes is to form a basis for the calculation of the positions of the individual grain holes.

4.5.4 Disc location

Manual positioning of the sample discs on the sample carousel can not be precise on a $10--100\,\mu$m scale. Furthermore, every time the sample is lifted into the measurement position some uncertainty in the position of the sample disc relative to the laser system will be introduced. Thus, it is necessary to determine the exact location of the sample disc relative to the laser system on each occasion before any measurements are carried out. The three location holes at the periphery of the disc are used for this purpose. The position of the location holes are determined by scanning the laser beam at reduced power ($\sim 4\%$) across the periphery of the disc. The power is reduced during the location hole scans to minimise the amount of scattered light that might reach grain holes adjacent to the location holes. A photo-diode in the measurement chamber is positioned in such a way that it will be struck by laser light reflected from the surface of the sample disc. When the laser beam passes over a location hole the intensity of the reflected light decreases significantly.

Figure 4.13 shows an example of the measured reflection during a location scan. Scanning is performed in both X and Y directions and these measurements form the basis for the calculation of the centre of the location hole. This process is repeated for the three locating holes. Originally, only two location holes were used, but it proved advantageous to introduce the third location hole in order to be able to account for all the degrees of freedom in the system. The following section contains a short mathematical description of the calculations carried out before OSL measurements are initiated. The calculations were undertaken as part of this thesis when it became clear that there was a fault in the original algorithm, which resulted in systematic errors in location. They have now been incorporated into the control software.

The centres of the location holes are located at a distance r ($4000\,\mu$m) from the centre of the disc. If θ is the angle of rotation, then the coordinates of the location hole centres are given by (see Figure 4.14a):

$$\begin{aligned}(x_1, y_1) &= (0, 0)\\ (x_2, y_2) &= (-2r\sin\theta, 2r\cos\theta)\\ (x_3, y_3) &= (\sqrt{2}r\cos(\theta+\pi/4), \sqrt{2}r\sin(\theta+\pi/4))\end{aligned}$$

when the centre of Hole 1, Hole 2 and Hole 3 are given as $(x_1, y_1), (x_2, y_2)$ and (x_3, y_3) respectively.

However, the disc might not lie exactly in the xy-plane of the mirrors (e.g. the plane of the heater plate is at angle to the xy-plane). This can be compensated by introducing two linear distortion factors l and m, where l is the distortion in the x-direction and m is in the y-direction. The coordinates are then given by:

$$\begin{aligned}(x_1, y_1) &= (0, 0)\\ (x_2, y_2) &= (-2rl\sin\theta, 2rm\cos\theta)\\ (x_3, y_3) &= (\sqrt{2}rl\cos(\theta+\pi/4), \sqrt{2}rm\sin(\theta+\pi/4))\end{aligned}$$

The two mirrors steering the laser are placed as close as possible at right angles to each other. If they are not exactly at right angles (i.e. the coordinate system is not strictly Cartesian) an angular distortion φ is introduced into the system (see Figure 4.14b). This can be compensated for, so that $(x', y') = (x - y\tan\varphi, y/\cos\varphi)$ Finally, the origin of the laser coordinate system is not necessarily located in the centre of hole 1. Thus, the system must be translated (see Figure 4.14c). The correlation between the measured centres

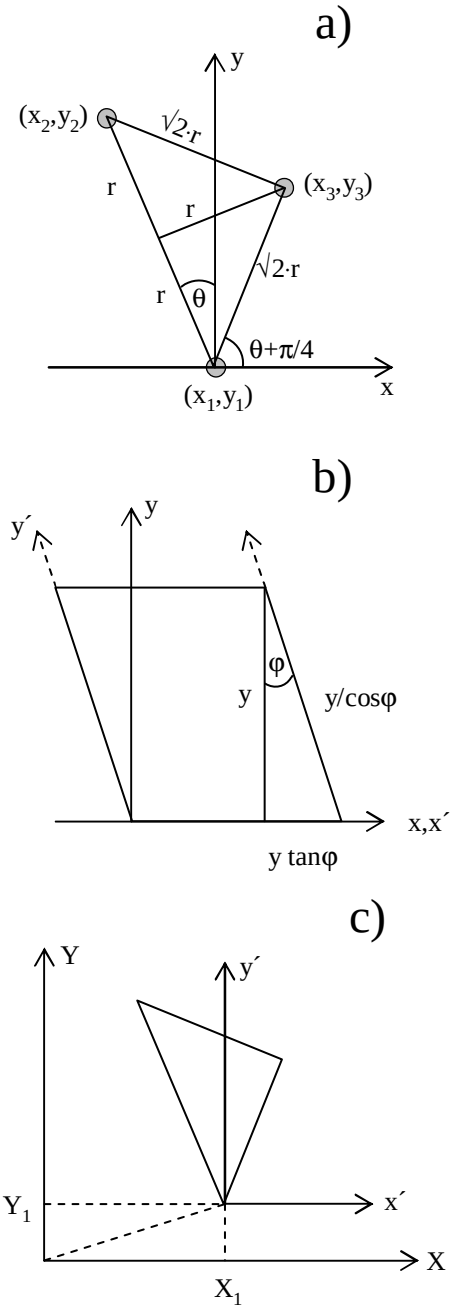

Figure 4.14: Diagram showing the parameters used in the calculations of the grain hole positions. **a)** Perfect geometry. **b)** Diagonal distortion. **c)** Translation.

(X, Y) of the location holes and the centres in the (x', y') system is given by $(X, Y) = (x' + X, y' + Y)$. Thus

$$
\begin{aligned}
(X_1, Y_1) &= (x'_1, y'_1) \\
(X_2, Y_2) &= (2r(m\cos\theta\tan\varphi - l\sin\theta) + X_1, 2rm\cos\theta/\cos\varphi + Y_1) \\
(X_3, X_3) &= (r(m(\sin\theta + \cos\theta)\tan\varphi + l(\cos\theta - \sin\theta)), rm(\sin\theta + \cos\theta)/\cos\varphi)
\end{aligned}
$$

These equations can be simplified by introducing four entities A, B, C and D:

$$A = \frac{X_2 - X_1}{2r} = m\cos\theta\tan\varphi - l\sin\theta \tag{4.1}$$

$$B = \frac{Y_2 - Y_1}{2r} = m\frac{\cos\theta}{\cos\varphi} \tag{4.2}$$

$$C = \frac{X_3 - X_1}{r} = l\,(\cos\theta - \sin\theta) + m\,(\sin\theta + \cos\theta)\tan\varphi \tag{4.3}$$

$$D = \frac{Y_3 - Y_1}{r} = m\frac{\sin\theta + \cos\theta}{\cos\varphi} \tag{4.4}$$

We are now left with four equations with four unknowns (θ, φ, m and l), which easily can be solved to yield:

$$\theta = \arctan\left(\frac{D}{B} - 1\right) \tag{4.5}$$

$$\varphi = \arcsin\left(\frac{CD - BC - AD + 2AB}{2B^2 + D^2 - 2BD}\right) \tag{4.6}$$

$$m = B\,\frac{\cos\varphi}{\cos\theta} \tag{4.7}$$

$$l = \frac{B^2\sin\varphi - AB}{\cos\theta\,(D - B)} \tag{4.8}$$

From these equations it is possible to calculate the position of individual grain holes by using the known geometrical relationship between the positions of the location holes and the grid of grain holes.

The three correction factors l, m and φ are machine dependent – particularly φ. Typically, the two linear distortion factors l and m are usually a few percent less than 1 (e.g. 0.98). The value of the diagonal distortion factor φ is typically $-0.5\,^\circ$, but has in one case been observed to be $-2.5\,^\circ$.

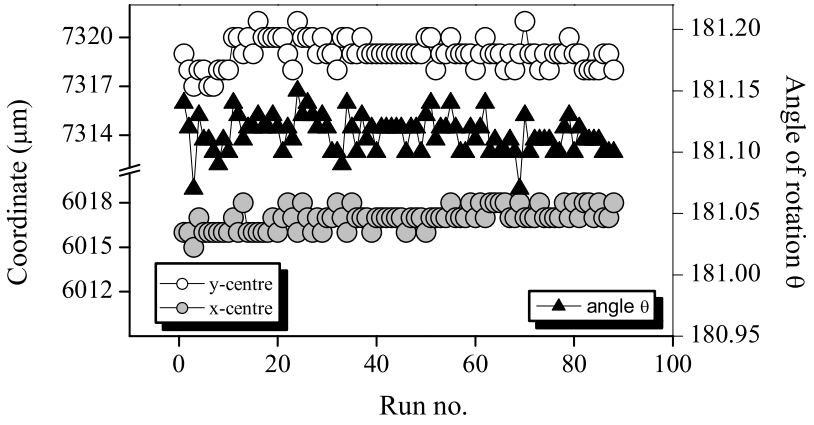

Figure 4.15: Precision of the disc location routine using the single grain attachment. The calculated positions of centre of a disc as a function of cycle number (left axis). The calculated angle of rotation as a function of run number (right axis).

4.5.5 System reproducibility

Precision of the location routine

Before an OSL measurement is undertaken the system must find the three location holes. If all three holes are located successfully, the software then calculates the positions of each of the 100 grain holes based on the known geometry between the location holes and the grain positions. Thus, it is very important to determine how well the system is able to determine the position of a sample disc. In order to determine how reproducibly the system is able to locate a disc (i.e. to successfully scan the three location holes), a disc was located 88 times. Because every time the disc is lifted into the measurement position or put back on the sample carousel it may rotate slightly or move laterally, the 88 different location routines were performed without lowering the lift. In Figure 4.15 the measured angle of rotation and the calculated values of the centre position of the disc are plotted as a function of run number. Ideally, each location routine should result in the same angle of rotation and value for the disc's centre position. The average angle of rotation is $181.11\,^\circ$ with a standard deviation of $0.01\,^\circ$. The average calculated value of the centre position is $6017\,\mu$m and $7317\,\mu$m for the x- and y-direction respectively. The standard deviations of the calculated x- and y-values are $0.7\,\mu$m ($\sim 0.012\%$) and $0.9\,\mu$m ($\sim 0.012\%$). These figures translate into a maximum error at the locating holes of $2.2\,\mu$m (3σ, x-direction) and $2.6\,\mu$m (3σ, y-direction).

Accuracy of the location routine

The system can be set up to determine the position of the individual grain holes by scanning the laser beam across the surface of the disc, while measuring the intensity of the reflected laser light (analogous to the procedure used in the location routine). The difference between the calculated and the measured position of a given grain hole can thus be compared. However, the individual grain holes are drilled one at a time and therefore might be slightly off-set with respect to each other. In order to determine the accuracy of the software calculations, the grain holes were defined to coincide with the location holes themselves. After successful location of a disc, the system predicted the position of the three "grain holes" (in this case identical to the location holes). If the software is able to calculate these positions accurately, they should be identical to the measured positions of the three location holes. This was tested using 20 different discs placed at different angles of rotation. The differences between the measured and calculated positions ranged between -1 and $2\,\mu$m and the average difference was $0.2\,\mu$m with a standard deviation of $0.7\,\mu$m ($n = 120$). Rounding errors in the computer calculations are assumed to be responsible for the small difference between the measured and calculated values. No systematic dependence on angle of rotation was observed.
For one disc the grain search routine was performed 51 times. The relative standard deviations of the determined positions for all three location holes were 0.01% (comparable to the precision determined in the location routine, section 4.5.5) and the average difference between the calculated and the measured position was -0.16μm with a standard deviation of $0.06\,\mu$m ($n = 306$). Thus, it is concluded that the system is able to determine the position of a disc both precisely and accurately.

Locating individual grain holes

In the preceding sections it has been shown that the single grain OSL system is able to determine the position of a disc very reproducibly. In this section the ability of the system to steer the laser spot to the centre of individual grain holes is examined. The location routine was performed on an empty disc (i.e. not loaded with grains) and the grain hole search was then initiated (without lowering the lift) and repeated 2,500 times (i.e. 25 times on each of the 100 grain holes). The individual position of each of the 100 grain holes was defined to lie as specified in section 4.5.3. In this test the average off-set (between predicted and measured hole centres) on the x-axis was $2.7\,\mu$m (standard deviation was $6.5\,\mu$m) and on the y-axis $14.1\,\mu$m (standard de-

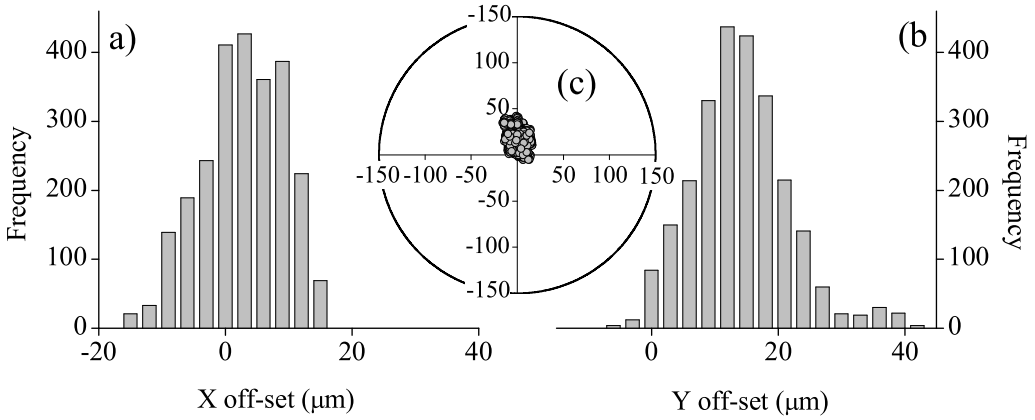

Figure 4.16: Accuracy and precision of the location routine in locating individual grain holes. The grain hole search routine was repeated 2,500 times. **a)** Frequency histogram of the off-set on the x-axis. **b)** Frequency histogram of the off-set on the y-axis. **c)** The off-sets on the y-axis as a function of the corresponding off-sets on the x-axis. The circle represents the dimensions of a grain hole.

viation was 7.6 μm). The results are shown in Figure 4.16. The important conclusion to draw from this test is that the 20 μm laser spot would have entirely entered each 300 μm grain hole even in the worst case. Given the accuracy and precision found when relocating the three location holes (previous section) it is presumed that most of the variability seen above is in the manufacturing of the disc.

4.5.6 Reproducibility of an OSL measurement

In single-aliquot dose evaluation procedures is it essential to perform reproducible measurements of the luminescence from a single grain. To test the reproducibility of the single grain system a disc was loaded with 100 quartz grains. The grains had previously been heated to 850 °C to completely empty any prior trapped charge and to sensitise them to ensure that measurement of the instrument reproducibility was not limited by poor counting statistics. The grains were repeatedly dosed (15 Gy), preheated (260 °C, 10 s) and stimulated with the green laser for 0.83 s at 90% power. This measurement cycle was repeated 15 times. In Figure 4.17 the integrated OSL signal from the first 0.03 s of stimulation is plotted against the measurement cycle number for a representative selection of grains. Most grains show a change in OSL response as a function of cycle number. To remove any systematic effects (originating from the phosphor itself), the data are fitted with a straight line and to pro-

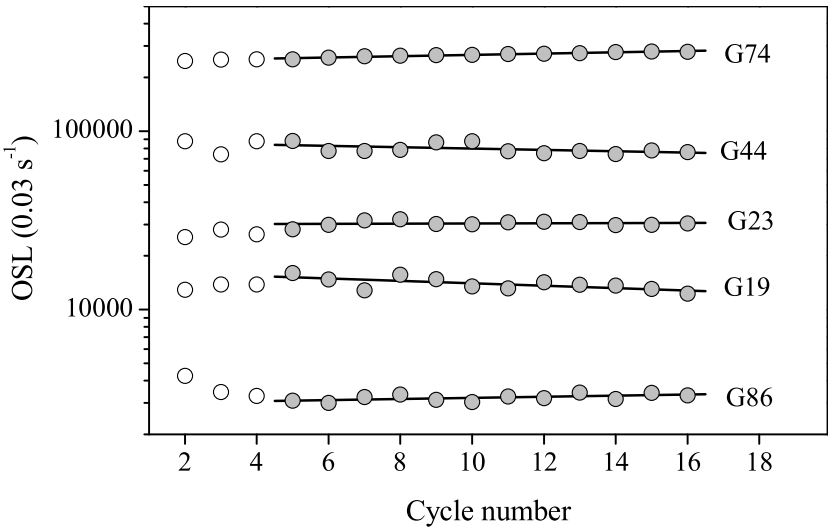

Figure 4.17: A zeroed quartz sample was dosed, preheated and stimulated with the green laser 15 times in total. The integrated OSL signal from the first 0.03 s of stimulation is plotted as a function of run number for a representative selection of grains (grain 19, 23, 44, 74 and 86). Note the logarithmic scale. Assessment of the instrument reproducibility by means of a linear fit to all the data points (filled and unfilled symbols) gives a value of ∼2%. If the first three points are omitted from the calculations a value of ∼ 1% is obtained. See text for details.

vide a measure of the instrument reproducibility σ_{inst} the relative deviations from the fitted line (m_2) are compared with the deviations expected from counting statistics (m_1).

$$\left.\begin{aligned} m_1 &= \sqrt{\frac{\sum_{i=1}^{n}\left(\frac{s_i}{N_i}\right)^2}{n}} \\ m_2 &= \sqrt{\frac{\sum_{i=1}^{n}\left(\frac{\Delta_i}{F_i}\right)^2}{n}} \end{aligned}\right\} \rightarrow \sigma_{inst} = \sqrt{m_2^2 - m_1^2} = \sqrt{\frac{\sum_{i=1}^{n}\left(\left(\frac{\Delta_i}{F_i}\right)^2 - \left(\frac{s_i}{N_i}\right)^2\right)}{n}} \tag{4.9}$$

where N is the integrated OSL count, s is the standard deviation of N, F is the fitted value, Δ is the difference between the integrated OSL count and the fitted value and n is the total number of measurements.

The results from these calculations are shown in Figure 4.18. Negative values of σ_{inst} are obtained when the deviation expected from counting statistics is larger than the observed deviation. In those cases the individual estimates of

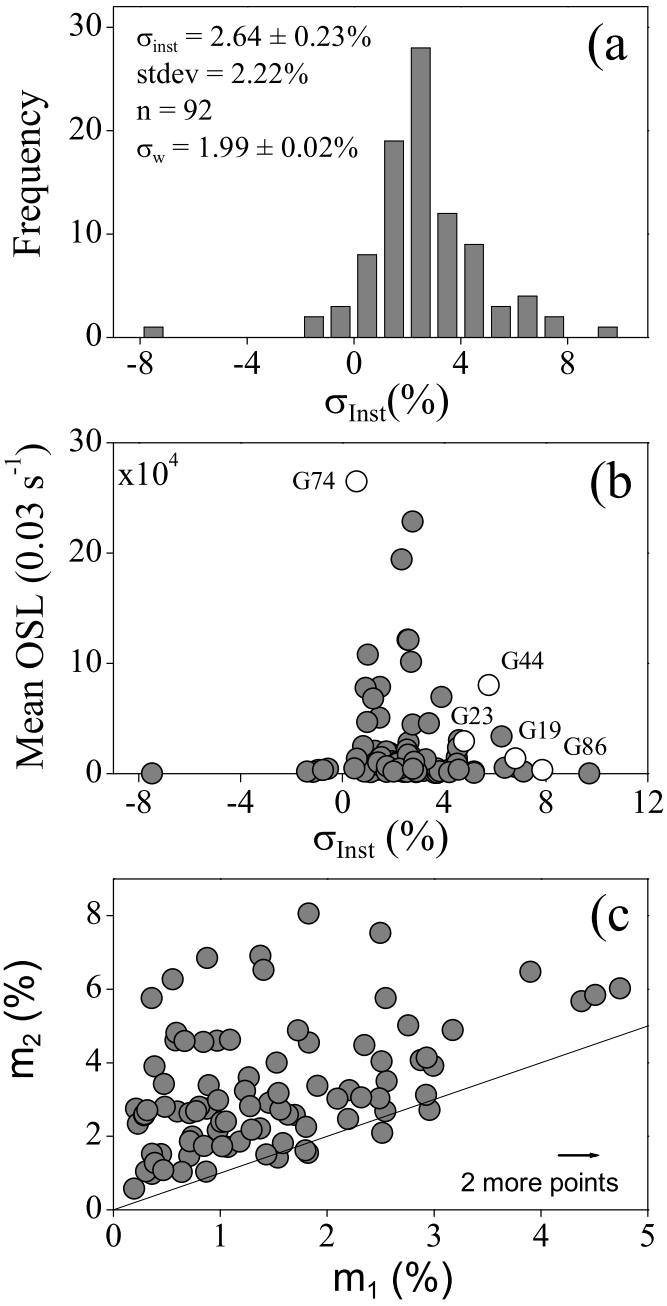

Figure 4.18: Assessment of the single grain attachment instrument reproducibility using a linear fit and the first 0.03 s of stimulation. **a)** Frequency histogram of the individual estimates of instrument reproducibility σ_{inst}. **b)** The average integrated OSL signal as a function of the individual estimates of the instrument reproducibility. Unfilled symbols represent the grains shown in Figure 4.17. **c)** The observed relative deviations from the linear fit as a function of the expected relative deviations from counting statistics. Two points with the following coordinates have been omitted from this graph: (6, 11) and (11, 8). The line represents $m_1 = m_2$.

instrument reproducibility has been assessed as

$$\sigma_{inst} = -\sqrt{m_1^2 - m_2^2} \tag{4.10}$$

Of the 100 grains measured, 92 grains gave a detectable luminescence signal. The weighted mean of these 92 estimates of the instrument reproducibility is $1.99 \pm 0.02\%$. In the SAR protocol a minimum of six OSL measurements are needed to estimate an unknown dose. Thus, the scatter arising from instrument reproducibility alone should be approximately 4.9% ($\sqrt{6}\times 1.99\%$). The implication of this is that the dose in a grain of quartz cannot be determined to better than 5%.

One problem with estimating the instrument reproducibility by repeatedly dosing, preheating and stimulating is that the sensitivity of individual grains often changes. There is no evidence in the literature that sensitivity change occurs linearly, which means that deviations from a straight line might not be representative of the system's reproducibility. For most of the 92 grains in this experiment (see Figure 4.17) the initial three measurement cycles deviate significantly from a straight line – presumably because of sensitivity change. If one were to remove the initial three measurements from the data set, the result would be a significant reduction in scatter and thereby a smaller instrument reproducibility (weighted mean $1.06 \pm 0.02\%$). If the "curvature" seen in the initial three measurements is caused by changes in sensitivity an alternative approach is to try to correct for theses changes in sensitivity by applying a test-dose to produce a corrected OSL response (i.e. the first measurement is divided by the second, the third by the fourth and so on). The result of this procedure is shown for three different grains (44, 19 and 74) in Figure 4.19a, c and e (open circles). The uncertainties on the individual points are within the symbols. If the test-dose correction is working properly, one would expect all corrected points to lie (within uncertainty) on a line given by: $y = 1$. From the corrected data the instrument reproducibility has been assessed using:

$$\sigma_{inst}^2 = \left(\frac{s_Y}{\overline{Y}}\right)^2 - \frac{1}{n}\sum_{i=1}^{n}\left(\frac{s_i}{Y_i}\right)^2 \tag{4.11}$$

where Y_i is the corrected OSL value, $\overline{Y}$ is the average of Y_i, s_Y is the standard deviation of $\overline{Y}$ and s_i is the estimated uncertainty on Y_i based on counting statistics. The estimates of instrument reproducibility from grains 44, 19 and 74 are 9.9%, 9.0% and 0.6%, respectively. Using this approach the weighted mean of all 92 estimates of the instrument reproducibility is $2.28 \pm 0.03\%$. In the SAR protocol three test-dose corrected OSL measurements are needed to

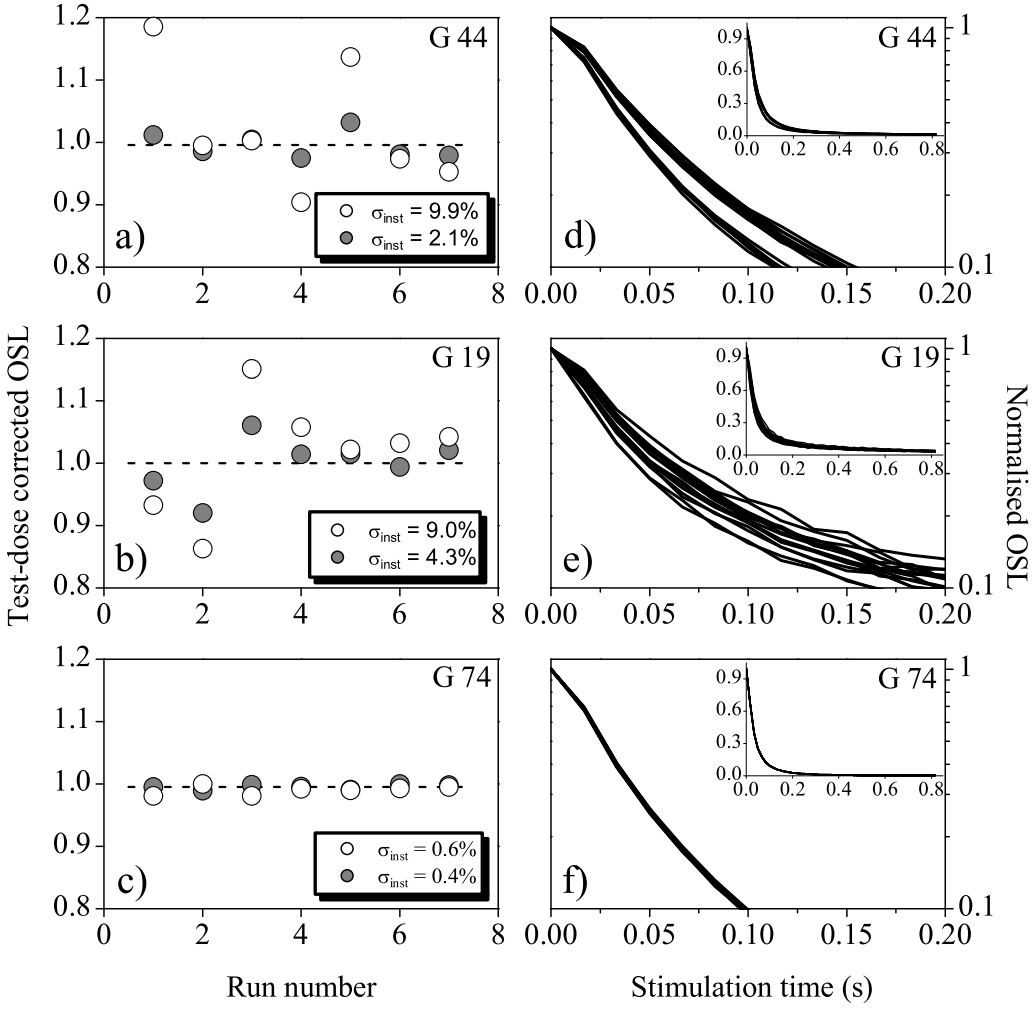

Figure 4.19: Reproducibility of the single grain system using test-dose corrected OSL signals from three grains. In **a)**, **b)** and **c)** the test-dose corrected OSL signals are plotted as a function of run number for grains 44, 19 and 74 respectively. Unfilled symbols: integration of the first 0.03 s. Filled symbols: integration of the first 0.57 s. The dashed horizontal line represents the average of the data represented by the filled symbols. In **d)**, **e)** and **f)** the normalised decay curves for the three grains are shown. Note the change in slope at 0.03 s of stimulation caused by the rise time of the laser.

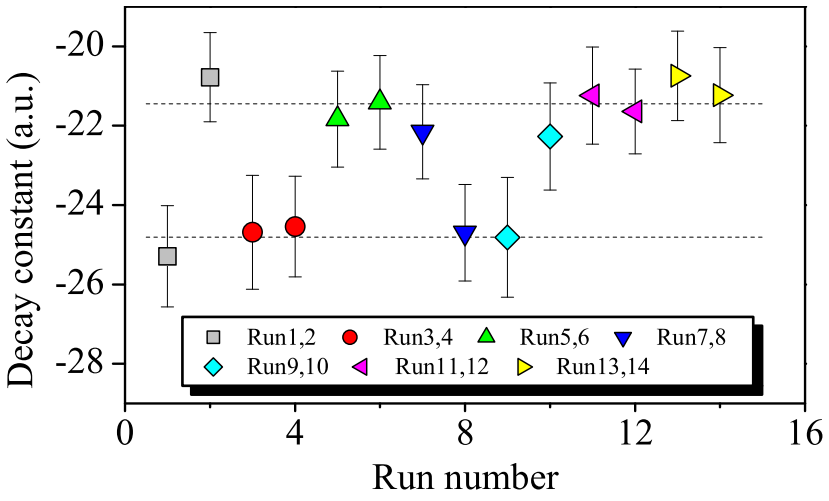

Figure 4.20: Initial decay constants for grain 44 (see Figures 4.17, 4.18b and 4.19a,d) as a function of run number. The decay constants fall broadly into two distinct groups.

estimate the unknown dose. Thus, the scatter arising from instrument reproducibility alone should be approximately 4% ($\sqrt{3}\times 2.28\%$) in a dose estimate. Normally, only the initial part of the OSL signal is used in analyses. Thus, an underlying assumption for the validity of comparing OSL signals is that the initial decay rates remain constant in the different OSL measurements. In Figure 4.19b, d and f, the normalised decay curves for the three grains are shown. The insets show the entire decay curves. Ideally, these decay curves should have the same decay rate and hence fall on top of each other. This is clearly not the case in Figure 4.19d, where the curves fall into two groups with different decay rates. This is further illustrated in Figure 4.20, where the initial decay constant for these decay curves are plotted against the run number. The decay constant α has been determined by fitting an expression of the form: $\ln y = \alpha x + \beta$ to the first 5 data points (excluding the very first point).

Varying decay rates caused by the instrument can most easily be explained by variations in the effective stimulation power. Differences in effective stimulation power can be attributed to the fact that the focused laser beam stimulates only a small part of a grain. Internal scattering within the grain hole is relied on to illuminate the entire grain. If this scattering is not completely uniform and/or reproducible, one might expect the observed decay rate of the OSL signals from a given grain to vary slightly from run to run, as different volumes of the grain are illuminated with slightly different intensi-

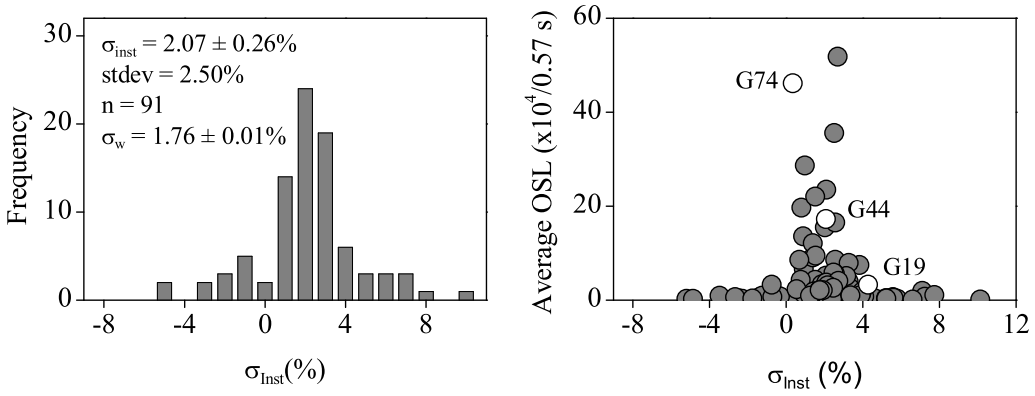

Figure 4.21: Assessment of the single grain attachment instrument reproducibility using test-dose corrected OSL signals and the first 0.57 s of stimulation. a) Frequency histogram of the individual estimates of instrument reproducibility σ_{inst}. b) The average integrated OSL signal as a function of the individual estimates of the instrument reproducibility.

ties from one measurement to another. It is also known that the sample disc rotates slightly between OSL measurements and that the grains move within the holes of the sample disc during heating. Thus, the grains will change their orientation slightly with respect to the laser beam from one measurement to another. This will accentuate any effect of non-uniform illumination.

Differences in stimulation power can also be attributed to the reproducibility of the laser itself. In section 4.5.2 the reproducibility of the laser was investigated and it was concluded that the relative standard deviation of the laser intensity is $\sim$2%. Thus, it is expected that the decay rate will vary for different stimulations, since the decay rate of the emitted OSL is proportional to the stimulation power. However, if the sample is stimulated for a sufficiently long time all the OSL will eventually be emitted. Thus, if one were to expand the integration interval to encompass the entire decay curve, it would be expected that the effect of variations in stimulation power in different measurements would be minimised.
The filled symbols in Figure 4.19a, c and e represent the same data as the open circles (integrated over the first 0.03 s of stimulation), but in this case the decay curves have been integrated over approximately 0.57 s of the stimulation time. The scatter has clearly been reduced and the individual estimates of instrument reproducibility are 2.1, 4.3 and 0.4% for grains 44, 19 and 74, respectively. In Figure 4.21 the individual estimates of the instrument reproducibility σ_{inst} using the first 0.57 s of stimulation for all 92 grains are shown. Integrating a larger part of the OSL signal has decreased the weighted mean of the instrument reproducibility from 2.3% to 1.8%, which implies a

minimum uncertainty on an estimate of dose of ∼3% if fully integrated signals are used. Thus, by increasing the integration interval, the instrument reproducibility has been decreased by approximately 1.4%. This is further investigated in Chapter 6.

4.6 Summary

In this chapter the important characteristic features of the Risø TL/OSL luminescence reader have been described. This instrument is capable of measuring thermoluminescence (TL) and optically stimulated luminescence (OSL). The available stimulation light sources in the conventional Risø reader are blue and infrared LEDs; the reproducibility of the blue LEDs is approximately 0.3%.
The Risø single grain attachment has also been characterised. This attachment enables routine measurements of individual sand-sized grains. The available stimulation sources are two focused lasers emitting at 532 nm (green) and 830 nm (infrared) respectively. The reproducibility of the green laser was found to be approximately 2%.

5 A Feasibility Study on Unheated Quartz

5.1 Introduction

Retrospective accident dosimetry based on luminescence methods usually involves the use of quartz extracted from heated (sensitised) materials such as house bricks, tile ceramic or pottery (Bailiff, 1997; Bøtter-Jensen, 2000; Bøtter-Jensen et al., 2000b; Bøtter-Jensen and Murray, 2001). Heating of these materials during manufacture will thermally release any stored charge and sensitise the quartz. However, unfired building materials, such as concrete and mortar, are much more widespread in the industrial and office environment, and it could therefore be valuable to investigate the suitability of using unheated materials as retrospective dosimeters. Sand for building materials is quarried from geological deposits containing a natural dose; this may be > 100 Gy, depending on the age of the deposit. The basic premise in applying OSL successfully to unheated materials is that the quartz grains in the sand used for building materials was optically zeroed during the process of quarrying, transport and manufacture. However, it is likely that not all grains received a sufficient exposure to light to adequately zero the natural geological dose, so it cannot be assumed that all grains contained a negligible dose at the time of construction. As a result the material will often contain a wide distribution of doses prior to the event of interest, with only some (if any) grains containing an effectively zero dose. The main challenge in using such materials as retrospective dosimeters is in identifying these well-zeroed grains, when an accident dose has been superimposed on the natural dose distribution. Another challenge is that these types of materials may be only weakly sensitive to radiation, thus requiring many measurements to be undertaken in order to obtain a satisfactory dose distribution.

The work presented in this chapter reports on measurements of the natural (geological) dose distribution in a modern concrete sample and describes the preliminary attempts to measure a dose depth profile in a simulated concrete brick (prepared using the modern concrete sample), which was given a known dose in the laboratory. The simulated concrete brick was made of layers of commercial premix concrete, inter-spaced with thermally annealed quartz to measure a reference dose depth profile through the brick. The brick was irradiated with 662 keV (^{137}Cs) photons to a dose of 5 Gy in quartz to the front of the brick. The absorbed dose-depth curve derived from the heated quartz is compared with the dose-depth curve predicted using Monte Carlo calculations. Dose distributions from quartz extracted from the concrete layers are presented and the derived doses are compared with the known dose-depth profile.

The dose distribution in each sample (both unirradiated and irradiated) was measured using 1) small aliquots each comprising of approximately 65 quartz grains and 2) single grains extracted from the concrete.

5.2 Experimental details

The sample measured in this preliminary study was a commercial premix concrete purchased at the local hardware store. The premix concrete was divided into two portions. Immediately after purchase quartz grains were extracted from one portion by sieving and treatment with HCl, H_2O_2 and HF in the usual way (Wintle, 1997). The other portion was used to construct a simulated concrete brick. This simulated concrete brick was constructed using a cardboard box with internal dimensions $5 \times 12 \times 24$ cm. A schematic drawing of the brick is shown in Figure 5.1. The brick was divided into 23 sections using 3 mm thick corrugated cardboard dividers. To determine the dose-depth profile in the brick, sachets containing 200 mg of sensitised quartz (500 °C for 1 hr) were placed in front of each slice. The brick was then filled with a commercial premix concrete and irradiated with 662 keV photons from a collimated ^{137}Cs point source. A dose of 5 Gy in quartz (considered similar to the lethal threshold dose to humans[1]) was given to the front of the brick. Quartz grains were then extracted from the individual concrete slices in the same manner as described above. An automated Risø TL/OSL reader, model Risø TL/OSL-DA-15, was used for the OSL measurements of small

[1] $LD_{50/30}$ (Lethal Dose 50/30): the dose of radiation expected to cause the death of 50% of the expected population within 30 days. For single whole body acute radiation exposure, the $LD_{50/30}$ is in the range from 4 to 5 Sv.

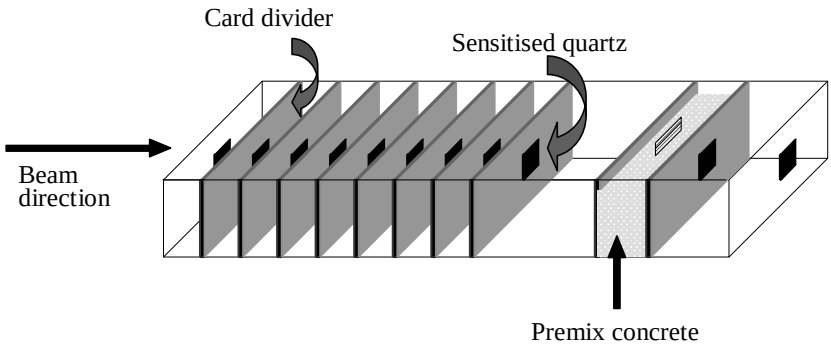

Figure 5.1: Layout of simulated brick; each division contained a sachet of sensitised quartz and was filled with dry concrete mixture.

multi-grain aliquots. The stimulation light source was a blue LED (470 ± 30 nm) array delivering $50\,\mathrm{mW/cm^2}$ at the sample (Bøtter-Jensen et al., 2000a). Small aliquots (2 mm diameter) were used for the concrete samples, each containing 65 ($\sigma = 10$) grains. About 2% of the aliquots were rejected because of feldspar contamination (as detected using IR-OSL). Single grain measurements (grain size: $212 - 250\,\mu\mathrm{m}$) were carried out on an automated Risø reader fitted with a single grain laser attachment (Bøtter-Jensen et al., 2000a). The stimulation light source is a $10\,\mathrm{mW\,Nd:YVO_4}$ solid state diode-pumped laser emitting at 532 nm, which is focused on to each of 100 grains mounted on a special sample disc.

All analyses employed the SAR protocol (Murray and Wintle, 2000). A preheat of 200 °C for 10 s and a test dose of between 2 and 4 Gy was used for all the measurements.

5.3 Dose-depth profile

The sensitised quartz samples inter-spacing the concrete slices were measured using large aliquots (> 1000 grains) and the SAR protocol. The results are plotted as a function of depth into the brick in Figure 5.2. Each point is an average of at least 18 measurements and has a standard error of < 1%. The continuous line was calculated using a Monte Carlo (MCNP) based model (Lauridsen, 2000, private communication). The Monte Carlo code MCNP (Monte Carlo N Particle) used is a general purpose, continuous-energy, generalised-geometry, time-dependent coupled Monte Carlo transport code (Briesmeister, 1986). The absorbed doses were calculated in the actual geometry for each mm depth into the simulated concrete brick over the en-

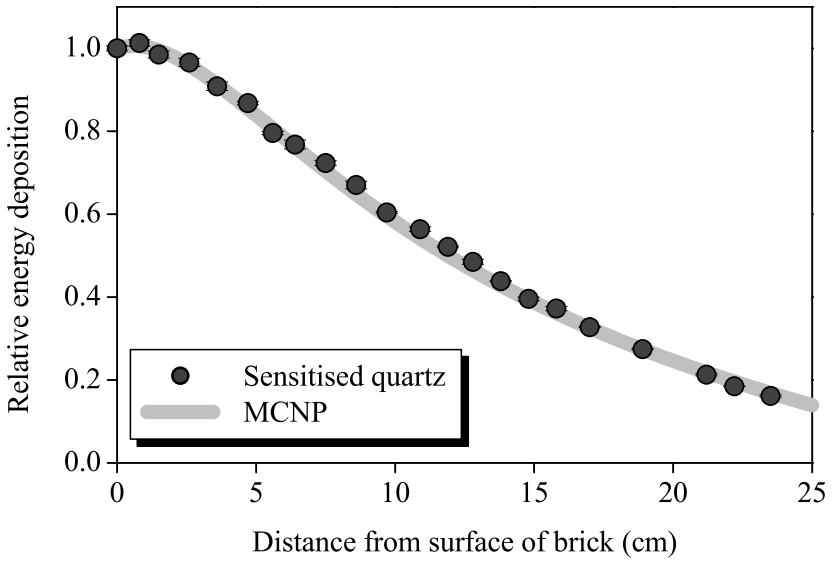

Figure 5.2: Comparison of Monte Carlo calculated depth-dose profile with that measured using sensitised quartz. The width of the grey line reflects the calculated uncertainties in the Monte Carlo prediction.

tire cross-section (240 mm). The measured dose-depth profile agrees very well with the calculated profile.

5.4 Small aliquot measurements

5.4.1 Natural dose distribution

If an accident dose superimposed on a natural dose distribution is to be determined accurately it is important that at least some of the grains in the sample were adequately zeroed at manufacture. One way to investigate how effectively the grains were zeroed at the time of manufacture is to measure the natural dose distribution in modern analogues. The measured natural dose distribution from small aliquots of quartz from the natural (e.g. unirradiated) premix concrete is shown as a histogram in Figure 5.3a. The average dose is 10.9 ± 1.5 Gy ($n = 183$) and the weighted mean 0.62 ± 0.01 Gy (weighted by counting statistics). The estimated doses range from 0.07 ± 0.04 Gy to 134.6 ± 15.3 Gy. Only aliquots with statistical uncertainties on the natural test dose $< 15\%$ have been included in the histogram. The distribution is clearly asymmetrical. For a well-zeroed sample the dose distribution is expected to be tight and symmetrical. A skewed distribution with a tail towards higher

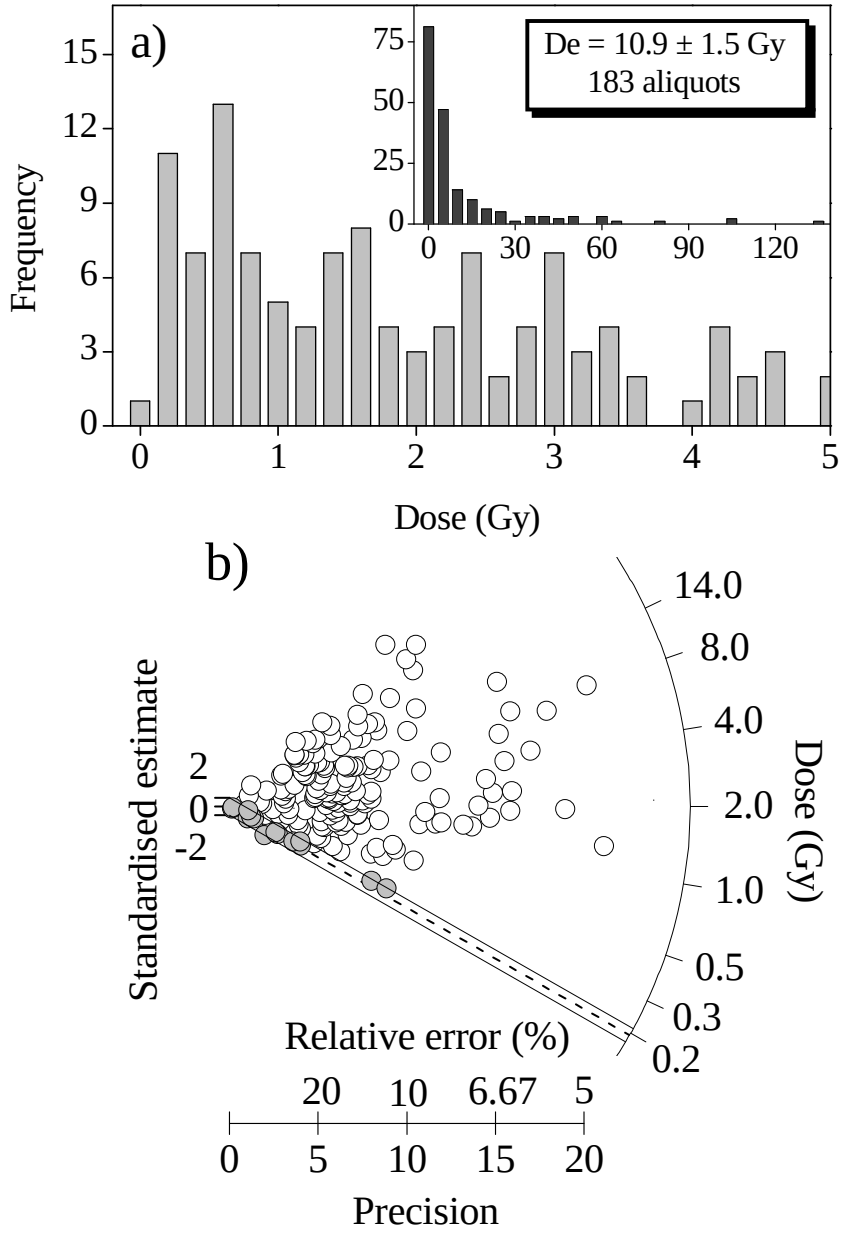

Figure 5.3: Doses measured in small aliquots of quartz extracted from unirradiated concrete. **a)** Histogram, using only those results with a natural test dose known to better than 15% ($n = 183$); the arithmetic average is given in the inset. **b)** Radial plot, showing the results selected for inclusion in the average result of 0.28 ± 0.05 Gy ($n = 18$).

doses indicates contamination with a small percentage of poorly zeroed grains (Olley et al., 1998, 1999). Thus, the natural dose distribution in this concrete premix is poorly bleached.
Murray et al. (1995) suggested using the lowest 10% of a distribution obtained using small aliquots to identify well-zeroed aliquots, whereas Olley et al. (1998, 1999) suggested using the lowest 5%. Using the lowest 5% gives a mean dose of 0.18 ± 0.02 Gy ($n = 9$). Weighting the results with respect to their uncertainties gives an average dose of 0.20 ± 0.02 Gy. Using the lowest 10% the corresponding numbers are 0.26 ± 0.02 Gy ($n = 18$) and 0.23 ± 0.01 Gy (see Table 5.1). Neither of these values are consistent with zero. However 7% of the individual results were consistent with zero (within $\pm 2\sigma$). In a histogram all data points are weighted equally, irrespective of the precision with which they are known. A radial plot (Galbraith, 1990), where each result is plotted together with its relative statistical uncertainty may be more informative. In a radial plot a result D_i with standard uncertainty s_i will plot at the coordinates

$$(x_i, y_i) = \left(\frac{D_i}{s_i} \, , \, D_i \, \frac{\ln D_i - \ln D_0}{s_i} \right) \tag{5.1}$$

Thus, the x-axis plots the precision (D_i/s_i) (here defined as the reciprocal of standard uncertainty) with which a result is known. The more precise an individual result is the further to the right it plots. The y-axis represents a scale of standardised estimates of logarithmic dose centred at a reference value D_0 and having unit standard uncertainty. D_0 is usually chosen to be the weighted mean of the results, but can in principle be any (positive) value. $\ln D_i - \ln D_0$ is the *slope* of a line drawn from the origin to (x_i, y_i). Thus, the estimates of dose D_i are represented by slopes. All points falling on a straight line drawn from the origin will have the same dose D_i. A line of zero slope ($y = 0$) corresponds to $D_i = D_0$. The radial dose (log) scale has been added to ease the interpretation of the radial plot. If each D_i has the same expectation value μ the points (x_i, y_i) should scatter homodastically, with unit standard deviation, about a straight line through $(0, 0)$ having slope μ (Galbraith, 1988). If $D_0 = \mu$ then all results with $-2 < y_i < 2$ are statistically consistent within 2σ of the expectation value. Thus, for a perfect Gaussian distribution 95% of the results fall within this $\pm 2\sigma$ band.

Figure 5.3b presents the same data as in Figure 5.3a but as a radial plot. The width of the $\pm 2\sigma$ band is calculated on the basis of the entire data set. In an attempt to identify the well bleached grains, the $\pm 2\sigma$ band has been subjectively positioned to cover the low dose edge of the distribution. Only about 10% of the data points (14 out of the 183 aliquots) appear in the band. The

		Depth (cm)	Expected Dose (Gy)	Lowest 5%			Lowest 10%			Radial plot		N
				D_e (Gy)	D_w (Gy)	n	D_e (Gy)	D_w (Gy)	n	D_w(Gy)	n	
Small aliquots	Slice 1	0.5	4.88 ± 0.04	4.15 ± 0.19	4.04 ± 0.21	9	4.74 ± 0.17	4.62 ± 0.16	18	4.84 ± 0.19	41	180 (336)
	Slice 2	1.3	4.87 ± 0.04	4.17 ± 0.39	1.99 ± 0.12	10	4.76 ± 0.22	3.07 ± 0.10	21	5.29 ± 0.15	44	208 (288)
				4.59 ± 0.17	4.61 ± 0.21	10	4.98 ± 0.12	5.02 ± 0.13	21			207
	Slice 3	2.0	4.80 ± 0.03	5.05 ± 0.12	4.97 ± 0.25	8	5.28 ± 0.08	5.23 ± 0.17	17	5.63 ± 0.17	37	167 (384)
	Slice 4	3.1	4.61 ± 0.03	3.12 ± 0.87	0.34 ± 0.05	6	4.08 ± 0.51	0.65 ± 0.05	12	5.39 ± 0.17	43	123 (384)
				4.67 ± 0.15	4.74 ± 0.23	6	4.92 ± 0.11	4.94 ± 0.15	12			121
	Slice 7	6.1	3.89 ± 0.03	3.74 ± 0.14	3.83 ± 0.17	6	4.07 ± 0.13	4.08 ± 0.13	12	4.78 ± 0.13	65	119 (336)
	Slice 12	11.4	2.68 ± 0.02	2.50 ± 0.11	2.47 ± 0.13	8	2.73 ± 0.08	2.76 ± 0.08	16	2.79 ± 0.11	22	157 (384)
	Slice 18	17.5	1.56 ± 0.02	1.57 ± 0.07	1.56 ± 0.06	7	1.69 ± 0.05	1.67 ± 0.04	13	1.76 ± 0.06	24	130 (192)
	Natural			0.18 ± 0.02	0.20 ± 0.02	9	0.26 ± 0.02	0.23 ± 0.01	18	0.20 ± 0.01	14	183 (288)
Single grains	Slice 1	0.5	4.88 ± 0.04	2.37 ± 0.21	2.04 ± 0.18	7	2.98 ± 0.20	2.56 ± 0.15	14	4.89 ± 0.08	75	143 (12,000)
	Slice 2	1.3	4.87 ± 0.04	1.71 ± 0.14	1.89 ± 0.13	6	2.25 ± 0.16	2.14 ± 0.10	13	5.13 ± 0.08	71	123 (9,600)
	Slice 3	2.0	4.80 ± 0.03	2.56 ± 0.19	2.49 ± 0.18	4	2.96 ± 0.23	2.74 ± 0.16	9	4.79 ± 0.08	54	86 (7,200)
	Slice 14	13.3	2.30 ± 0.02	1.08 ± 0.09	1.15 ± 0.15	8	1.34 ± 0.09	1.46 ± 0.09	15	2.32 ± 0.05	72	154 (12,000)

Table 5.1: Summary of results from quartz extracted from the premix concrete using small aliquots as well as single grains. **Depth** is the distance from the front of the brick to the sample. **Expected dose** is the dose expected from the measurements of the thermally annealed quartz inserted in front of each slice. $\boldsymbol{D_e}$ is the arithmetic mean, $\boldsymbol{D_w}$ is the weighted mean (weighted with respect to counting statistics) and **n** is the number of included results in the dose estimation. **N** is the number of results included in the distribution (the value given in parenthesis is the total number of measured aliquots).

average dose of the points falling within this band is 0.28 ± 0.05 Gy ($n = 14$) and the weighted mean is 0.20 ± 0.01 Gy, similar to the lowest 5% and 10% approaches.

5.4.2 Irradiated dose distributions

Quartz extracted from seven different slices of the irradiated brick was measured using small aliquots (the results are summarised in Table 5.1). In Figure 5.4 small aliquot data from six of these slices are presented as dose histograms. Only results with an uncertainty on the natural test dose $< 15\%$ have been included in the histograms. The black vertical line represents the expected dose for that particular slice. This expected dose was derived from the measurements of the sensitised quartz inserted between the individual concrete slices. Adding a dose on top of the natural dose distribution has clearly shifted the distributions towards higher doses as expected. The expected doses coincide reasonably with the leading edges of the distributions. Applying the lowest 5 or 10% approach gives dose estimates close to the expected dose with the exception of slice 4 (Figure 5.4d), where the presence of two precisely known results ($D_e = 0.17 \pm 0.05$ Gy and $D_e = 0.53 \pm 0.16$ Gy) causes a significant underestimation of the added dose – particularly when using the weighted mean. Similarly in slice 2, a single outlier ($D_e = 0.91 \pm 0.14$ Gy) causes the underestimation. Omitting these outliers results in dose estimates consistent with the added dose using both the lowest 5 and 10% approaches.

Figure 5.5 presents the small aliquot data obtained from slice 12 (11.4 cm into the brick). Results from 157 aliquots have been included (those with uncertainty on the natural test dose $< 15\%$). From the dose-depth profile measured with the sensitised quartz an added dose of 2.68 ± 0.02 Gy is expected at this depth. The lowest 5% approach gives a mean dose of 2.50 ± 0.11 Gy ($n = 8$) and a weighted mean of 2.47 ± 0.13 Gy. The corresponding numbers using the lowest 10% approach are 2.73 ± 0.08 Gy ($n = 16$) and 2.76 ± 0.08 Gy. The results are also plotted on a radial plot in Figure 5.5b. The positioning of the $\pm 2\sigma$ band is subjective, but it has again been placed to cover the lower dose edge of the distribution. Twenty two aliquots are located in the $\pm 2\sigma$ band giving an average of 2.92 ± 0.09 Gy and a weighted mean of 2.79 ± 0.11 Gy.

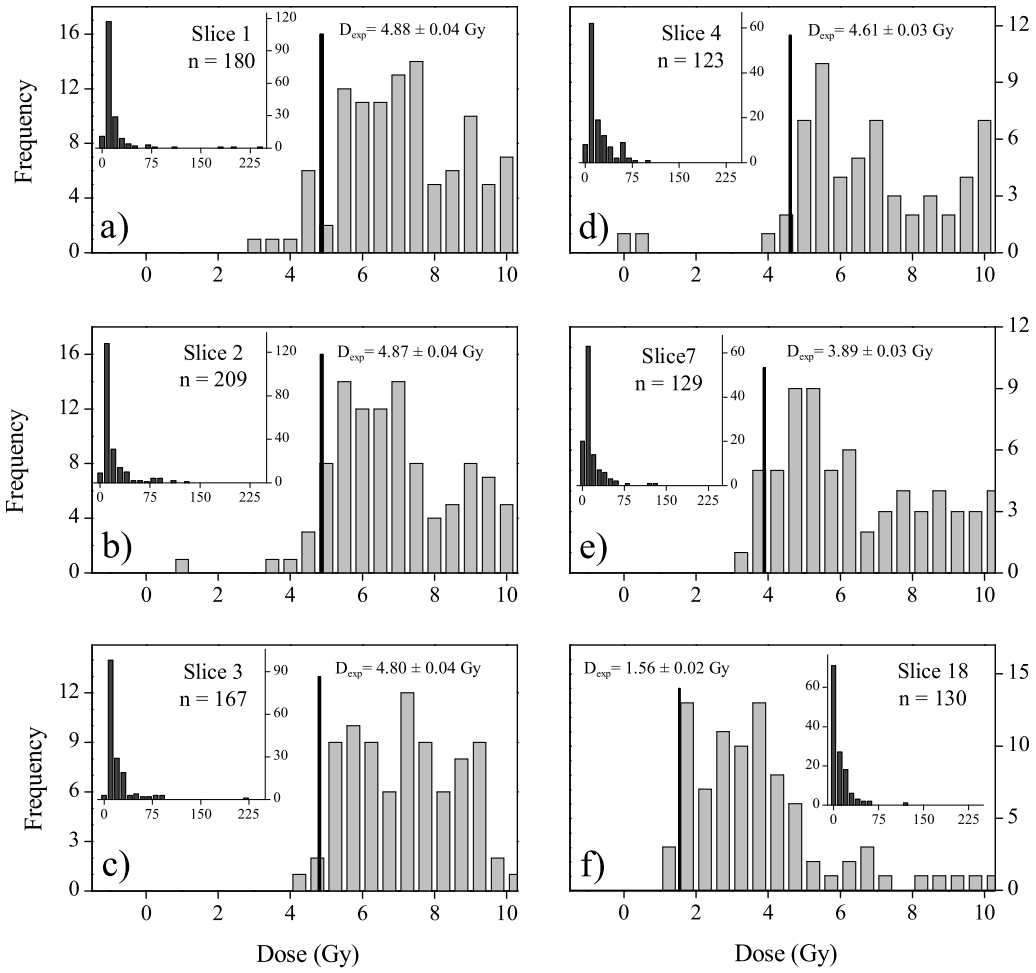

Figure 5.4: Doses measured in small aliquots of quartz extracted from slices 1–4, 7 and 18 located at depths of 0.5, 1.3, 2.0, 3.1, 6.1 and 17.5 cm into the brick respectively. Only results with a natural test dose known to better than 15% have been included in the diagrams. The vertical black lines represent the expected doses.

5.5 Single grain measurements

Single grain measurements were carried out on four different slices (slice 1, 2, 3 and 14) for comparison with the small aliquot data. The data are presented as dose histograms in Figure 5.6 on page 85, where the black vertical line represents the expected dose. The single grain dose distributions appear as wide and asymmetrical as the small aliquot distributions. In the small aliquot data the leading edge of the dose distributions coincided with the expected dose, but in the single grain data a distinct dose population is centred

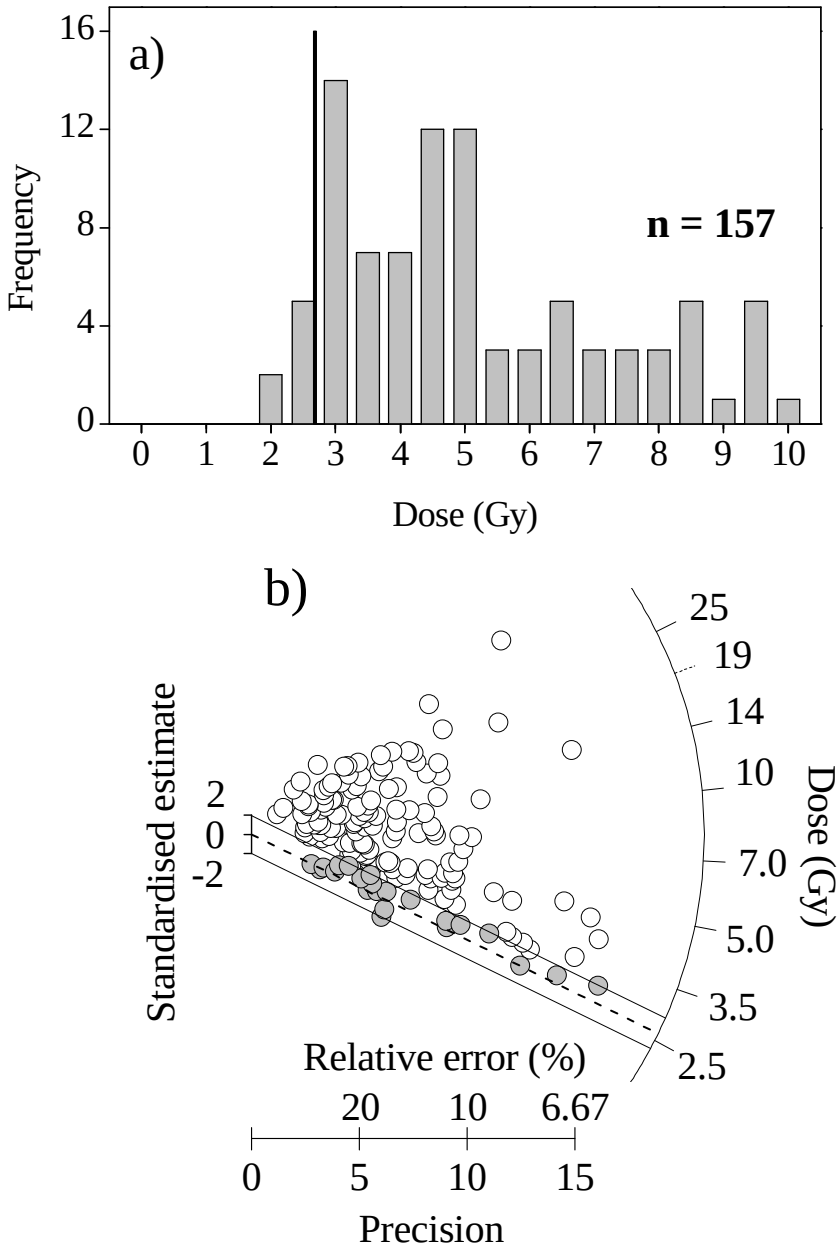

Figure 5.5: Doses measured in small aliquots of quartz extracted from slice 12 (11.4 cm into the brick) of the simulated brick (expected dose 2.68 ± 0.02 Gy). **a)** Histogram, using only those results with a natural test dose known to better than 15% ($n = 157$); the vertical black line represents the expected dose. **b)** Radial plot, showing the results selected for inclusion in the average result of 2.92 ± 0.09 Gy ($n = 22$) and a weighted mean of 2.79 ± 0.11 Gy .

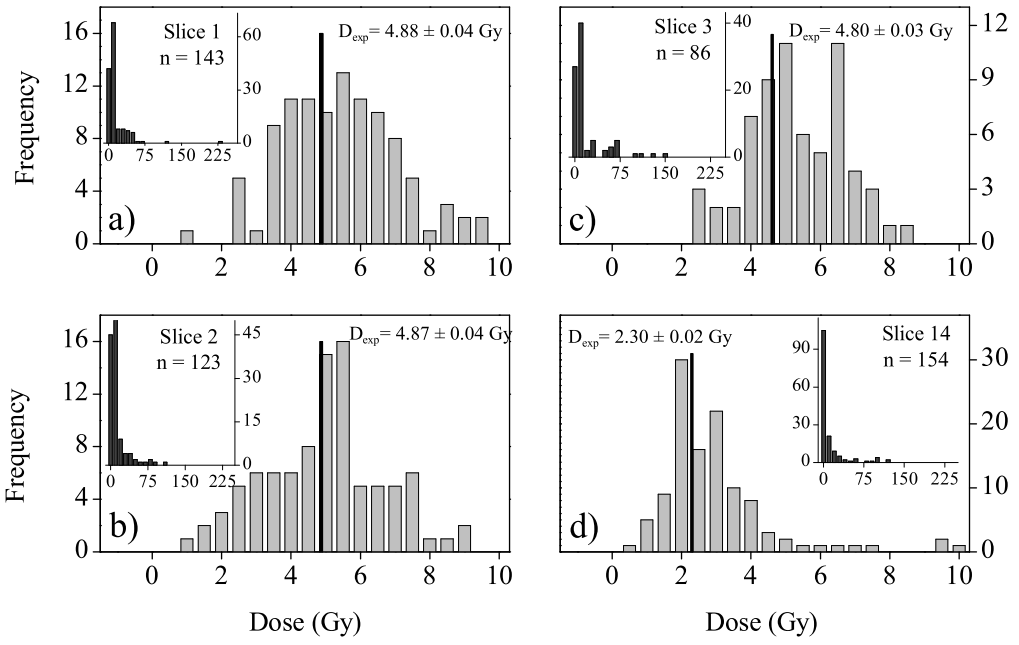

Figure 5.6: Dose distributions measured using single grains of quartz. Only results with a natural test dose known to better than 15% have been included. The vertical line represents the expected dose.

on the expected value. In the small aliquot data approximately 30% of the results were consistent with the expected dose (consistent within 2σ using the uncertainty calculated on the basis of counting statistics for the individual dose estimates). In the single grain data the corresponding number is approximately 60%. This implies that this sample did contain a significant proportion of well-zeroed grains. Using the lowest 5 or 10% approach on the single grain data underestimates the added dose significantly (see Table 5.1).

In Figure 5.7 radial plots of the single grain data from slice 1 and slice 2 are shown. Of the 12,000 grains measured from slice 1 (Figure 5.7a) only 143 were accepted in the distribution (uncertainties on the natural test dose $<$ 15%). Seventy five grains are located in the $\pm 2\sigma$ band giving an average of 6.5 ± 0.8 Gy and a weighted mean of 4.89 ± 0.08 Gy (weighted by counting statistics). Of the 9,200 grains measured from slice 2 (Figure 5.7b) only 123 were accepted in the distribution. Seventy one grains are located in the $\pm 2\sigma$ band giving an average of 5.8 ± 0.4 Gy and a weighted mean of 5.13 ± 0.08 Gy. All single grain results are summarised in Table 5.1.

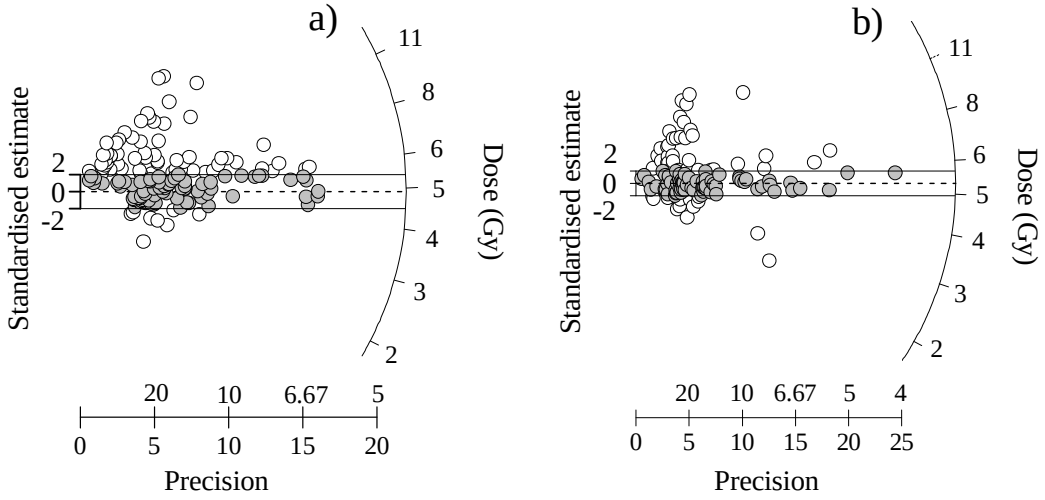

Figure 5.7: Radial plots of single grain results. Only results with a natural test dose known to better than 15% have been included. **a)** Results from slice 1 ($n = 143$). The filled symbols represent the results selected (using the radial plot method) for inclusion in the weighted average of 4.89 ± 0.08 Gy ($n = 75$). **b)** Results from slice 2 ($n = 123$). The filled symbols represent the results selected for inclusion in the weighted average of 5.13 ± 0.08 Gy ($n = 71$).

Figure 5.8 summarises the small aliquot results, calculated using the lowest 5% approach and the radial plot method and single grain results using the radial plot method. The broad line represents the absorbed dose depth curve measured using the sensitised quartz (Figure 5.2). Using the lowest 5% approach gives dose estimates consistent with the expected doses (when obvious outliers have been removed from the data), whereas the subjective radial plot method slightly overestimates the expected dose. However, the agreement between the small aliquot data and the expected curve is surprisingly good.

Measurements of incompletely bleached samples using multiple-grain aliquots would be expected to result in an overestimation of the lowest dose in the sample. This overestimation is caused by the measurement of a mixed population of bleached and unbleached grains in each aliquot. In an incompletely bleached sample the probability of selecting only well-bleached grains increases as the number of grains in an aliquot decreases and as the fraction of well-bleached grains increases (Olley et al., 1999). Nevertheless, although this sample is poorly bleached (Figure 5.3), analysis of the small aliquot data returns the correct answer (Figure 5.8).

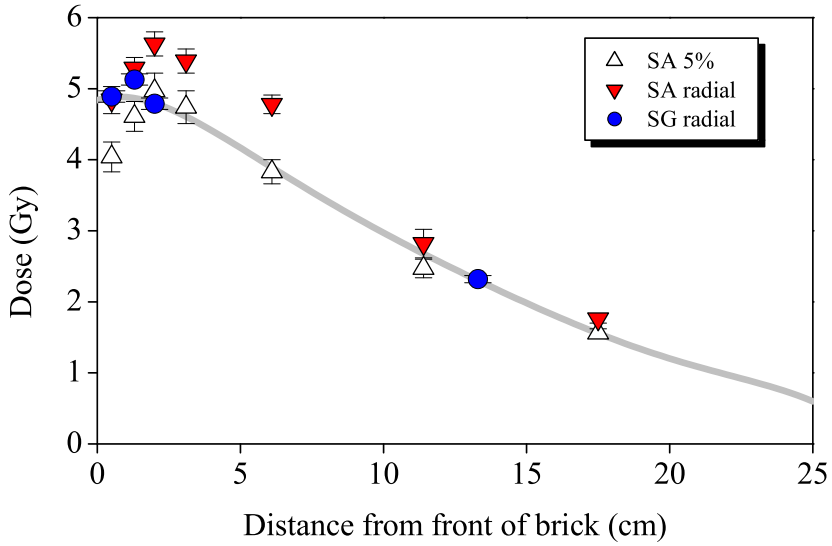

Figure 5.8: Comparison of small aliquot (SA) results derived from the first 5% of histograms (triangles), radial plots (inverted triangles) and single grain (SG) results (circles) with the predicted depth-dose curve.

The single grain measurements show that there is a large variability in the intensity of the OSL signal obtained from different grains. Figure 5.9 shows the normalised cumulative light sum for the natural signal and from the natural test signal plotted against the proportion of grains for slice 1 (as suggested by Duller and Murray, 2000). All 12,000 measured grains were ranked in order of descending brightness and the OSL intensities added. If the intensities of the OSL signals were similar for all grains, the cumulative light sum would be strictly proportional to the proportion of grains. However, for slice 1 about 80% of the natural light comes from only 1% of the grains and only 2.5% of the grains gave a statistical uncertainty on the natural test dose response of $< 30\%$. In the small aliquot measurements each aliquot contained about 65 grains, which means that each aliquot on average only contained 1–2 grains giving detectable light signal. In this case it appears that small aliquot analyses were almost indistinguishable from those from single grains. The difference between the natural and the natural test signal curves (Figure 5.9) could indicate that the sample was incompletely bleached. If the sample had been fully bleached the two curves could be expected to coincide (Duller and Murray, 2000).

It is important to note that using the Risø single grain OSL attachment (Bøtter-Jensen et al., 2000a) 4,800 single grains can be measured in the same

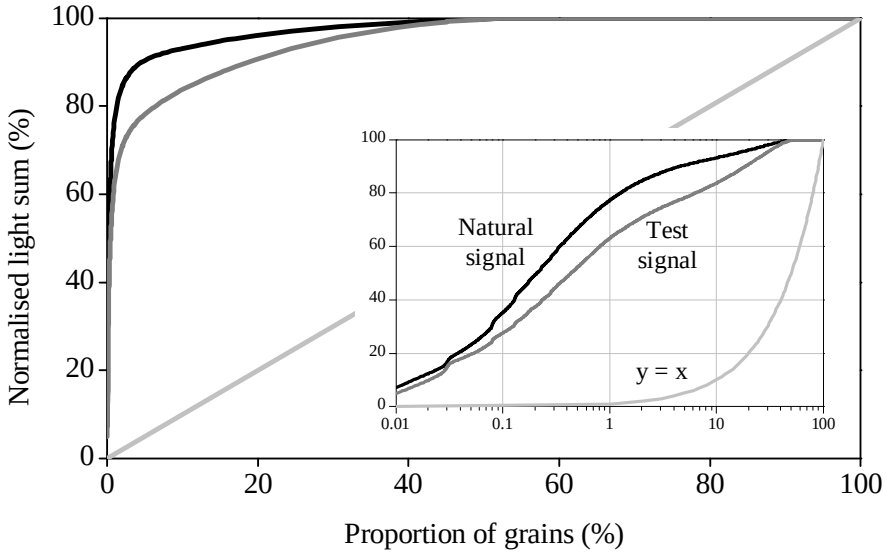

Figure 5.9: Cumulative light sum against proportion of contributing grains for natural and test dose signal obtained from the 12,000 grains measured from slice 1. The line $y = x$ represents an "ideal" sample where all grains contribute equally to the light sum.

time as it takes to measure 48 single aliquots in the standard Risø TL/OSL system (Bøtter-Jensen, 2000). Thus the single grain data not only avoid the problem of averaging the results from several bright grains, but also give a significantly faster throughput.

5.6 Conclusion

The dose-depth profile in a simulated concrete brick, measured using heated quartz, agreed very well with the profile calculated using the Monte Carlo MCNP code. Small aliquot measurements of the concrete before dosing showed that the concrete was poorly bleached. Small aliquot measurements of the irradiated concrete brick were made for seven different depths into the brick. Both averaging the lowest 5 or 10% of the results and using the radial plot method gave good agreement with the calculated profile.

Single grain measurements showed that only 2.5% of the grains measured gave detectable test dose signals. In effect this means that on average the small aliquots only contained 1–2 detectable grains, which probably explains why the small aliquot doses agreed with expectations. However, it is interesting to note the distinct difference between the small aliquot and single grain dose distributions. The single grain distributions clearly contains a well-

defined sub-population centred on the expected dose (Figure 5.6), whereas the small aliquot distributions contain a "continuum" of doses with the leading edge coinciding with the expected dose (Figure 5.4). This difference between the distributions is surprising, since the small aliquot and single grain analyses ought to be essentially indistinguishable from each other. This is discussed further in Chapters 7 and 8. Using the lowest 5 or 10% of the obtained single grain results significantly underestimates the expected dose. The presence of results giving a dose lower than the expected dose is at this stage attributed to uncertainties in the individual dose estimates. Using the radial plot method on the single grain measurements of the concrete slices gave good agreement with the calculated dose depth profile. It is concluded that measurement of individual grains from poorly zeroed building materials can provide useful information on accident doses.

Averaging the lowest 5 or 10% of the results is a somewhat arbitrary approach to determining a dose. Using such an approach may result in significant underestimation of the accident dose due to a normal spread in the results as a consequence of experimental uncertainties (Wallinga, 2001). In the radial plot method placing the $\pm 2\sigma$ band is subjective. In most cases the dose estimate is relatively insensitive to minor changes in the position of the $\pm 2\sigma$ band, but in some cases including or excluding a high precision point may change the dose estimate significantly. In placing the $\pm 2\sigma$ band one will tend to be biased by the precisely known results. The estimates of uncertainty have been purely based on counting statistics. In order to be able to interpret dose distributions correctly it is important to establish whether other factors besides incomplete bleaching and counting statistics also contribute to the observed spread in the data. This question is addressed in the next chapter.

6 Sources of Variability in Single Grain Dose Distributions

In luminescence based measurements of dose distributions in unheated mineral samples, the observed spread in dose values is usually attributed to four main factors: fluctuations in the number of photons counted, incomplete zeroing of any prior trapped charge, heterogeneity in dosimetry and instrument reproducibility. In order to interpret correctly measured dose distributions in retrospective dosimetry it is important to understand the relative importance of these components, and to establish whether other factors also contribute to the observed spread. In this preliminary study, dose distributions have been studied using single grains of heated and laboratory irradiated quartz. By heating the sample, the contribution from incomplete zeroing was excluded and at the same time the sample was sensitised. The laboratory gamma irradiation was designed to deliver a uniform dose to the sample. Thus, it was anticipated that statistical fluctuations in the number of photons counted and instrument reproducibility, both quantifiable entities, should be able to account for all the observed variance in the measured dose distributions. This assumption is examined in detail in this chapter and the origins and importance of the residual variance in the data discussed.

6.1 Introduction

Over the past 10 years optically stimulated luminescence (OSL) has proven to be a powerful technique for retrospective dose determinations used in the dating of archaeological and geological materials (Roberts, 1997; Murray and Olley, 2002) and in reconstruction of radiation doses following a

nuclear accident (Bailiff, 1997; Bøtter-Jensen, 2000; Bøtter-Jensen et al., 2000b). It is well-known that zeroing of the OSL signal during daylight exposure is a heterogeneous process, with some grains being more completely reset than others (Murray and Olley, 1999). Thus, in samples where the residual trapped charge in all grains has not been fully zeroed at deposition, a significant improvement in accuracy can, in principle, be obtained by measuring the dose distribution on a grain-by-grain basis (Roberts et al., 1998; Olley et al., 1999; Bøtter-Jensen et al., 2000a; Jain et al., 2002; Thomsen et al., 2002b). Determining the dose in individual grains should allow the identification and rejection of poorly-zeroed grains from the population used to estimate the burial dose. However, this selection process requires that poorly-bleached grains can be distinguished from well-bleached grains. Even a well-bleached dose population will contain some range of dose values, because of factors such as statistical variations in the number of photons counted, grain-to-grain variation in the environmental dose rate, and the reproducibility of the measurement system. Only if the characteristics of a relevant well-bleached distribution are known can one hope to separate the results making up the well-bleached distribution from other "contaminating" results. Estimates of uncertainty on dose estimates from individual grains are usually based on estimates of variance derived from the number of photons observed (i.e. counting statistics), sometimes with an additional component to allow for instrument reproducibility (Duller et al., 2000). Many authors have reported that the luminescence signal intensity varies considerably from grain to grain (e.g. McFee and Tite, 1994; Murray and Roberts, 1997; Duller et al., 2000) and as a result estimates of uncertainty vary considerably from one individual dose estimate to another. Thus, even a well-bleached dose distribution contains a wide range of uncertainties, and as a result, a wide range of doses. Because of this variation in associated uncertainties, display and analysis of multiple dose estimates is complex. Simple histograms are inadequate, because they ignore the uncertainty information, and many other methods of display have been suggested; radial plots (Galbraith, 1990), plots of OSL sensitivity against dose (Duller et al., 2000) and uncertainty weighted histograms (Duller et al., 2000) seem to be the most commonly used.

One important question to ask of the data published so far is whether the associated uncertainties adequately describe the variability in these data. In one of the earliest single-grain dose studies Murray and Roberts (1997) examined an aeolian deposit from Western Australia, which was confidently expected to be well-zeroed. It was found that the individual estimates of uncertainty based on counting statistics were significantly smaller than the observed spread in the data. After a detailed discussion of the potential origins

of this spread, it was attributed to heterogeneity in external beta dosimetry. Roberts et al. (1999) found a substantial spread in single grain dose estimates from Jinmium rock shelter. This was attributed to heterogeneity in external beta dosimetry, incomplete zeroing (to account for large doses) and post-depositional intrusion of younger grains (to account for small doses). The measurement protocol (using a single test-dose-corrected regeneration point) was validated by applying a second regenerative dose. If this second dose was treated as unknown, Roberts et al. (1999) found that they were able to measure this unknown dose accurately, which gave them confidence that the protocol used was applicable and that their estimates of uncertainty accounted for the observed variability. Duller et al. (2000) used the SAR protocol (Murray and Wintle, 2000) to measure single grains of quartz extracted from an aeolian dune sand from Tasmania expected to be well-zeroed. Only 81% of the measured doses were within 2 standard deviations of the mean dose (with estimates of uncertainty based on counting statistics and instrument reproducibility). The SAR protocol is intended to correct for changes in sensitivity that may occur during sequential measurement cycles. To check whether the protocol has adequately corrected for sensitivity changes, it is usual to repeat the measurement of one of the regenerated dose points at the end of the measurement sequence. Duller et al. (2000) treated this repeat point as an unknown and used the observed spread in the doses to asses the reliability of the estimates of uncertainty on the individual dose estimates. They found that these estimates of uncertainty were able to account for the observed spread in the laboratory regenerated data, and therefore concluded that the additional scatter observed in the natural dose estimates was probably due to grain-to-grain variations in external dosimetry, and bioturbation. Duller et al. (2000) introduced an instrument reproducibility component into their calculations because Duller et al. (1999) had explicitly measured the instrument reproducibility of an automated Risø reader fitted with a single grain laser attachment, using both Al_2O_3:C and quartz from a modern Australian dune sand. Both samples were given a beta dose in the instrument and measured. The relative standard deviations of the measured doses were 6.7% and 12% for Al_2O_3:C and the quartz sample, respectively, and this difference was attributed primarily to counting statistics.

A common feature in all these studies is that none of the natural single grain measurements gave dose distributions statistically consistent with the mean dose, even for samples expected to be well-bleached. All the tests used to verify that the estimated uncertainties were correct have involved giving the sample a beta dose in the measurement instrument, which (if the measurement protocol is performing well) is essentially the same as determining the instrument reproducibility. This work attempts to take these tests a step

further. First, a simple model to describe the summing of the various source of uncertainty in laboratory measurements is developed, and then used to strip out the contribution from counting statistics from other sources of variability. All the tests use a natural sedimentary quartz sample, which has been heated to completely zero any prior dose, and to sensitise the grains, and so ensure the presence of many precisely known results (at least in terms of counting statistics). The contribution to the observed variance in dose estimates from a laboratory gamma irradiated sample is examined, and the instrument reproducibility is then measured directly. Finally, the origins and importance of the residual variance in the data are discussed.

6.2 Experimental details

6.2.1 Samples

A sedimentary quartz sample ($212 - 250\,\mu$m fraction, lab code 004807) was heated at 850 °C for 1 hour and thereby completely zeroed and sensitised. A portion was given a known gamma dose by loading it into a $50 \times 50 \times 5$ mm glass cell with 2 mm wall thickness and 1 mm internal spacing. This volume was filled with quartz grains, and the entire package irradiated in darkness using a 662 keV ^{137}Cs gamma beam perpendicular to one 50×50 mm face. From Monte Carlo modelling it is anticipated that the grain-to-grain dose variability should be $< 1\%$ (Nathan, personal communication). A further portion was first loaded into single grain discs (see below) and then beta irradiated in the Risø TL/OSL reader. The dose range employed in these irradiations was between 5 and 11 Gy. Two further samples were also used to illustrate dose distributions from natural quartz; both came from an archaeological site at Öggestorp, Sweden. One sample (lab code 010413) was a heated stone taken from a fireplace and the other (lab code 010414) was taken from an aeolian sand layer immediately above the hearth. Details of these two samples can be found in Baran et al. (2003). All three samples were measured using both single grains of quartz as well as small aliquots containing ∼60 grains each.

6.2.2 Instrumentation

Single grain measurements were carried out using an automated Risø reader fitted with a single-grain laser attachment (Bøtter-Jensen et al., 2000a). The stimulation light source is a 10 mW Nd:YVO_4 solid-state diode-pumped laser emitting at 532 nm, which is focused to a spot $< 20\,\mu$m in diameter on the

aluminium sample disc. In the present work, grains were stimulated for 1 s. Each sample disc contains 100 holes, 300 μm deep by 300 μm in diameter, on a 10 by 10 grid with 600 μm spacing between hole centres. Visual inspection under red light confirmed that a maximum of one grain was loaded into each hole. *In situ* irradiations were made using a calibrated ^{90}Sr/^{90}Y beta source providing a dose rate of 0.18 Gy/s to quartz in the single grain discs.

An automated TL/OSL reader, model Risø TL/OSL-DA-15, was used for the OSL measurements of small aliquots. The stimulation light source was a blue LED (470 ± 30 nm) array delivering 50 mW/cm^2 at the sample (Bøtter-Jensen et al., 2000a). The small aliquot measurements of sample 004807 were carried out at 10% power with a neutral density filter in front of the PM tube. This sample is sufficiently sensitive to saturate the photomultiplier tube at the doses involved here, unless the stimulation power is reduced and neutral density filters are employed.

6.2.3 Method of analysis

All analyses made use of the single-aliquot regenerative-dose (SAR) protocol (Murray and Wintle, 2000) with four regeneration doses, a recuperation measurement (regeneration dose = 0 Gy) and a repeat dose (corresponding to both one regeneration dose and the expected (unknown) dose). A preheat of 260 °C for 10 s, a cutheat of 160 °C and a test dose of 2 Gy were used for all the measurements. Only grains giving a "natural" test dose (i.e. first measurement cycle) response known to better than 20% (based on counting statistics; see section 6.3) and a recycling ratio within two standard deviations of unity were included in the following analysis. All dose estimates have been derived by linear interpolation between two regenerated dose points. In the dose range used in this study (5-11 Gy) the measured growth curves were close to linear, making the use of linear interpolation valid. All estimates of uncertainty on the results from individual aliquots (i.e. single grains or small aliquots) were based only on photon counting statistics as described in section 6.3.

6.3 Estimating the uncertainty

In estimating the uncertainty on the integrated background corrected OSL signal, Poisson statistics is assumed. The measured signal, Y (number of emitted photons as a function of time) is recorded in consecutive time inter-

vals of equal length (channels). If y_i is the number of counts in channel i then the total number of counts in the n first channels Y_n is given by:

$$Y_n = \sum_{i=1}^{n} y_i \tag{6.1}$$

Included in the measured signal Y is a background signal B which is largely unrelated to the OSL signal and corrections for this contribution must therefore be made. Conventionally, the background contribution is assumed to be constant in the stimulation interval and estimated using the last m channels of the measured signal (B_m), where the contribution from the rapidly decaying OSL signal can be considered to be negligible. The net OSL signal L_n is usually estimated from the first n channels by subtracting the estimated background signal from the measured signal. The number of channels m used in the background estimation is some multiple of n, i.e. $m = k \cdot n$. Thus, the net OSL signal in the first n channels is estimated by:

$$L_n = Y_n - \frac{B_m}{k} \tag{6.2}$$

Assuming that Y_n and B_m are Poisson distributed leads to the following estimate of uncertainty on L_n as discussed by Galbraith (2002):

$$s_{L_n} = \sqrt{Y_n + \frac{B_m}{k^2}} \tag{6.3}$$

where s_{L_n} is the estimated standard deviation of L_n.

All dose estimates in this work have been derived by linear interpolation between two regenerated dose points. Let R_1 and R_2 be the test dose corrected signals (L_1/T_1 and L_2/T_2) from two regenerated dose points with corresponding doses D_1 and D_2 respectively. The natural dose is then estimated to be:

$$D_n = \frac{R_n - R_1}{R_2 - R_1} (D_2 - D_1) + D_1 \tag{6.4}$$

where R_n is the natural test dose corrected signal.
The relative standard deviation of a sensitivity corrected luminescence signal R_i is given by:

$$\sigma^2_{R_i} = \left(\frac{s_{R_i}}{R_i}\right)^2 = \left(\frac{s_{L_i}}{L_i}\right)^2 + \left(\frac{s_{T_i}}{T_i}\right)^2 \tag{6.5}$$

where T_i is the luminescence signal from the i^{th} test dose.
Using the law of error propagation the standard deviation s_{D_n} on the estimated dose is calculated to be

$$s_{D_n}^2 = \left(\frac{D_2 - D_1}{R_2 - R_1}\right)^2 \times \left(s_{R_n}^2 + \left(\frac{1}{R_2 - R_1}\right)^2 \left[(R_n - R_2)^2 s_{R_1}^2 + (R_n - R_1)^2 s_{R_2}^2\right]\right) \tag{6.6}$$

where s_{R_n}, s_{R_1} and s_{R_2} are the estimated standard deviations of R_n, R_1 and R_2 respectively. No uncertainty on the beta source dose rate has been included in these calculations.

6.4 Dose distributions

To illustrate the nature of dose distributions, Figure 6.1 compares distributions measured using small aliquots (each of about 60 grains) with those using single grains of quartz for three different samples. The dose distributions are presented as histograms. In the insets to Figure 6.1 the OSL signal from the natural test dose is plotted against the equivalent dose. Thus, increasing values on the y-axis represent increasing precision. All three samples are thought to be well-zeroed and in all of them the small aliquot distributions are narrower (smaller relative standard deviation) than the corresponding single grain distributions; this is attributed to the presence of several light-emitting grains in each small aliquot, providing an averaged signal.

It is usually assumed that counting statistics account for the observed variability. If this turns out not to be true, the residual variability is then attributed to incomplete bleaching and/or differences in external micro-dosimetry. Figure 6.1a and 6.1b present results from an aeolian sand (lab code 010414). These data were obtained using small aliquots and single grain measurements respectively. The relative standard deviation (RSD) σ_D of the small aliquot data is 17%, whereas for the single grain distribution it is 36%. The variability in this sample might be attributed to incomplete zeroing, variations in external micro-dosimetry and/or counting statistics. Figure 6.1c and 6.1d display results from the heated stone (lab code 010413). The RSD σ_D for the small aliquot measurements is only 4%, but 26% for the single grain measurements. In this heated sample incomplete zeroing does not contribute to the variability, but differences in micro-dosimetry and counting statistics might still be able to account for the additional variance observed in the

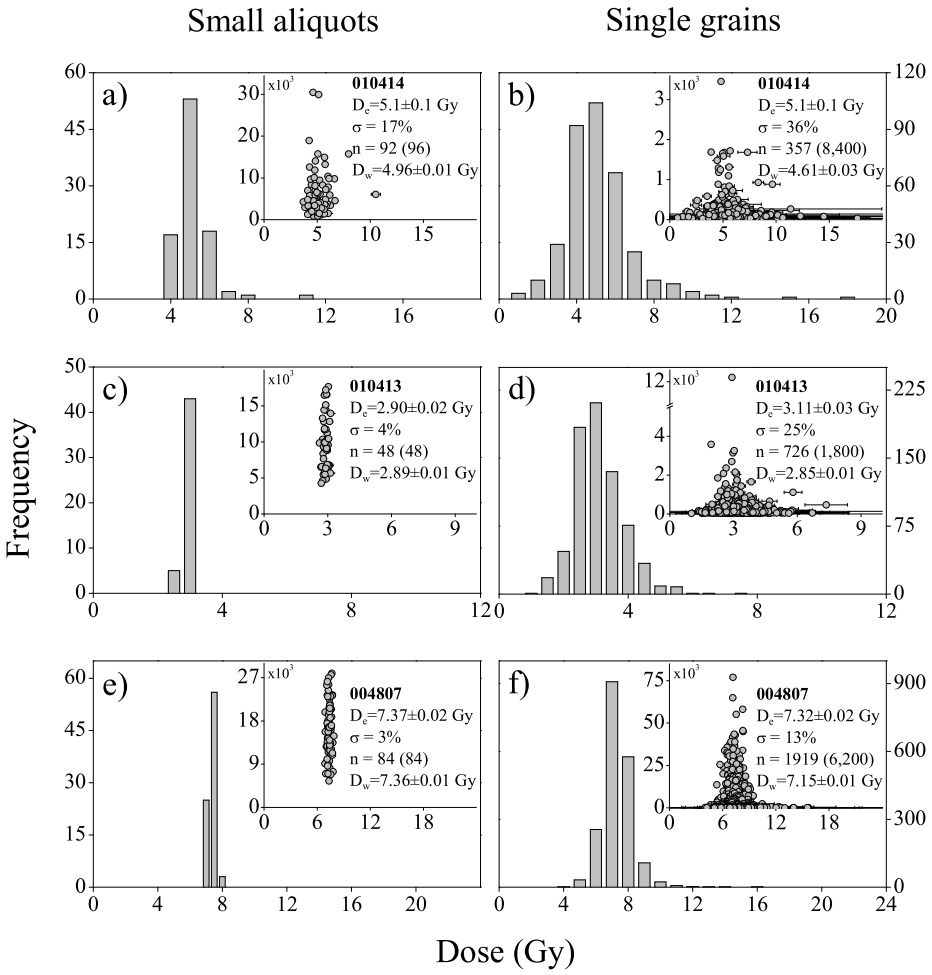

Figure 6.1: Comparison of measured dose distributions using small aliquots (**a**,**c**,**e**) each comprising of ∼60 grains with those from single grains of quartz (**b**,**d**,**f**) for three different samples, all believed to have been well-zeroed. Distributions are presented as histograms; the insets show the measured OSL signal from the natural test dose plotted against the equivalent dose. D_e is the mean equivalent dose and D_w is the weighted mean. n is the number of accepted results and the number in parenthesis give the number of measured aliquots. **a)**,**b)** Quartz extracted from an aeolian sand (lab code 010414). **c)**,**d)** Quartz extracted from a heated stone sample (lab code 010413). **e)**,**f)** Sedimentary quartz sample (lab code 004807) heated to 850 °C and gamma irradiated in the laboratory.

single grain data set compared to the small aliquot results. Figure 6.1e and 6.1f present results from the sedimentary quartz sample that was first heated to 850 °C, thereby excluding the contribution to the observed variance from incomplete zeroing. The sample was then irradiated using a 662 keV ^{137}Cs source in a geometry designed to ensure uniformity of dose (see section 6.2), thereby excluding any potential contribution from micro-dosimetry (spread in dose $< 1\%$). The sample absorbed a dose of 7.4 Gy. Despite close control over zeroing and dosimetry the RSD σ_D for the small aliquot measurements is 3%, and 13% for the single grain measurements. The objective of this work is to examine whether counting statistics and instrument reproducibility can account for all the observed variance in such ideal single grain dose distributions.

6.5 Modelling the expected variance

It is straightforward to estimate the uncertainty σ'_g in each estimate of dose arising from photon counting statistics only, because all dose estimates were derived by linear interpolation between two test-dose corrected OSL signals from two regenerated doses (see section 6.3). If the width of a dose distribution is dominated by the variance arising from the number of photons counted in each luminescence measurement, then the observed relative standard deviation σ_D of the distribution should be similar to the individual relative estimates of uncertainty in dose σ'_g (predicted relative standard deviation) i.e. a distribution containing dose estimates with individual σ'_g in the range of, say, 5 to 6% should have an overall observed RSD in the same range. A measured dose distribution will contain a range of individual standard deviations, thus it is necessary to divide the distribution into intervals according to σ'_g. If the RSD (σ_d) of the data contained within these intervals are calculated and plotted against σ_g (midpoint of interval) one would expect a directly proportional relationship of unit slope if the observed variance is dominated by counting statistics. However, the measurement instrument cannot be perfectly reproducible, and it is assumed that all measurements will have a count-rate independent relative variance (P_2^2) arising from this source. Thus, it is expected that the total (observed) relative variance is given by:

$$\sigma_d^2 = (P_1 \cdot \sigma_g)^2 + P_2^2 \tag{6.7}$$

where σ_g is the midpoint of the interval of individual RSD and σ_d is the observed RSD of the dose estimates in the interval. The constant (P_1) is

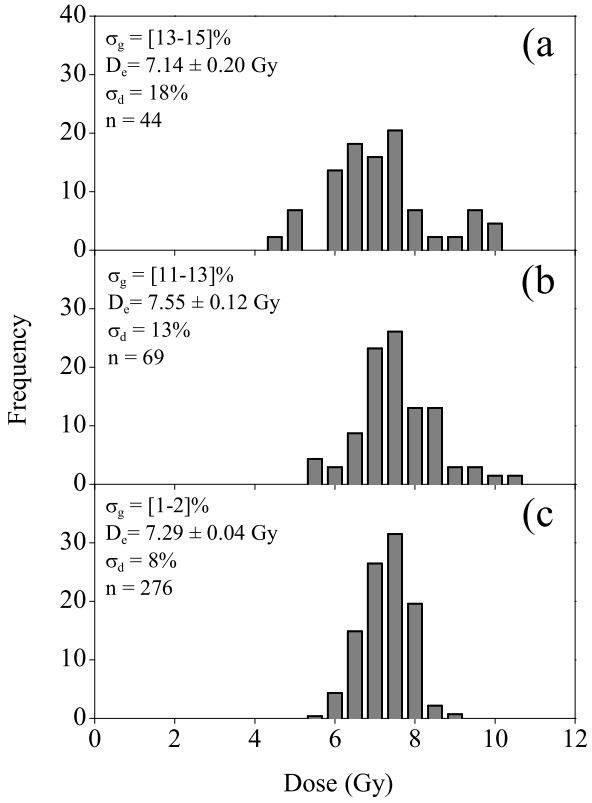

Figure 6.2: Dose histograms of the measured distribution shown in Figure 6.1f. Each histogram has been normalised to contain 100 grains. **a)**,**b)** and **c)** Results with observed individual relative standard deviations in the intervals 13-15%, 11-13% and 1-2% respectively.

expected to be unity, but it is defined to allow for the possibility of non-random loss of pulses in the counting electronics.

The dose histogram shown in Figure 6.1f includes all the single grain results from the gamma irradiated sample that met the selection criteria outlined in section 6.2. The distribution is symmetric and has an unweighted mean of 7.32±0.02 Gy (n =1919) and a RSD of 13%. The relative standard deviations of doses calculated for individual grains σ'_g (based only on counting statistics) range between 0.45 and 200%. The same data set is used to derive Figure 6.2, but Figures 6.2a, 6.2b and 6.2c show only results with individual relative standard deviations in the intervals 13–15%, 11–13% and 1–2%, respectively. These histograms have all been normalised to contain 100 grains. It is to be expected that the histograms should have the same mean value and that they

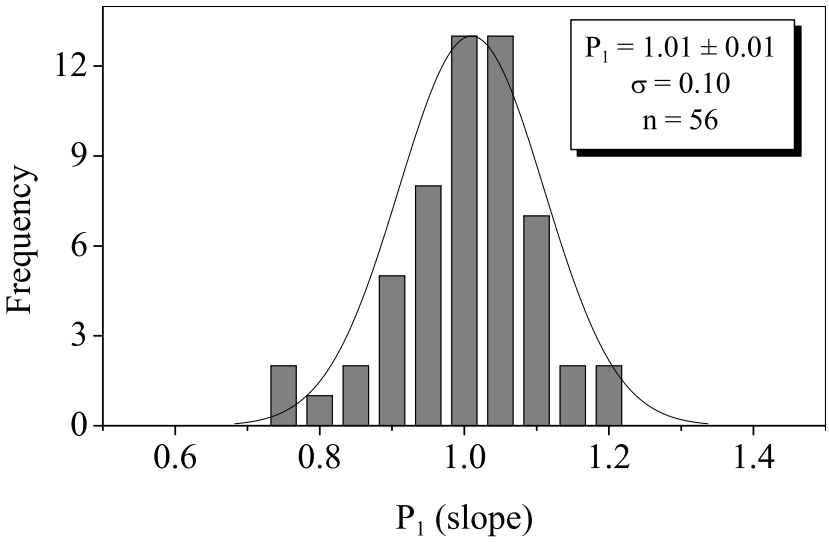

Figure 6.3: Histogram of the slopes P_1 (see Equation 6.7) for all data sets measured in this study.

will become taller and narrower as the RSD on individual results decreases. In Figure 6.2a and 6.2b, the observed RSD σ_d is similar to the range of individual estimates of uncertainty on each grain, but this is clearly not the case in Figure 6.2c, where the observed RSD σ_d is 8%, in contrast to the range of predicted individual standard deviation of 1-2%.
The uncertainty s_{σ_d} on an observed RSD σ_d derived from n points is given by $s_{\sigma_d} = \sigma_d/\sqrt{(2(n-1))}$ (Topping, 1955). In any regularly spaced set of uncertainty intervals, the number of results in each interval will vary, and so the uncertainty s_{σ_d} on the observed σ_d will also vary. To avoid this, the calculated standard deviations of the individual dose estimates are sorted in ascending order, and then grouped into bins containing 21 points. The standard deviation σ_d is then calculated for each bin. This results in a data set of observed σ_d values with a constant relative uncertainty $s_{\sigma d}$, but varying bin width (i.e. intervals of σ'_g). The value of σ_g used in equation 1 was that associated with the central value of σ_d in the interval (the 11^{th} point). The validity of Equation 6.7 has been tested by examining how close the slope P_1 is, on average, to unity. Figure 6.3 shows a distribution of all 56 calculated values of P_1 derived in this study. The mean is 1.011 ± 0.013, confirming that P_1 is indistinguishable from unity, as expected.

6.6 Gamma irradiation

The OSL signal from each grain in Figure 6.1f was integrated over the first 0.03 s of stimulation (2 channels) and corrected for the background contribution (using a signal based on integration over the last 0.2 s (12 channels)). In Figure 6.4a these data are displayed on a radial plot (Galbraith, 1990), where each result is plotted against its RSD, σ'_g. In a radial plot all points having the same dose estimate lie on a straight line connecting the origin on the y-axis and the dose value on the circular scale to the right. The use of the standardised estimate for the y-axis allows the $\pm 2\sigma$ band to be plotted (solid lines in Figure 6.4a). If the relative standard deviations σ'_g used on the x-axis of the radial plot adequately describe the variability in the data, 95% of the points should lie within this $\pm 2\sigma$ band. In Figure 6.4a the central dose value (dashed line) has been set to the calculated weighted mean of the sample. Only 60% of the results (displayed as filled circles) lie within the $\pm 2\sigma$ band, in contrast to the expected 95%. No difference was found setting the central dose value to the arithmetic mean. In Figure 6.4b the OSL signal from the natural test dose (a measure of the sensitivity) is plotted against the estimated equivalent dose. Those results within $\pm 2\sigma$ of the weighted mean are displayed as filled circles (same points as in Figure 6.4a); the points outside $\pm 2\sigma$ as open circles. It is obvious from both Figure 6.4a and 6.4b that the observed variability is significantly larger than that expected from counting statistics alone. In Figure 6.4c the observed RSD (σ_d) is plotted as a function of the predicted RSD (σ_g). The best fit of Equation 6.7 to these data is also shown. The slope of the curve is 1.02 ± 0.05 and the intercept with the y-axis is $7.8 \pm 0.2\%$. Thus, from the model used to construct Equation 6.7, it might be deduced that the 7.8% intercept corresponds to instrument variability. The next section describes experiments designed to measure this component of variability directly.

6.7 Instrument reproducibility

6.7.1 Reproducibility of an OSL measurement

The instrument reproducibility of the Risø single grain reader was examined by repeatedly dosing, preheating and stimulating a single grain disc loaded with 100 grains. In each measurement cycle the sensitivity of each grain changed slightly; to account for this sensitivity change a test dose correction has been made in the usual manner (Murray and Wintle, 2000). A measure of the instrument reproducibility was obtained by subtracting, in quadrature,

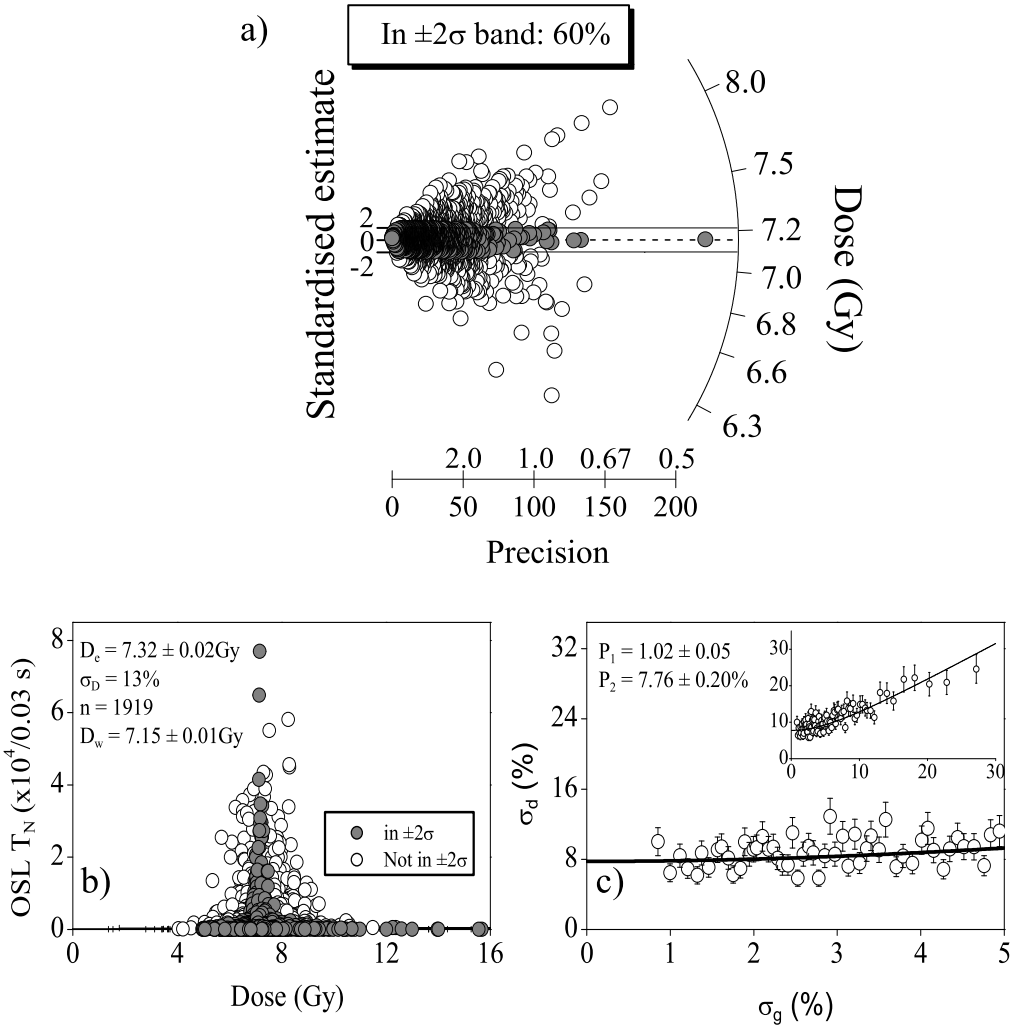

Figure 6.4: Laboratory irradiated sample (lab code: 004807) containing a well-known gamma dose. Estimates of uncertainty on the individual results have been based only on counting statistics and the OSL signals were integrated over the first 0.03 s of stimulation. **a)** Radial plot of the dose estimates. Filled circles represent those data points that are consistent with the calculated weighted mean ($\pm 2\sigma$), whereas the open circles are the remainder. Only 60% of the results fall within the $\pm 2\sigma$ band (filled circles) in contrast to the expected 95%. Note: the x-axis has two scales; lower scale shows the precision and the upper scale shows the relative standard deviation RSD. **b)** Shows the same data as in a). The integrated OSL signal from the natural test dose plotted as a function of measured dose. The filled circles represent points consistent with the calculated weighted mean (same as in a)). **c)** The observed RSD as a function of the predicted RSD of the data set shown in a) and b). The inset shows the full curve. The solid line is the best fit of Equation 6.7 to the data.

the uncertainty calculated to arise from counting statistics from the observed RSD, to give 100 estimates of the instrument reproducibility. The weighted mean of these 100 estimates (each involving two OSL measurements) is 2.28± 0.03%. In the SAR protocol three test-dose corrected OSL measurements are needed to estimate the unknown dose. Thus, the scatter arising from instrument reproducibility alone should be approximately 4% ($\sqrt{3} \times 2.28\%$), which is significantly lower than the 8% determined in the gamma irradiation experiment described above.

6.7.2 Dose recovery

To confirm this preliminary estimate of instrument reproducibility a dose recovery experiment was carried out in which the sample was loaded into single grain discs, bleached using the green laser and then given a beta dose of 7 Gy in the single grain reader. The grains were then measured using the SAR protocol. The results from this experiment, calculated using the first 0.03 s of stimulation, are shown in Figure 6.5a and 6.5b. Compared to the results from the gamma irradiated sample (Figure 6.4) the plot of the natural test-dose OSL against the estimated dose shows a significant reduction in scatter (Figure 6.5a) – especially among the well-known points; plotting the observed RSD σ_d against the predicted RSD σ_g (Figure 6.5b) gives an intercept of $4.87 \pm 0.10\%$, only a little larger than the ∼4% expected from instrument reproducibility.

The single grain measurement system illuminates each grain in turn by steering a focused laser spot from one grain to another. This process is likely to introduce error, and so instrument reproducibility was also estimated using single grains measured on a conventional Risø luminescence reader (model Risø TL/OSL-DA-15). Here, single grains of quartz from the gamma irradiated sample were mounted at the centre of flat aluminium discs (one grain per disc) and bleached using blue LEDs. They were then given a beta dose. This dose was measured in the usual way, using the SAR protocol. The OSL signal from each grain was integrated over the first 0.8 s of stimulation (total stimulation time was 40s) and corrected for the background contribution (using a signal based on integration over the last 16 s). Plotting the observed RSD (σ_d) against the predicted RSD (σ_g) gave an intercept of $2.6 \pm 0.2\%$ (data not shown). This is significantly lower than the ∼5% obtained above using the single grain reader, and suggests that the more complex stimulation source in the single grain system does introduce some additional error.

The stimulation source in the conventional Risø reader is an array of blue LEDs, focused to illuminate the entire disc (9.7 mm in diameter) and so provides a uniform illumination of the sample. In the single grain reader

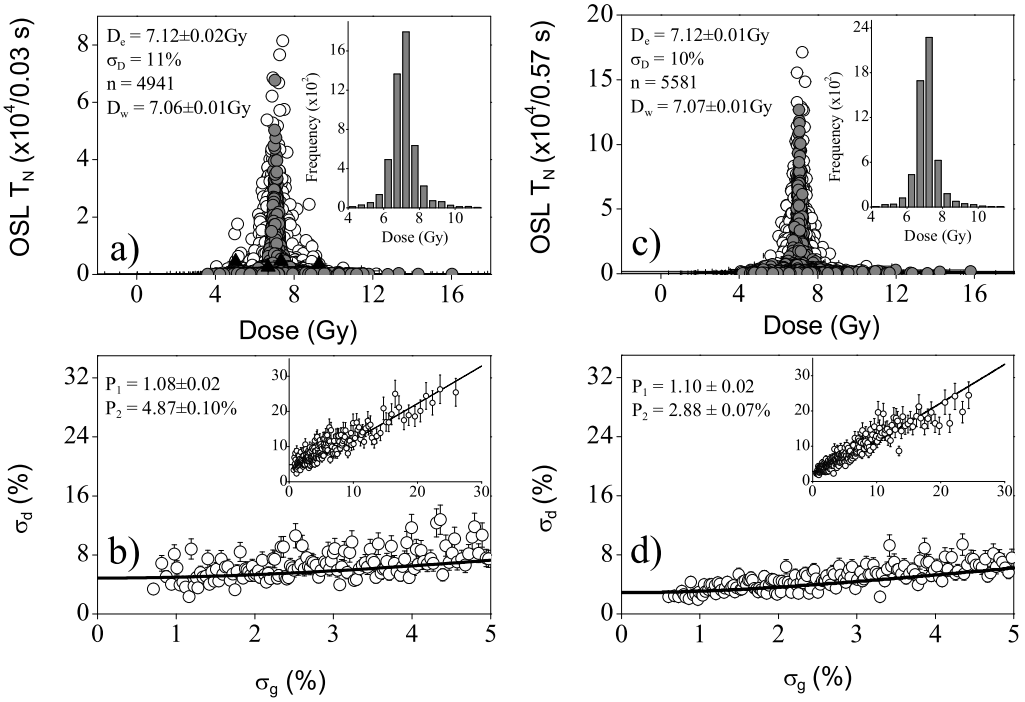

Figure 6.5: Results from a dose recovery experiment, in which a laboratory heated and irradiated sample was bleached in the reader, given a beta dose and then measured using the SAR protocol. **a)** The OSL signal is integrated over the first 0.03 s of stimulation. Only 72% of the results (filled symbols) are consistent with the calculated weighted mean. Four results are shown as filled triangles (from left to right): D18G40, D9G58, D4G79 and D23G14. Also see Figure 6.6. **b)** Observed relative standard deviation (RSD) as a function of the predicted RSD and the best fit to the data from a) using Equation 6.7. **c)** Same data set as above but the OSL signals have been integrated over the first 0.57 s of the stimulation time. 77% of the results are statistically consistent with the calculated weighted mean compared to the 72% in a). Thus, increasing the integration interval reduces the observed variability. **d)** Observed RSD as a function of the predicted RSD and the best fit to the data from c) using Equation 6.7.

a tightly focused green laser ($< 20\,\mu$m in diameter) is steered to the centre (standard deviation of $7\,\mu$m) of the grain hole before being switched on. Internal scattering within the grain hole is then relied on to illuminate the grain. If this scattering is not completely uniform and/or reproducible, one might expect the observed decay rate of the OSL signals from a given grain to vary slightly from run to run, as different volumes of the grain are illuminated with slightly different intensities from one measurement to another. In section 4.5.2 (Laser reproducibility) it was determined that the laser power fluctuates with a relative standard deviation of approximately 2%. If this is

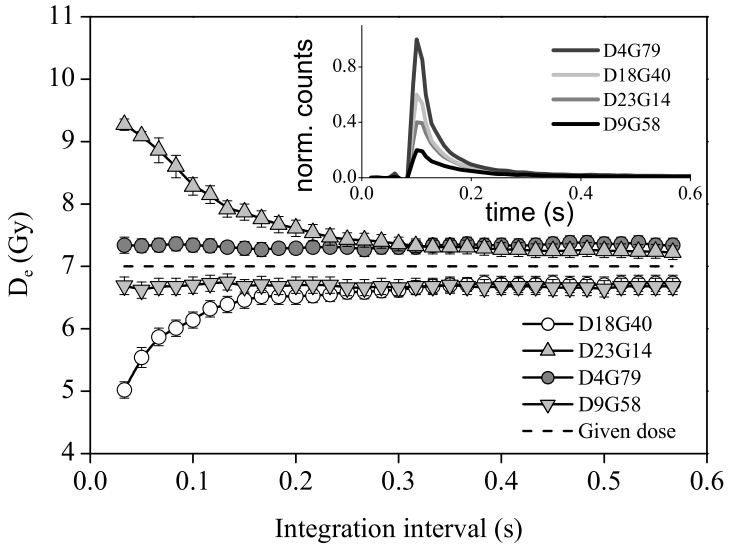

Figure 6.6: Dependence of estimated dose on OSL signal integration area for 4 different grains (shown as triangles in Figure 6.5a). The normalised OSL decay curves for the natural signal for the grains are shown in the inset.

the only additional source of variation in a single-grain reader compared to a conventional reader, integration of the full single grain OSL curves would be expected to reduce any such effect. In Figure 6.6 the dependence of estimated dose on signal integration area is shown for four different grains (see also Figure 6.5a). One grain (D18G40) provided a dose estimate ($D_e = 5.02 \pm 0.13$ Gy) significantly lower than the mean, when only the first 0.03 s of the stimulation time was included. However, if > 0.5 s of stimulation is included, the dose estimate is 6.73 ± 0.18 Gy, much closer to the given dose of 7.0 Gy. In another case (D23G14) the original dose estimate was 9.27 ± 0.11 Gy, much larger than the expected value, but including > 0.5 s of stimulation brings the dose estimate down to 7.22 ± 0.16 Gy. In the third and fourth cases (D4G79 and D9G58) no significant dependence on the length of integration interval is observed. These data suggest that it should be possible to improve the observed dose distribution (and thereby bring down the calculated P_2 value) by simply integrating a greater part of the measured signals. Although making use of only the first 0.2 s of stimulation in the signal integration removes most of the dose dependence on integration interval, the remainder of this study employs the first 0.57 s. The data displayed in Figure 6.5c, and 6.5d are derived from the same experimental results as Figure 6.5a, and 6.5b, but use the first 0.57 s of stimulation. The overall standard deviation (σ_D) has only decreased by about 1%, but it is clear that the scatter

among the more precisely known results has decreased significantly. Plotting the observed RSD (σ_d) against the predicted RSD (σ_g; Figure 6.5b) provides an intercept P_2 of $2.88 \pm 0.07\%$, consistent with the intercept determined using the conventional reader ($2.6 \pm 0.2\%$). Increasing the integration interval on the instrument reproducibility data set (section 6.7.1) in the same manner reduces the estimate of instrument reproducibility from 2.3% to about 1.7%, which implies a minimum P_2 value of about 3% ($\sqrt{3} \times 1.7\%$), consistent with the observed value of about 2.9%. Increasing the integration interval on the data set obtained using the conventional reader had no significant effect ($P_2 = 2.8 \pm 0.2\%$). Returning to the data set of Figure 6.4, the intercept obtained when measuring the gamma irradiated sample on the single grain reader using only the first 0.03 s of the signal was 7.8%. Increasing the integration interval to include the first 0.57 s of the stimulation time decreases the intercept to $7.2 \pm 0.2\%$. However, it was shown above that instrument reproducibility contributes only about 2.9% to the scatter in dose estimation, which leaves a further 6.6% ($\sqrt{7.2^2 - 2.9^2}$) unaccounted for.

6.7.3 Source uniformity

One explanation for the increase in scatter between the beta and the gamma experiments could simply be that the beta source is not delivering a spatially uniform dose. Spooner and Allsop (2000) examined the spatial variation of dose-rate from a ^{90}Sr/^{90}Y beta source and found that the dose rate could vary by 15% across a 10 mm sample area for a source/sample distance of 15 mm. A non-uniform beta dose rate would not affect the beta experiment used to examine instrument reproducibility, because the rotation of sample discs during a standard SAR measurement sequence is usually small ($< 2\,^\circ$), but it could have a large effect on the comparison between beta and gamma irradiations. To investigate the effect of source non-uniformity, the mean dose measured in each sample hole using the gamma irradiated quartz was calculated, using data from 3500 different single grain measurements (i.e. an average of 35 results per grain hole). All discs were within 1% of the same angular orientation on the sample wheel. These data provide a calibration dose rate for each grain location. The standard deviation of all the averaged measurements is about 5%, which means that beta source non-uniformity cannot contribute more than $\sim 5\%$ to the overall variability. Applying the 100 different source calibrations to the individual results in the gamma irradiated data set reduced the calculated intercept from $7.2 \pm 0.2\%$ to $6.2 \pm 0.2\%$, so it is still not possible to account for 5.5% ($\sqrt{6.2^2 - 2.9^2}$) of the observed uncertainty in the data.

To complete the testing of the reliability of the single grain reader, the dose distribution from 552 single grains of the gamma irradiated quartz was measured on a conventional Risø reader using blue LEDs as the stimulation source (one grain on each disc). The intercept derived from this dose distribution was $6.0 \pm 0.3\%$, consistent with the intercept determined using the single grain reader. Because all the grains are centrally placed on the sample disc, source variability should not contribute to this intercept, and so agreement between the intercept obtained using the single grain reader ($6.2 \pm 0.2\%$) and the conventional reader ($6.0 \pm 0.3\%$) confirms that the two principal additional sources of variability arising from the use of the single grain reader have been identified, i.e. non-uniform stimulation and non-uniformity of beta dose. The first of these can be avoided in these experiments by increasing the integration time; the second by using a calibration table. The remainder of this chapter is concerned with the identification of the origins of the additional 5.5% uncertainty.

6.8 Other possible sources of variance

6.8.1 Acid treatment

One of the differences between these controlled experiments and the measurement of natural samples is that the natural samples are dosed before any chemical treatment in the laboratory. Although not directly relevant to the sources of variance in the gamma irradiated sample, it is important to demonstrate that the additional variance does not arise because of the absence of chemical treatment. Therefore, part of the gamma irradiated sample was treated with HF (15 min) and HCl (40 min) after dosing, but before measurement. Integrating the first 0.57 s of the decay curves and applying the correction for source non-uniformity gave a slope of 0.99 ± 0.05 and an intercept of $6.4 \pm 0.2\%$. This intercept is indistinguishable from the result obtained using the gamma irradiated sample with no chemical treatment after the irradiation. It is concluded that chemical etching of grain surfaces does not contribute to the variance in the results.

6.8.2 Handling – gamma irradiation

Another significant difference between the beta (section 6.7.2) and the gamma experiment (section 6.6) is the handling involved. In the beta experiment the grains were irradiated after placing them in the single grain discs whereas in the gamma experiments the grains were irradiated in bulk and then loaded

into the single grain discs. In loading single grain discs there is a significant amount of handling of individual grains. In order to investigate if this has any effect on the observed dose distribution an experiment was performed in which the grains were gamma irradiated after loading – in this way disturbance of the grains was kept to a minimum. An unirradiated heated quartz sample was loaded into single grain discs, which were then placed in custom-made aluminium containers (each taking up to 4 single grain discs) with a 3 mm lid pressed against each disc to provide build-up of the secondary electron flux and to ensure that grain movement is minimal. The discs were irradiated using a ^{137}Cs gamma beam in such a way that all grains received the same exposure. Finally, the discs were measured in the usual manner in the single grain reader. After correction for beta source non-uniformity these measurements gave a slope of 0.99 ± 0.06 and an intercept of $6.3 \pm 0.3\%$, indistinguishable from the result for the gamma irradiation performed in bulk (Figure 6.4). The same grains were then bleached and given a beta dose in the reader. The discs were then replaced in the sealed aluminium containers and shaken vigorously, before repeating the measurement in the Risø single grain reader. Plotting the observed RSD (σ_d) against the predicted RSD (σ_g) gave a slope of 0.86 ± 0.06 and an intercept of $4.7 \pm 0.2\%$, which is significantly higher than the intercept determined in the dose recovery experiments. Finally, the same grains were bleached, given a beta dose in the reader, and then measured without any disturbance of the grains. This experiment gave a slope and intercept of 1.05 ± 0.04 and $1.7 \pm 0.2\%$; this intercept is actually slightly lower than found in the earlier beta dose recovery experiments (section 6.7.2). Thus, it is concluded that the increase found as a result of shaking the grains is probably real.

6.8.3 Handling – beta irradiation

To further investigate the effects of handling, a sample was beta irradiated in bulk. It was first mounted on aluminium discs using a 3 mm spray mask size and silicone oil as an adhesive. The sample was given a beta dose of about 6 Gy, the grains washed off the discs with acetone, and then loaded into single grain discs. If handling is not a contributing factor to the observed variance in the data, this experiment ought to return the same answer as the dose recovery experiment described above. However, the data gave a slope of $P_1 = 1.07 \pm 0.06$ and an intercept of $P_2 = 7.6 \pm 0.2\%$. The beta source calibration table showed that the standard deviation of the beta doses delivered to grain positions located within a 3 mm diameter spot at the centre of the disc is 2%. The subsequent irradiations in the single grain discs can therefore be corrected for beta source non-uniformity as before, although

correction does not change the results significantly, i.e. $P_1 = 1.16 \pm 0.06$, and $P_2 = 7.7 \pm 0.2\%$.

To interpret the handling experiments, the first assumption is that the gamma irradiations provide a uniform dose distribution, independent of grain size and orientation. This is likely, given the results of Monte Carlo modelling (section 6.2) and the presence of build-up material (glass in section 6.2 and aluminium in section 6.8.2) of very similar mass attenuation and absorption characteristics compared to quartz. Keeping the grains in – as far as possible – fixed positions did not change the apparent scatter in dose in the gamma irradiated grains. However, deliberately introducing movement did apparently increase the width of the distributions from the same grains following a subsequent beta irradiation (section 6.8.2). Similarly, beta irradiating grains on a separate disc, and then moving them into the holes on a single grain disc also increased the distribution width. These observations are all consistent with the concept of a non-uniform beta dose within a quartz grain. Wintle and Murray (1977) determined that $\sim 200\,\mu$m of quartz is required to achieve isotropic electron flux, when an unattenuated beta spectrum from ^{90}Sr/^{90}Y source crosses the air/quartz interface. Beta irradiations in the Risø reader are performed without the presence of build-up material. It is thus likely that the degree of isotropy (and thus dose deposition) will be dependent on grain shape and orientation, although this will be compensated to some degree by the aluminium of the sample disc surrounding the grain on all sides except the top. This hypothesis is examined in the next section.

6.8.4 Dose build-up

Wintle and Murray (1977) measured a fractional depth-dose curve for a ^{90}Sr/^{90}Y beta plaque source using aluminium absorbers placed directly on top of fine grains of CaF_2 (natural) on an aluminium disc (see inset in Figure 6.7; open symbols). The initial rise in the curve is steep; indicating that – if the curve applies to the Risø single grain reader beta irradiations – small differences in grain size and shape may result in the deposition of varying doses from grain to grain. Wintle and Murray found that the depth-dose curve flattens off at a depth of between 100 and 200 μm, suggesting that placing an aluminium absorber of that thickness in front of the irradiator would result in more uniform dose deposition. However, the depth-dose curve measured by Wintle and Murray was obtained using an open source with no collimation and thin dosimeters ($4 - 11\,\mu$m). The irradiation geometry in the Risø reader is different; there is a 125 μm thick beryllium window in front of the source with a 2 mm thick steel ring above the Be window and a 1 mm thick brass ring beneath it; both 10 mm in internal diameter. These differences in

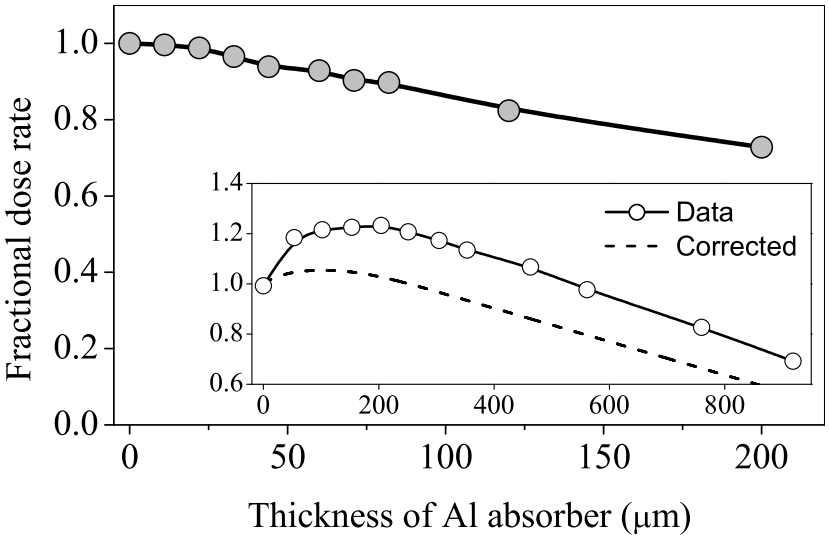

Figure 6.7: Fractional dose-depth curve measured using the Risø reader using blue LEDs and $212-250\,\mu$m grains in single grain discs. The inset shows the data obtained by Wintle and Murray (1977) and the same data averaged over a mean path length of $133\,\mu$m. See text for details.

irradiation geometry means that the curve measured by Wintle and Murray may not be applicable to beta irradiations performed in the Risø reader. The dose-depth curve dependency has been measured directly by using different thicknesses of aluminium absorbers placed directly underneath the irradiator, with single grains in a standard single grain disc as dosimeters (Figure 6.7). The light stimulation source used was blue LEDs, stimulating all grains in the disc at once. This experiment is quite different from Wintle and Murray's in that the dosimeters used here integrate from the exit surface of the aluminium absorber to approximately $200\,\mu$m, but this is the geometry relevant to this problem. The curve measured by Wintle and Murray can be corrected (to first order) by averaging. In order to calculate this the average grain is assumed to be spherical with a radius of $100\,\mu$m, which means that the average path length through the sphere is $\sim 133\,\mu$m (ICRU Report 33, 1980). Thus, averaging the first $133\,\mu$m ought to give a ratio comparable to the ratio determined in this experiment. This curve is plotted in the inset to Figure 6.7 as a dashed line. The increase in dose for small absorber thickness is now very small, but still detectable. In contrast, the curve measured using the Risø reader shows no build-up region, suggesting that scattering in the beryllium window and collimation system softens the beta spectrum sufficiently to achieve a more isotropic electron flux at the air/quartz interface.

However, the deposited dose will depend on grain size and orientation due to attenuation of the flux as it passes through the grains. Using the fractional dose-depth curve in Figure 6.7 it is possible to estimate the relative dose deposited in grains of different shapes, and then derive an estimate of the effect that different grain sizes/shapes will have on the distribution. Determination of this contribution to variability in the data has been attempted by considering the range of doses delivered to cylinders of varying radii, with the long axis lying normal to the beta source face. From visual observation it is very unusual that the width of grains is less than half their length, and grains are constrained to have the largest characteristic length lying between 212 and 250 μm (the sieve interval). Using the dose-depth curve of Figure 6.7, the doses deposited in cylinders of radius between 50 and 100 μm have been considered, and then these doses were normalised to that absorbed by a 115 μm radius sphere. The RSD of such doses is 2%; this is small compared to the $\sim$ 6% RSD unaccounted for in the controlled experiments using gamma irradiated quartz (section 6.7.3). If the distribution of luminescence centres within grains is uniform then the dose variation with depth is very unlikely to account for a large fraction of the residual variability, although these primitive calculations are not regarded as definitive.

6.9 Small aliquot results

Figure 6.1e shows the dose distribution for small aliquot measurements of the laboratory heated and gamma irradiated sample (lab code 004807). The distribution has a RSD of 3%; significantly less than the 13% obtained for the single grain dose distribution. If these data are used to plot the observed RSD σ_d as a function of predicted RSD σ_g, the calculated intercept (P_2) is 2.5 ± 0.6%. This is indistinguishable from the measured instrument reproducibility of 2.6 ± 0.2%. The large uncertainty on the small aliquot intercept (P_2) can be explained by the fact that only 84 small aliquots were measured. Each interval/bin has throughout this study contained 21 results, giving in this case just 4 intervals. Reducing the number of results in each bin to 11 (i.e. 8 intervals) gives an intercept of 2.6 ± 0.2%, again consistent with the observed instrument reproducibility. Thus, it is concluded that in multi-grain aliquots, counting statistics and instrument reproducibility alone can account for the observed variance in the data. This is not true for single grains.

6.10 Conclusion

One of the major advantages of using single grains in OSL dose determinations is the possibility of identification and rejection of poorly-zeroed grains. However, in order to be able to identify the well-zeroed part of the dose distribution, the characteristics of such a distribution must be predictable. This study used a heated and uniformly gamma irradiated quartz sample to ensure that incomplete bleaching and non-uniform dosimetry do not contribute to the observed variance in the dose distribution. It has been shown that the observed variability in the data is consistent with the sum (in quadrature) of a component which depends on the number of photons detected from each grain, and a fixed component independent of light level. The latter is in turn made up of several quantified contributions, including spatial variation in beta source activity, variation in illumination intensity from measurement to measurement, and other sources of instrument reproducibility such as sample positioning, measurement timing, etc. Taken together, all these sources contribute some 5.6% to the total residual uncertainty of 7.8% left when the contribution from counting statistics is removed. Thus there remains about 5.5% ($\sqrt{7.8^2 - 5.6^2}$) unaccounted for. Some of this probably arises from variable attenuation of the beta particles through the sample; this effect is thought to be small compared to the remaining unaccounted variability, but definitive calculations remain to be undertaken.

It is concluded that, at this stage, the dose in a single grain of quartz cannot be measured to better than about 6.2%, no matter how bright the OSL signal is. In natural samples, it is unwise to integrate the whole OSL signal, because of the contributions from various slowly bleaching components, and so in routine use only the first part of the OSL signal should be used. Unfortunately the illumination intensity in the single grain reader is not completely reproducible, and so the use of only the first part of the OSL signal adds further variability to measurements, to give an overall standard deviation of about 7.2%. For the beta source, if corrections are not made for the spatial variability, the minimum possible standard deviation in a single grain measurement becomes 7.8%. This latter component is likely to be very dependent on individual irradiation sources; it is known that more recent beta sources (since about 2000) can have spatial variations considerably larger than the 5% measured on the old source used here. This extra variance is not present in small aliquot data, for which it is sufficient to allow for instrument reproducibility (2.9%) in addition to uncertainties arising from fluctuations in the number of photons counted. In conclusion, in interpreting single grain dose distributions, it is recommend that an uncertainty of at least 8% is added to all uncertainties based on counting statistics alone. This implies that all

grains giving more than a few hundred counts in the initial part of the OSL signal should be given equal weight in subsequent dose distribution analysis.

7 OSL Dosimetry using Concrete Samples

7.1 Introduction

In this chapter dose distributions derived from OSL measurements of single grains of quartz extracted from two industrially produced concrete blocks, one unirradiated and the other irradiated normal to one face in the laboratory using ^{137}Cs gamma photons are presented.

In a previous study (see Chapter 5), the distribution of doses in grains extracted from a bag of premix concrete was investigated using both small aliquots and single grains of quartz. However, this dry concrete mixture was produced for the retail "do-it-yourself" market, and is not necessarily representative of the concrete used in industrial buildings. In the present study single grains of quartz extracted from cast concrete blocks obtained directly from the manufacturer are examined. The quartz grains were extracted separately from both the bulk and the surface of the concrete blocks, because the surfaces were expected to be better bleached as a result of light exposure during storage, transportation and subsequent use as building material. Nevertheless, most of the analyses in this study have focused on the bulk material, because most industrial concrete is poured, and cast *in situ*. Grains were extracted both from the unirradiated concrete block and the irradiated concrete block. The OSL dose-depth profile for the irradiated block was determined by measuring the dose distributions from single quartz grains extracted from slices taken across sections of the block. A standard statistical criterion was used to identify the well-bleached grains in the distributions, and the resulting dose-depth profile has been validated by comparison with that predicted using Monte Carlo (MCNP-code) calculations. Finally the minimum detection limits for this material have been derived.

7.2 Experimental details

A $6 \times 14 \times 20$ cm concrete block was incorporated in the centre of a concrete wall constructed in front of a laboratory standard ^{137}Cs point source, so that the 6×14 face of the block was exposed at the front face of the wall. The wall was irradiated such that its face received a dose of 5.0 Gy. The block was then sliced, normal to the direction of the gamma beam, into 14 sections each $\sim$ 15 mm thick and quartz grains were extracted from the individual sections by treatment with HCl and HF followed by sieving. Large aliquots of the quartz extract were screened for feldspar contamination using IRSL stimulation and the HF treatment repeated if any detectable IR signal was measured. Single grain measurements were carried out on quartz grains extracted from four of these concrete slices, using an automated Risø reader fitted with a single grain laser attachment (Bøtter-Jensen et al., 2003). The stimulation light source is a 10 mW $Nd:YVO_4$ solid-state diode-pumped laser emitting at 532 nm, which is focused sequentially on to each of 100 grains mounted on a special aluminium sample disc. Laboratory irradiations were made using a calibrated ^{90}Sr/^{90}Y beta source mounted onto the reader. All measurements were carried out using the SAR protocol (Murray and Wintle, 2000) with a preheat of 200 °C for 10 s, a cut-heat of 160 °C and a test dose of 4 Gy.

7.3 Results

7.3.1 Unirradiated concrete block

Figure 7.1 displays a histogram of the dose results obtained from single grain measurements on the $212 - 250\,\mu$m quartz fraction extracted from an unirradiated portion of bulk concrete (i.e. not including surfaces). A total of 14,400 grains from this sample were measured, of which only 236 grains gave a detectable light signal (defined here as grains with uncertainties on the natural (i.e. first) test dose, based on photon counting statistics, of $< 20\%$). The estimated doses range from -0.9 ± 0.7 Gy to 137 ± 59 Gy and the average dose was calculated to be 26.5 ± 1.8 Gy ($n = 236$). The dose distribution is clearly asymmetric indicating that the sample was poorly bleached.

However, in a histogram all data points are given equal weight, irrespective of the precision with which they are known. A meaningful histogram ought to only display data points with similar uncertainties, and so a stricter selection criterion has been applied. The histograms in Figure 7.2 contain only dose measurements that have either a relative uncertainty (based on counting statistics) of less than 15% or an absolute uncertainty of less than 0.5

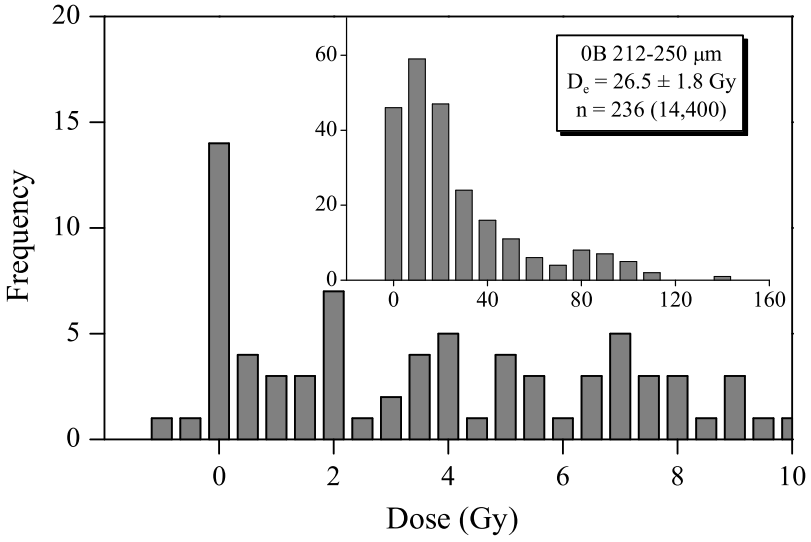

Figure 7.1: Natural doses measured from single grains of quartz ($212-250\,\mu$m fraction) extracted from an unirradiated portion of the bulk concrete. All results included in the figure have uncertainties on the natural test dose, based on photon counting statistics, of $< 20\%$. The average dose is 26.5 ± 1.8 Gy ($n = 236$).

Gy. Single grain measurements on heated quartz given a well-defined gamma dose in the laboratory have shown that the dose in a single grain cannot be determined to better than approximately 10% regardless of grain sensitivity (see Chapter 6). If special attention is given to source non-uniformity corrections and signal integration the additional error can fall to approximately 6%. Such corrections were not made in this data set. Thus, all data points in Figure 7.2 have an additional 10% uncertainty combined in quadrature with the uncertainty derived from photon counting statistics. As a result the overall uncertainty associated with each data point in the rest of this study ranges between 10 and 18%. Restricting accepted equivalent dose estimates only to these with this range of associated uncertainties reveals that the grain population is not as poorly bleached as first assumed (compare Figures 7.1 and 7.2b). The natural distributions for grain sizes of: $150-180\,\mu$m, $212-250\,\mu$m and $355-400\,\mu$m are shown in Figure 7.2a, 7.2b and 7.2c, respectively. One might expect larger grain sizes to give a better recovery (i.e. percentage of grains giving detectable signals) because of the larger volume of the grain, but only a slight improvement was found, suggesting that grain volume is not an important factor controlling grain sensitivity. It was also expected that different grain sizes might be bleached to different degrees, but no significant

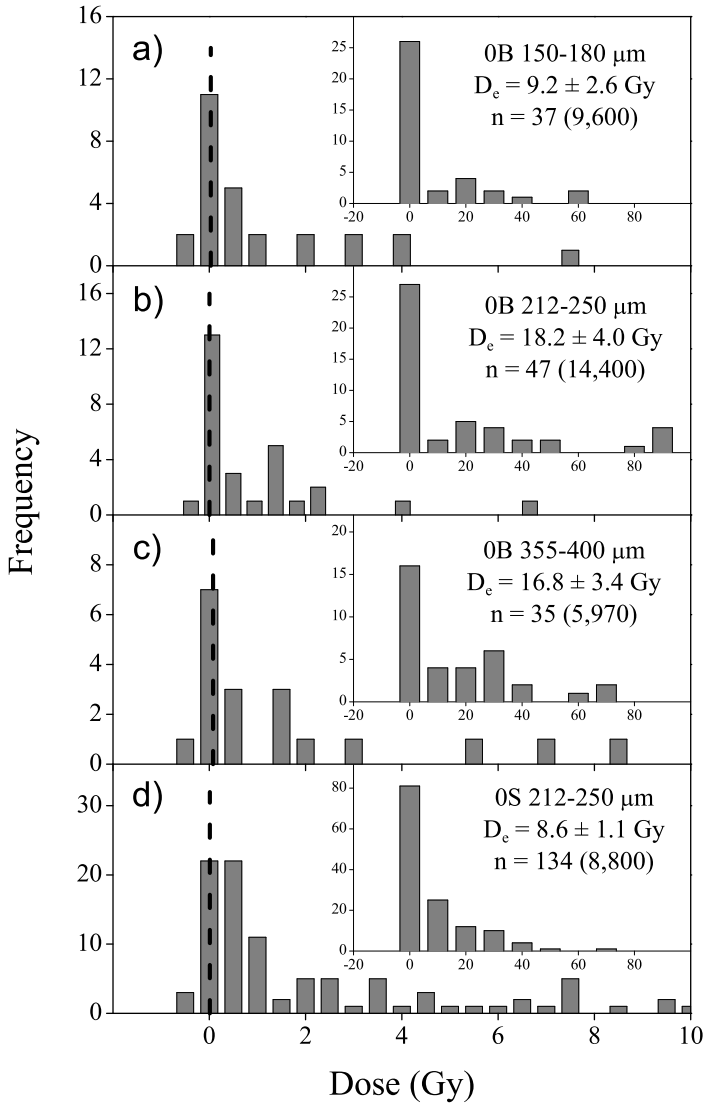

Figure 7.2: Dose histograms of the natural dose distribution in the concrete. All results included here have either a relative uncertainty (counting statistics) of less than 15% or an absolute uncertainty of less than 0.5 Gy. **a)**, **b)**, **c)** Histograms of the natural doses measured in single grains of quartz extracted from an unirradiated portion of the bulk concrete for grain sizes of $150-180\,\mu$m, $212-250\,\mu$m and $355-400\,\mu$m, respectively. **d)** Dose histogram for the surface layer of the block. The dashed lines represent the estimated dose of the well-bleached grains.

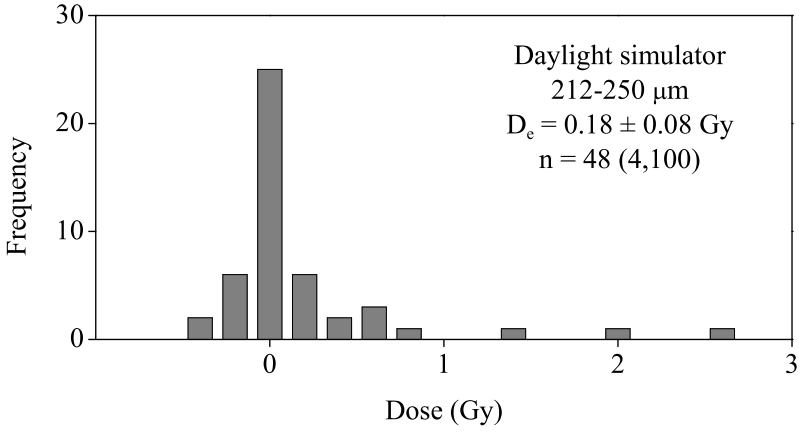

Figure 7.3: Dose histogram showing the results obtained from the portion of the bulk unirradiated sample, which was bleached under a daylight simulator for 1 hour. The average dose is 0.18 ± 0.08 Gy ($n = 48$).

differences between the measured distributions were found. All distributions show a significant number of grains close to the origin, indicating that these grains were completely zeroed before or during the manufacturing process. A dose histogram for the quartz extracted from the surface layer of the block (Figure 7.2d) is also presented. It was expected that the grains from the surface layer would be better bleached than the grains extracted from the bulk material, but no significant difference between the surface and bulk results was found. The most likely explanation is that in extracting the grains from the surface layer, too thick a layer of grains was included, with many originating from the bulk of the brick, rather than the surface.

To demonstrate the appearance of an ideally bleached distribution a portion of the $212 - 250\,\mu$m fraction from the bulk unirradiated sample was illuminated under a daylight simulator for 1 hour. The resulting dose histogram is shown in Figure 7.3. The average dose is 0.18 ± 0.08 Gy ($n = 48$) and the weighted mean 0.016 ± 0.008 Gy. This experiment demonstrates that if grains are well-bleached, we are able to accurately and precisely measure a zero dose (0 Gy), suggesting that the doses close to zero in Figure 7.2 are meaningful.

7.3.2 Laboratory irradiated concrete block

The data from quartz grains extracted from the irradiated concrete block are presented as dose histograms (all dose estimates with a relative statistical

uncertainty $< 15\%$ or an absolute statistical uncertainty $< \pm 0.5$ Gy) as well as radial plots (all grains giving a natural test dose response with a relative uncertainty of $< 20\%$) in Figure 7.4. All results have an additional uncertainty of 10% added in quadrature. For the first slice (1B $\sim$ 2 mm into the block) the first part of the distribution is centred on approximately 5 Gy, which is consistent with the leading edge of the radial plot. As we move further into the block, the lowest part of the histogram moves closer and closer to zero (the dashed lines represent the estimated added doses). It should be noted that all four radial plots display a well-defined upper limit to the dose distributions; this presumably reflects the original geological dose in this material, and is derived from grains which have not received significant light exposure before measurement.

7.3.3 Dose estimation

One of the major problems when dealing with incompletely bleached materials is to identify the well-bleached grains, i.e. identify those grains which should be included in the estimation of the added dose. It is clear that attention must be focused on the low-dose part of the distribution, but how do we decide which data points to include in the final dose estimation?
The standard error, α, on the weighted mean Z, can be calculated in two ways:

$$\alpha_{ex}^2 = \frac{\sum_{i=1}^{n}(x_i - Z)^2/\sigma_i^2}{(n-1)\sum_{i=1}^{n} 1/\sigma_i^2} \qquad \alpha_{in}^2 = \frac{1}{\sum_{i=1}^{n} 1/\sigma_i^2} \tag{7.1}$$

where x_i are the individual dose estimates, Z is the weighted average, σ_i are the individual estimates of uncertainty on the dose estimates x_i, and n is the total number of measurements. The first estimate, α_{ex}, combines information on both the individual estimates of uncertainty (σ_i), and the deviation from the weighted mean ($x_i - Z$). If there is no additional source of variance in the data other than σ_i, then for large n, $\alpha_{ex} \approx \alpha_{in}$. These two estimates of the standard error can be considered as an "external" and an "internal" measurement of uncertainty on the mean value (Topping, 1955). For a large normal population, where σ_i accurately describes the uncertainty on each individual measurement, the ratio α_{in}/α_{ex} tends to unity, and the uncertainty on this ratio is $(2(n-1))^{-0.5}$.

This is illustrated for an *ideal* (computer simulated) distribution in Figure 7.5. 100 Gaussian distributions each with a mean value of 100 Gy were calculated. The relative standard deviation (RSD) of these 100 distributions

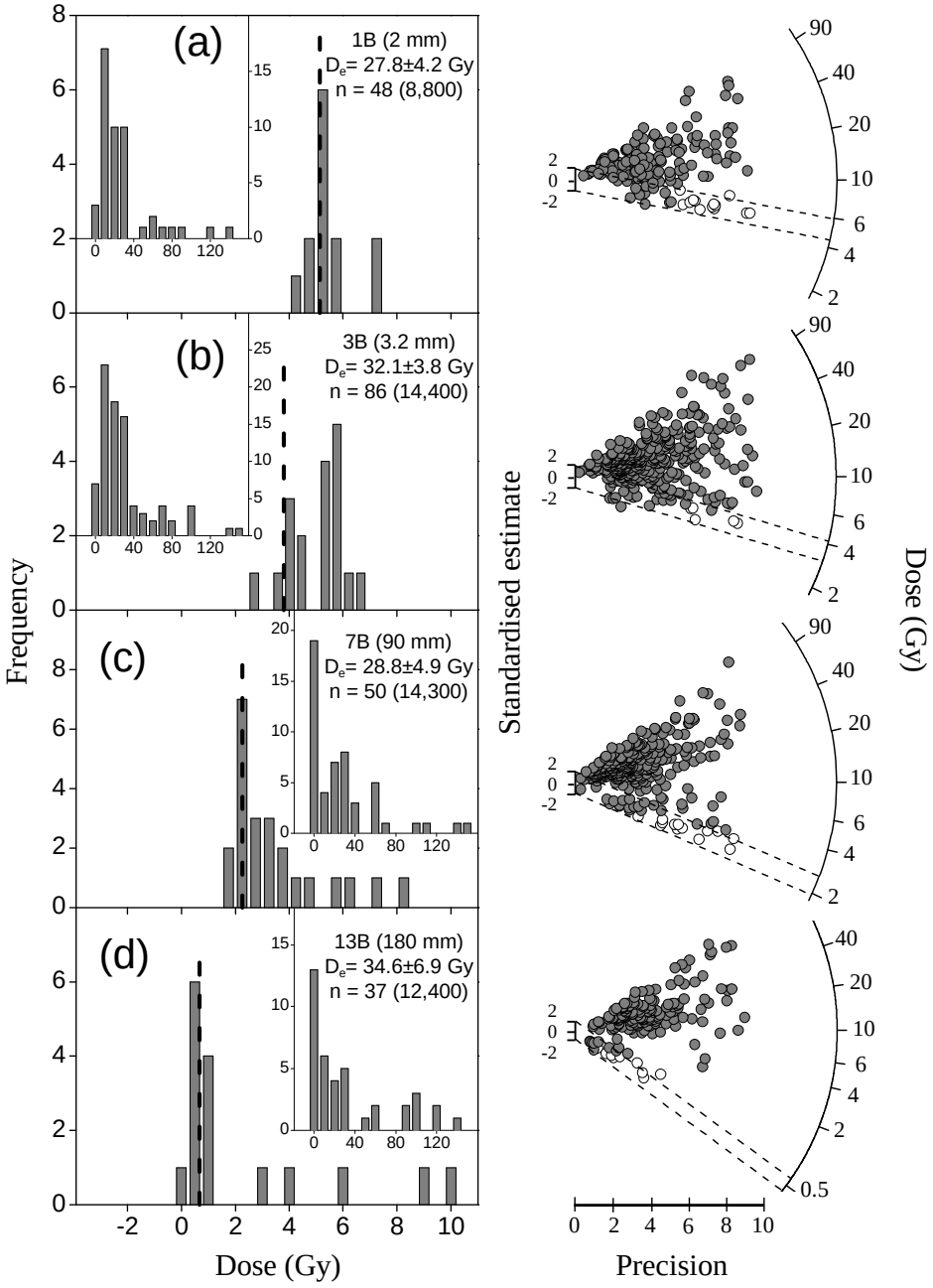

Figure 7.4: Results obtained at four different depths into the irradiated concrete brick. Dose histograms include results which have either a relative uncertainty of less than 15% or an absolute uncertainty of less than 0.5 Gy. The dashed lines represent the estimated added dose. The radial plots include all results with uncertainties on the natural test dose, based on photon counting statistics, of $< 20\%$. Unfilled circles represent points included in the estimation of the added dose. Results falling within $\pm 2\sigma$ of the estimated added dose lie within the dashed lines.

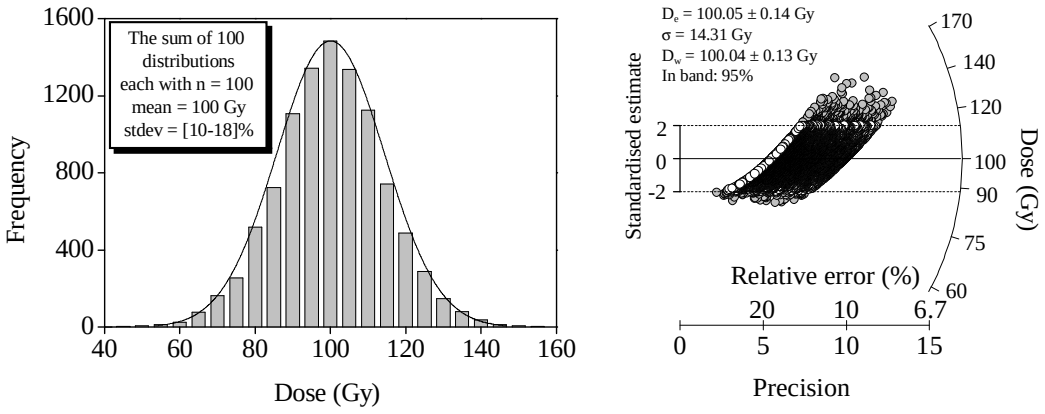

Figure 7.5: Ideal computer simulated Gaussian distribution. 100 points were extracted from 100 Gaussian distributions with identical mean (100 Gy) but varying standard deviations. The standard deviations varied between 10 and 18 Gy in intervals of 8/99 Gy (≈ 0.081 Gy). All 100 points extracted from a given distribution were assigned an uncertainty identical to the standard deviation of the distribution.

varied between 10 and 18% (i.e. the first distribution had a RSD of 10%, the next 10.081% and so forth). The points making up the individual distribution were each assigned an uncertainty identical to the standard deviation for the distribution. From each of these Gaussian distributions 100 points were randomly extracted and these points were combined to form a single distribution containing 10,000 points with individually assigned uncertainties ranging between 10 and 18 Gy. The resulting distribution has an average value $D_e = 100.05 \pm 0.14$ Gy ($n = 10,000$) and a weighted average $D_w = 100.04 \pm 0.13$ Gy. The distribution is shown as a histogram and as a radial plot in Figure 7.5. 95% of the individual points fall within $\pm 2\sigma$ of the mean value as expected. In Figure 7.6 the ratio R between the internal estimate of uncertainty α_{in} and the external estimate of uncertainty $\alpha_e x$ is plotted against the weighted mean. The points were sorted in increasing order, and α_{in} and α_{ex} calculated for $n = 2, 3, 4 \ldots$ etc. , beginning with the smallest value. Including all 10,000 points gives a ratio $R = \alpha_{in}/\alpha_{ex} = 0.990 \pm 0.007$. R is consistent with unity when at least all values between point 1 and point 9949 are included in the calculation, or when no more than point 1 to point 9994 are included. The weighted mean, Z, ranges between 99.879 ± 0.007 and 100.014 ± 0.007 Gy in the interval from point 9949 to 9994.

In Figure 7.7 the results from a heated and gamma irradiated sample (lab code 004707, see Chapter 6) are shown. The sample was heated to 850 °C to completely zero any prior OSL signal and then given a dose of 7 Gy in the laboratory using a ^{137}Cs source. The results are shown in a ra-

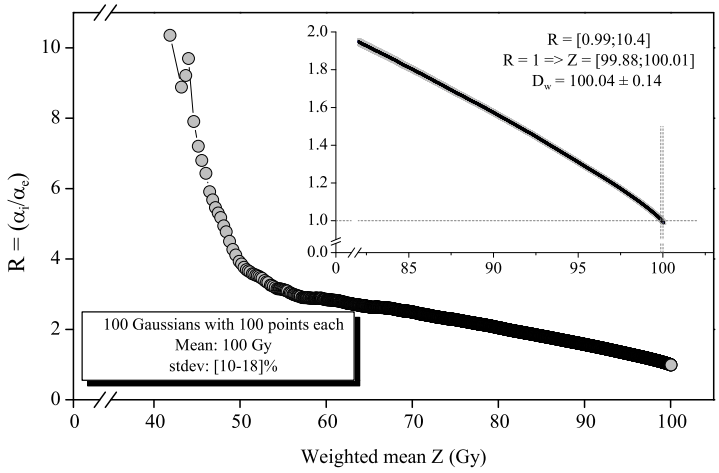

Figure 7.6: The ratio R between the internal estimate of uncertainty α_{in} and the external estimate of uncertainty α_{ex} is plotted against the weighted mean for a simulated Gaussian distribution.

dial plot in Figure 7.7a (the same data are displayed in Figure 6.1f). The uncertainty on the individual dose estimates are based purely on counting statistics. Only 60% of the results are consistent within 2σ of the average dose 7.32 ± 0.02 Gy, $n = 1919$. In Figure 7.7b R is plotted as a function of the weighted mean Z. $R = 0.30 \pm 0.02$ when all dose estimates ($n = 1919$) are included, confirming that the assigned uncertainties are not accounting for the observed variance in the data. When R is consistent with unity (point 53 to 97) the weighted mean ranges between 5.50 ± 0.03 and 5.64 ± 0.03, i.e. a significant underestimate of the known dose of 7 Gy. In section 6.6 it was argued that at least an additional 8% uncertainty should be added to the uncertainties arising from fluctuations in the number of photons counted to account for the observed variance. Figure 7.7c shows a radial plot of the same data as in Figure 7.7a, but with the additional 8% uncertainty added (in quadrature). 93% of the results are consistent within 2σ of the given dose of 7 Gy. In Figure 7.7d, R is plotted as a function of the weighted mean Z and when all dose estimates are included $R = 0.92 \pm 0.02$ ($n = 1919$). When R is consistent with unity (point 1753 to 1788) the weighted mean ranges between 7.03 ± 0.02 and 6.91 ± 0.01 Gy.

Now consider the well-bleached distribution in Figure 7.3. Calculating R for all dose estimates gives $R = 0.57 \pm 0.10$ ($n = 48$), which is not consistent with unity, indicating that a few grains were not completely bleached. This is also clear from visual inspection of Figure 7.3. The ratio R is consistent

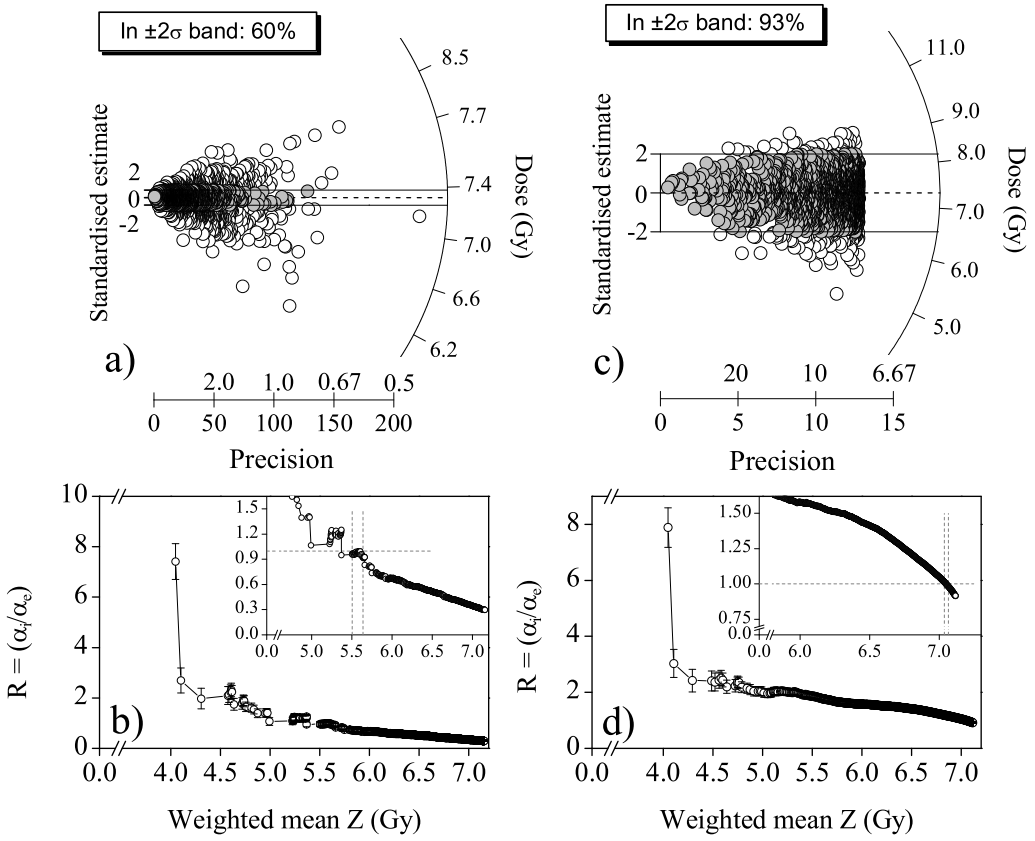

Figure 7.7: Application of the internal/external criterion to results from a laboratory heated and gamma irradiated sample (lab code 004807). **a)** radial plot of the same data displayed in Figure 6.4a. Only 60% of the results fall within the $\pm 2\sigma$ band centred on the average dose. **b**) R plotted as a function of the weighted mean Z. **c)** same as a) but with additional 7.8% of uncertainty. 93% of the results are now consistent with the average dose. **d)** same as b) but with additional 7.8% of uncertainty.

with unity when $n = 31$; i.e. when the lowest 31 dose estimates are included (out of a total of 48 estimates).

In a population where additional variance arises from incomplete bleaching, the ratio α_{in}/α_{ex} can be used to select that part of the lowest dose region of the distribution that contains only well-bleached grains. The doses are first sorted in increasing order, and α_{in} and α_{ex} calculated for $n = 2, 3, 4 \ldots$ etc. , beginning with the smallest dose. When $\alpha_{in}/\alpha_{ex} = 1 \pm (2(n-1))^{-0.5}$, the process is stopped and the grains included in the calculation to that point are assumed to be well-bleached. Some bias towards higher doses is inevitable in this approach, but it is demonstrated below that this is not significant for the data sets used here. It is also necessary to assume that there are no grains

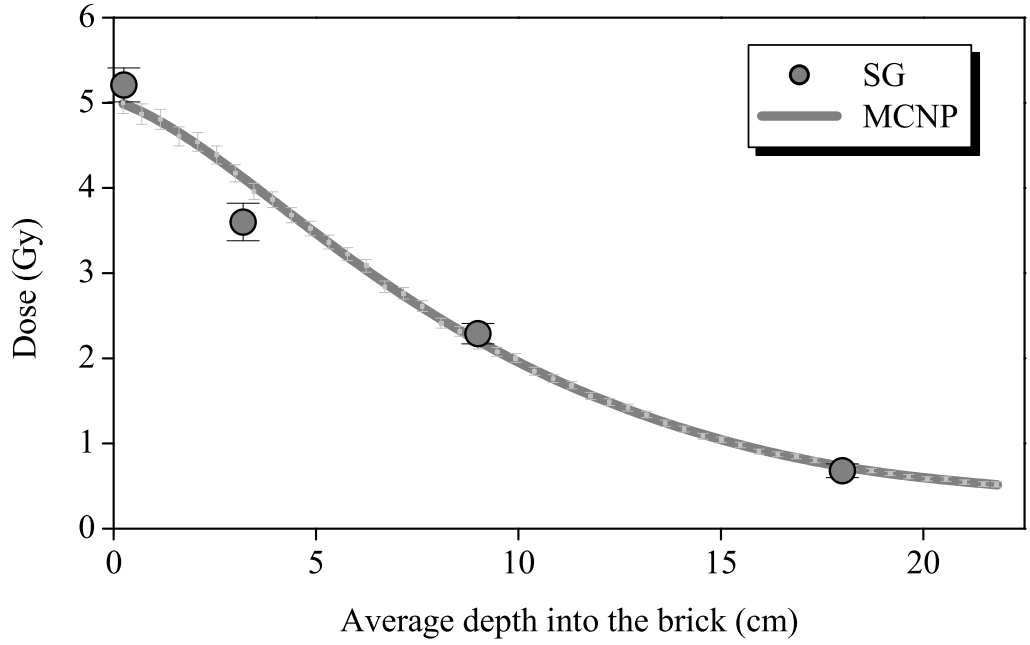

Figure 7.8: Estimates of the added dose (filled circles) plotted as a function of depth into the irradiated concrete block. The continuous line is the calculated dose-depth profile using a Monte Carlo (MCNP) based model (Lauridsen, 2002, private communication).

with a dose smaller than the dose of interest. That is a reliable assumption here, but it may not always be true in unconsolidated material.

Figure 7.8 shows the estimated doses using the above approach (filled circles) as a function of depth into the block. The continuous line was calculated using a Monte Carlo (MCNP) based model (Briesmeister, 1986), with the irradiation geometry and concrete composition as input parameters (Lauridsen, 2002, private communication).

The single grain measurements agree very well with the calculated values, confirming both the method of selecting the well-bleached grains, and the estimation of uncertainty associated with each average value. All single grain results are summarised in Table 7.1. Applying this approach to the zero-dose distributions of Figures 7.2a, 7.2b, and 7.2c (see dashed lines), estimates of 0.030 ± 0.015 Gy, 0.0040 ± 0.0035 Gy and 0.053 ± 0.035 Gy, respectively, were derived. This suggests a minimum detection limit of < 100 mGy (i.e. 3σ) for this sample. It should be noted that the quartz extracted from the concrete blocks was extremely insensitive ($\sim$ 95,000 grains were measured in this study) and therefore it took considerable instrument time to collect these data. However, it is known that many geological sources of

Sample	Estimated dose (Gy)	No. of results included	No. of grains measured
0B 150-180	0.030 ± 0.015	15	9,600
0B 212-250	0.0040 ± 0.0035	15	14,400
0B 355-400	0.053 ± 0.035	6	5,970
0S 212-250	0.040 ± 0.016	19	8,800
UV-bleached	0.030 ± 0.015	15	4,100
Slice 1B	5.21 ± 0.20	13	8,800
Slice 3B	3.60 ± 0.22	5	14,400
Slice 7B	2.29 ± 0.12	13	14,300
Slice 13B	0.51 ± 0.08	10	12,400

Table 7.1: Summary of the estimated doses. The label "0B" refers to the samples extracted from the bulk of the unirradiated concrete block. The label "0S" refers to the surface sample. The numbers gives the grain size used.

sand are considerably more sensitive than this material, and it is believed that this analytical approach has general application.

7.4 Synthetic aliquots

When measuring incompletely bleached samples using multi-grain aliquots overestimation of the lowest dose in a sample is expected, since it contains a mixed population of well-bleached and poorly-bleached grains. The study described above has focused only on single grain measurements. However, these data can also be used to investigate whether measurements of small aliquots (consisting of 100 grains) would give similar estimates of the added dose. This was examined by combining the OSL signals from individual single grain discs (each containing 100 single grains) to generate "synthetic aliquots". The OSL signals were combined by summing the light levels, and these OSL signals were then used to evaluate the equivalent dose in the usual manner.

Figure 7.9 shows the dose distributions obtained using these synthetic aliquots from the irradiated concrete slices. The dashed lines represent the expected added doses derived from Monte Carlo modelling. It is obvious that deriving a dose estimate from these distributions will lead to a significant

overestimate of the added dose. The single grain measurements showed that the light levels of individual grains vary significantly and that only about 2.5% of the grains give a detectable natural test dose response (i.e defined here as having a statistical relative uncertainty of $< 20\%$). This implies that in an aliquot containing 100 grains, only about 2–3 grains, on average, give detectable test dose signals. The measurements of the natural dose distributions (i.e. from the unirradiated concrete) revealed that about 0.3% of the measured grains gave an equivalent dose consistent with zero within 2 standard deviations, which implies that there would only be one well-bleached grain in every three aliquots.

Thus, although an overestimation of the dose due to the averaging effect is to be expected, it is surprising that the synthetic aliquot distributions overestimate the added dose so significantly. Analysis of the natural signals from the single grain measurements reveals that 8.7% of the grains gave a natural signal, while only 2.5% gave a detectable test dose signal. This suggests that small aliquots are averaging over a different suite of grains than single grains and thus overestimating the smallest possible dose. This is demonstrated by the significant offset in the dose distribution derived from the synthetic aliquots (see Figure 7.9). It is concluded that this particular sample is not suitable for multi-grain small-aliquot measurements.

7.5 Conclusion

It has been shown that it is possible to measure added doses in a sample of commercial concrete of well below 1 Gy using the OSL signal from single grains of quartz. Minimum detection limits are less than 100 mGy. The reliability of the dose estimates has been confirmed by comparison with the dose-depth profile derived from a Monte Carlo simulation.

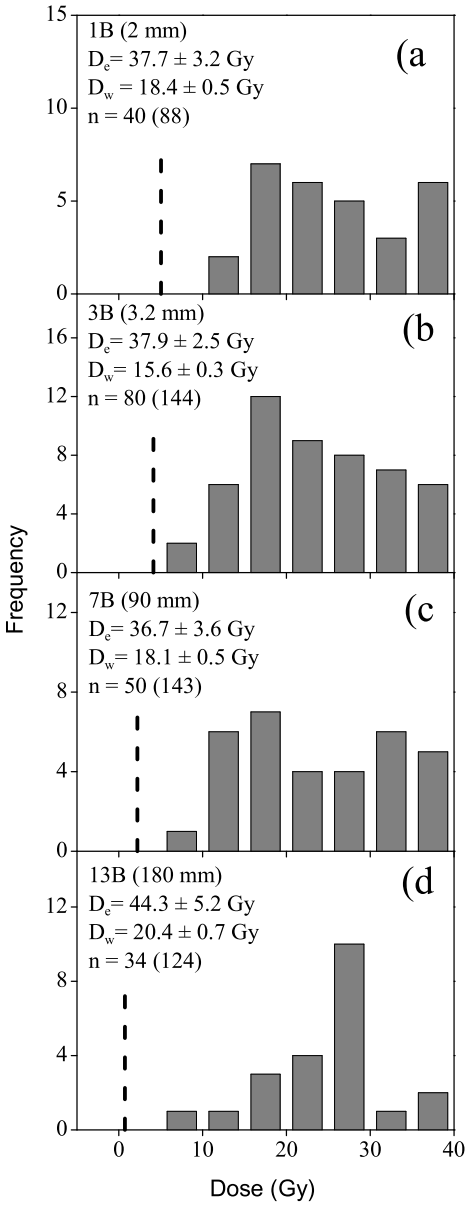

Figure 7.9: Synthetic aliquot dose distributions. The synthetic aliquots have been generated by combining the OSL signals from individual single grain discs (each containing 100 single grains). All included results have a relative statistical uncertainty on the estimated dose of less than 25%. The dashed lines represent the expected added doses derived from Monte Carlo modelling.

8 OSL Dosimetry using Mortar Samples

8.1 Introduction

In this chapter the suitability of using quartz extracted from mortar as retrospective dosimeters has been investigated. There are only few existing investigations using quartz extracted from mortar (e.g. Hong et al., 2001; Jain et al., 2002; Goedicke, 2003). The work described in Chapters 5 and 7 focused on quartz extracted from modern concrete samples. In these studies the apparent distribution of doses at the time of manufacture was measured and by laboratory irradiation a radiation accident was simulated. However, it cannot be assumed that recently manufactured samples will always be available after an accident, nor can it be assumed that laboratory doses accurately simulated natural or accident doses, which will often be absorbed at much lower dose rates. One way to address this question is to attempt to determine the dose in older unbleached materials of known age and dose rate, and thus known dose. In this chapter three different types of mortar extracted from a building built in 1964 had their OSL signals measured. These samples had only been exposed to the natural background radiation (i.e. no accident dose had been superimposed) and the dose accrued in quartz since construction was estimated to be 133 mGy (estimated by independent measurements of the dose rate in the material). The prime objective of this study was to measure the distribution of apparent doses in these samples and to investigate how accurately the known dose of 133 mGy could be measured.

The three different types of mortar (render, plaster and white wash) were sampled from a building built in 1964 (GSF - Forschungszentrum für Umwelt und Gesundheit, Germany). The three samples were distributed by GSF to the partners of the EU project "Luminate" as part of an exercise to intercompare dose evaluation methods using poorly-bleached materials.

In this chapter, thermal transfer in single grains of quartz is measured using the plaster sample (GSF2) and the grain size dependence of bleaching was investigated using the white wash sample (GSF3)in the size range 90 to 300 μm. The natural background distribution of doses is investigated using both small aliquots ($\sim$ 100 grains) and single grains of quartz. All three samples are poorly-bleached and only weakly sensitive to radiation (only about 0.3% of the single grains gave detectable light signals in response to a test dose of 4 Gy). The background dose accrued since construction of the building is estimated using four different methods: 1) simple average of all obtained results, 2) lowest 5% method, 3) probability plot method and 4) comparison of internal and external uncertainties. These dose estimates are compared with the expected dose.

8.2 Samples and the expected dose

The samples were collected at GSF in Münich, Germany on 17.7.01 and measured between 1.12.01 and 4.12.02. Dose-rate estimates were made on the render sample (GSF1) : 2.87 (beta, infinite matrix), 1.47 (gamma, infinite matrix) and 0.7 (observed environmental gamma) mGy/y (Göksu, 2002). These data imply a total minimum dose of 0.133 Gy (assuming $\sim$ 15% of gamma infinite matrix dose rate in the render, $\sim$ 85% of environmental gamma and 3% beta attenuation). Although the dose rates were measured on one sample only, it is expected that they would not vary significantly from sample to sample as they were all from the same building (Göksu, 2002).

8.3 Experimental details

Samples were treated with H_2O_2, HCl and HF to obtain a clean quartz extract. Large aliquots (8 mm) of the quartz extract were screened with an IR laser (830 ± 10 nm) for feldspar contamination, and the HF treatment was repeated if any detectable IRSL signal was measured. The samples were then sieved to recover the required grain sizes.

Small aliquots comprising 60 to 100 grains each were measured using an automated Risø TL/OSL reader (TL/OSL-DA-15) (Bøtter-Jensen et al., 2000a). Blue light stimulation used LEDs (470±30 nm) delivering 50 mW/cm^2 at the sample position after passing through GG-420 filters. Single grain measurements were carried out using the Risø single grain laser attachment. The stimulation light source was a 10 mW $Nd:YVO_4$ solid-state diode-pumped laser emitting at 532 nm, which can be focused sequentially onto each of 100

grains mounted on a special aluminium sample disc (Bøtter-Jensen et al., 2003). Laboratory irradiations were made using a calibrated $^{90}Sr/^{90}Y$ beta source mounted onto the reader and delivering 0.11 Gy/s to quartz. Detection optics consisted of Hoya U-340 ($\lambda_p \sim 340$ nm, FWHM 80 nm) filters in front of a bialkali photomultiplier tube (Electron tubes Ltd. 9235 QA). All measurements were carried out using the SAR protocol (Murray and Wintle, 2000) with a preheat of 200 °C for 10 s and a cut-heat of 180 °C (or 160 °C). Test doses ranged between 1 and 4 Gy.

8.4 Results and discussion

8.4.1 Thermal transfer in single grains of quartz

In the SAR protocol multiple heatings of the samples are required to remove unstable components from the regenerated signals. However, thermal stimulation may result in transfer of charge from light insensitive but thermally-stable traps into light sensitive traps. This phenomenon is referred to as thermal transfer (TT). TT is probably not important in older samples (Murray and Olley, 2002), but several authors have reported an increase of the equivalent dose as a function of preheat temperature for young samples (e.g. Murray and Clemmensen, 2001; Bailey et al., 2001; Rhodes, 2000; Wallinga et al., 2001). Murray and Olley (2002) suggested that TT may be common in samples in which the main OSL trap was adequately zeroed, but where less light sensitive traps such as the TL traps at 160 °, 240 ° and 280 °C retained a significant charge population. Heating the sample in the laboratory releases this charge population (or some of it) and a fraction may be retrapped at the OSL trap and thus give rise to a finite OSL signal even in the absence of any radiation dose since the last zeroing event.

Thermal transfer was investigated using the $212 - 250\,\mu$m grain size from sample GSF2. This sample was chosen as it was particularly poorly bleached having an average apparent dose of approximately 80 Gy (discussed later). Multiple step heating on the same grain was used (Jain et al., 2002); this provides the thermal-transfer dose distributions for each preheat temperature from the same set of grains. The grains were first bleached by green laser stimulation at 125 °C for 1 s, then held for 1,000 s at room temperature and subsequently bleached again for 1 s. This was followed by heating the disc (containing 100 grains) to 180 °C for 10 s (preheat), cooling down to room temperature and measurement of the OSL of individual grains at 125 °C stimulation temperature. The preheat temperature was increased in increments of 20 °C up to 300 °C and the single-grain OSL was measured

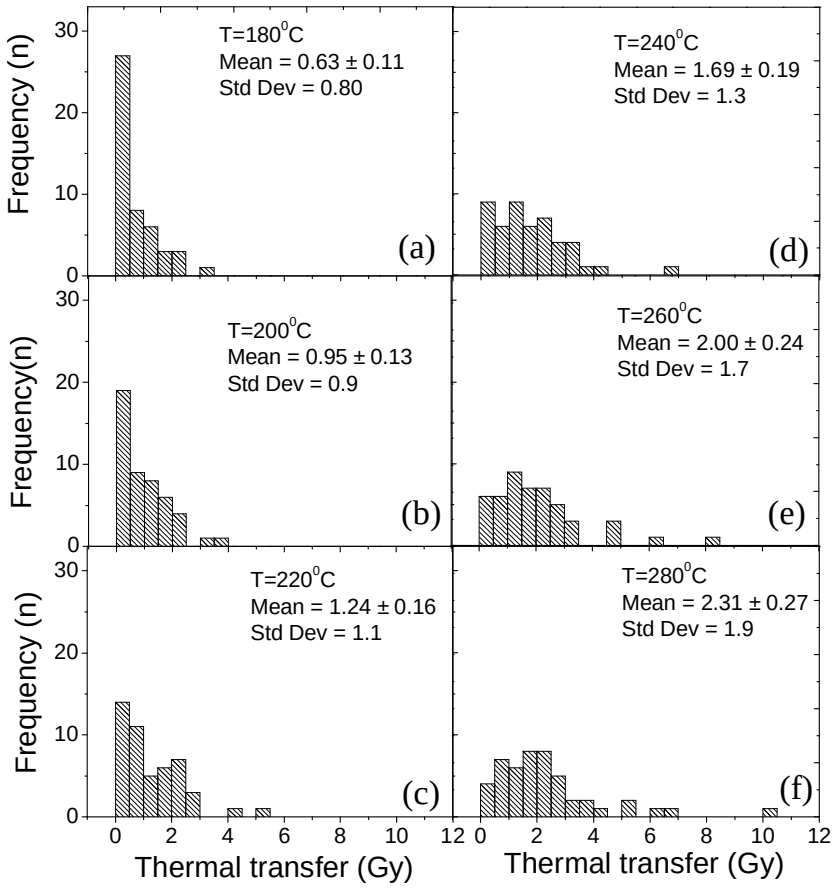

Figure 8.1: a to f) Histograms of thermal transfer (Gy) in 48 single grains of quartz from the sample GSF2 for preheat temperatures between 180 to 280 °C.

after each heating. Sensitivity changes after each OSL measurement were monitored using the OSL response to a test dose (1 Gy; cutheat: 160 °C). Finally, a dose-response curve was measured using the SAR protocol employing a preheat of 200 °C for 10 s and a cutheat of 160 °C for 10 s. A corrected cumulative thermal transfer OSL was then calculated for each preheat temperature (this is a sum of sensitivity corrected OSL at the given temperature and those at all preceding preheat temperatures) and interpolated on the growth curve to obtain a potential dose offset for the corresponding temperature (see Jain et al., 2002, for details). The contribution to thermal transfer from the test dose itself can be measured by repeating the above experiment after removing all the trapped charges (e.g. by heating to 500 °C), so that thermal transfer, if any, is caused by charge built up from the test doses; this was measured in few cases and was always insignificant.

The results from the TT experiment are plotted in Figure 8.1. Only 48 of a total of 8,400 measured grains were accepted using the criteria: a) relative uncertainty on the first test dose $< 30\%$, and b) first test dose OSL signal > 30 counts/0.1 s. This gives an overall recovery from the material of 0.57% (i.e. 0.57% of all grains measured were accepted). Because of low sensitivity, the thermal-transfer OSL decay curves in many grains had low signal-to-noise ratios; as a result, the cumulative thermal transfer decreased in a few grains with heating to higher temperatures. The frequency distributions of these results for preheats between 180 and 280 °C are plotted in Figure 8.1(a-f). At lower temperatures, the distributions are positively skewed, but relatively narrow, with the median < 0.5 Gy. However, at higher temperatures (> 220 °C), the distribution broadens, the median becomes significantly greater ($\sim$ 2 Gy), and there are individual values as high as 10 Gy. These observations suggest that some grains giving insignificant thermal transfer OSL at 180 °C do show significant but variable (from grain to grain) transfer at higher temperatures. Consequently, a preheat temperature of 200 °C was used for dose estimation. An increase in the mean and the variance of the thermal-transfer values with preheat temperature is seen in Figure 8.2a. The average increases from 0.63 ± 0.11 Gy at 180 °C to 2.31 ± 0.27 Gy at 300 °C consistent with thermal erosion of deeper light insensitive traps. In Figure 8.2b the OSL from the first test dose is plotted as a function of the cumulative thermal transfer at 300 °C. Grains with TT values larger than 4 Gy generally have test dose signals $< 1,000$ cps and therefore relatively large uncertainties (these estimates of uncertainty are based on counting statistics only). The precisely known TT values (i.e. test dose signals between 1,000 and 20,000 cps) lie between 0 and 4 Gy.

The variation in thermal transfer with the degree of bleaching of the OSL traps in the sample was considered in more detail. If it is assumed that TT is caused by transfer of charge from poorly-bleached light insensitive traps into the OSL trap, an inverse correlation between the TT and the degree of OSL bleaching might be expected. To investigate this, the ratio of OSL in the natural sample (prior to any preheat) and the first test dose OSL was taken as a surrogate for the extent of partial bleaching (L_n/T_1). These values should increase with the degree of poor bleaching. A plot of (L_n/T_1) against the thermal transfer at both 200 °C (Figure 8.3a) and 280 °C (Figure 8.3b) does not indicate any such inverse correlation. Even grains with very low (L_n/T_1) values (see Figure 8.3b, inset) show a significant thermal transfer, suggesting that none of the grains have had all the stored energy released by bleaching. Surprisingly, the thermal transfer in poorly bleached grains can be less than the maximum thermal transfer for the well bleached grains (Figure 8.3); this

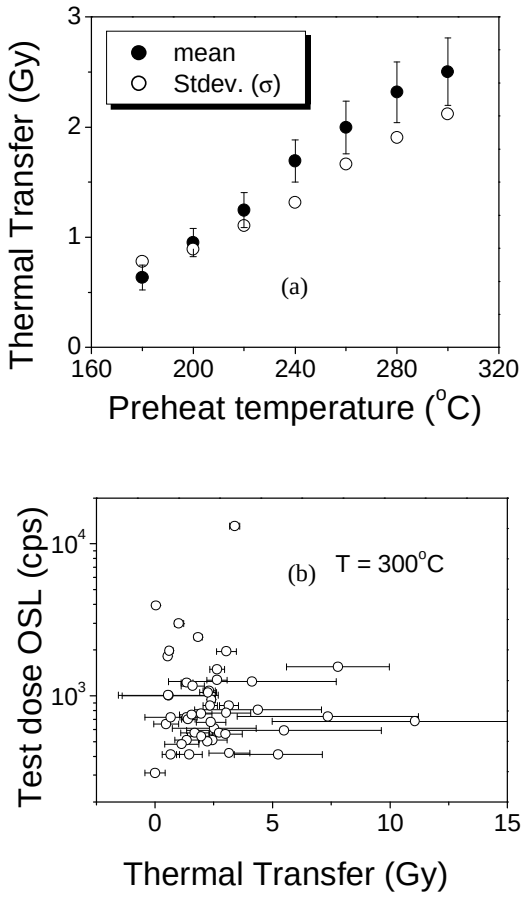

Figure 8.2: **a)** A plot of mean and standard deviation of the thermal transfer for each preheat temperature. The error bars on the mean values are the standard errors. **b)** A scatter plot of the cumulative thermal transfer at 300 °C versus the first test dose OSL response of the each grain.

can only occur if some of these poorly bleached grains have, by genesis, a smaller proportion of deep light insensitive traps, when compared to the OSL trap. Thus, the lack of an inverse relationship between TT and the degree of bleaching suggests that the light insensitive trap structure is highly variable from grain-to-grain in this sample. This is further supported by the increase in the variance as a function of preheat temperature as shown in Figure 8.1 and 8.2a (if the light insensitive trap structure had been the same for all grains thermal erosion should affect all grains equally and the variance would have remained constant). It can be inferred that thermal transfer can cause an increased variance with increasing preheat temperature in single-grain dose

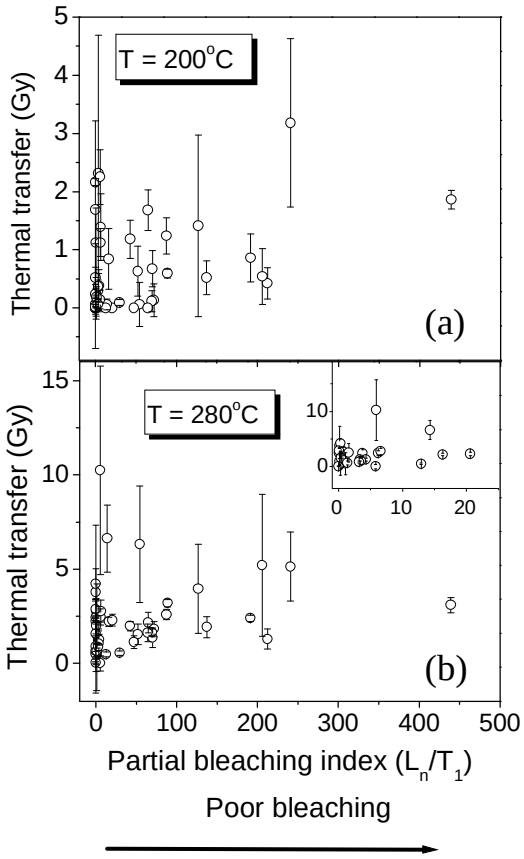

Figure 8.3: Relationship between thermal transfer and the extent of partial bleaching in individual grains for preheat temperatures of **a)** 200 °C and **b)** 280 °C.

distributions from samples containing incompletely bleached light-insensitive traps.

8.4.2 Estimated equivalent doses and dose distributions

In the following section it is attempted to derive the best possible equivalent dose estimates for the samples GSF1 (render), GSF2 (plaster) and GSF3 (white wash) using dose distributions obtained from measurements of single-grains and small-aliquots ($\sim$ 100 grains) of quartz. Since the dose of interest (i.e. the dose absorbed since construction) is small, closely spaced regeneration doses in the range between 0 to 6 Gy were used. Dose estimates $>$ 6 Gy

are based on linear extrapolation of the growth curve and therefore generally not well known. Dose estimates were derived using four different approaches:

§1. **Average**: a simple arithmetic mean.

§2. **Lowest 5% method**: uses the average of the lowest 5% of the dose estimates from a skewed dose population (Olley et al., 1998).

§3. **Probability plot (PP):** In the probability plot the cumulative frequency is plotted as a function of dose. Plotting a cumulative Gaussian distribution produces a sigmoidal curve. If this curve is displayed on a probability scale (i.e. the inverse of a cumulative Gaussian distribution), it will plot as a straight line (see Figure 8.4a). The advantages of using such probability plots are: 1) the tail ends of poorly-bleached distributions become more clearly visible on the probability axis, 2) the shape of the probability plot is not very sensitive to the bin size (unlike histograms), since it uses the cumulative frequency and 3) mixed dose populations can be identified by changes (or breaks) in the slope of the line (Jain et al., 2002).
The aim in this study is to identify the dose population most likely to have been adequately zeroed at construction (i.e. the lowest dose population) and to determine the accrued background dose from this population. In the probability plot method this sub-population is identified by the change in slope in the cumulative frequency (see Figure 8.4b). The accrued background dose is estimated by calculating the weighted mean of all results included in the identified sub-population. The bin-width was chosen to be the median of the absolute uncertainties of the dose estimates in the range from 0 to 1 Gy (the region of interest).

§4. **Comparison of internal and external uncertainties (IEU):** This approach is based on the ratio of the measurement of "external" (α_{ex}) and an "internal" (α_{in}) uncertainty (Topping, 1955) on the mean value. As discussed in section 7.3.3, for a large normal population, where σ_i accurately describes the uncertainty on each individual measurement, the ratio α_{in}/α_{ex} tends to unity, and the uncertainty on this ratio is $(2(n-1))^{-0.5}$. In a poorly bleached sample, the ratio α_{in}/α_{ex} can be used to select the lowest dose population arising from only well-bleached grains. This approach was used successfully by Thomsen et al. (2003a) to identify the lowest well-bleached grain population in a poorly bleached concrete sample.

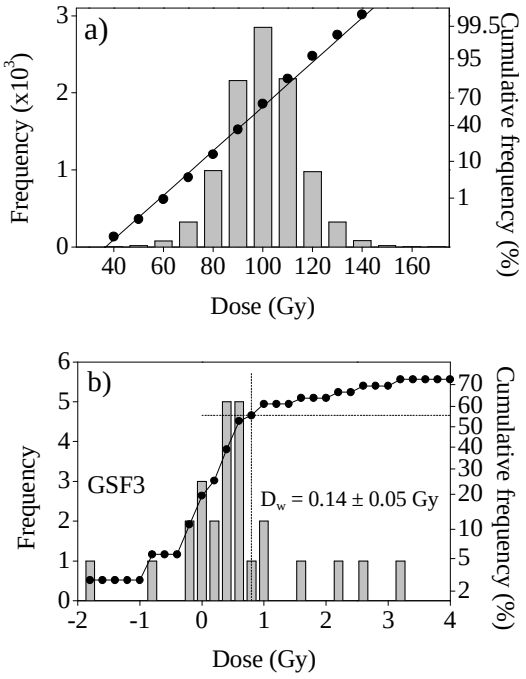

Figure 8.4: **a)** Dose histogram and probability plot of a computer simulated Gaussian distribution (see section 7.3.3 for further details). Also shown is a linear fit to the cumulative frequency data ($R^2 = 0.9981$). **b)** Estimation of dose from single grains of quartz extracted from GSF3 using the probability plot method. Only those values with relative uncertainties less than 30% or absolute uncertainties less than 1 Gy are plotted and the bin width is chosen from the median of error distribution. The lowest normal population is identified on the basis of the change in slope (dashed lines) of the probability plot (filled circles). The equivalent dose estimate is the weighted mean of the sub-population of doses below the slope change (i.e. < 0.8 Gy). See Figure 8.7c for the entire dose distribution obtained using single grains from GSF3.

Approaches §2, §3 and §4 all aim to identify the lowest meaningful doses in the population. While approach §2 is arbitrary, both §3 and §4 are based on the premise that the dose distribution in a well bleached sample is Gaussian.

The estimates of uncertainty on individual small aliquot dose estimates in this chapter are based purely on counting statistics. However, single grain uncertainties have an additional 10% relative uncertainty added in quadrature (see Chapter 6). Only results with a statistical relative uncertainty on the natural test dose $< 30\%$ have been included in the assessment of the dose absorbed since construction.

In histograms, all data points are given equal weight irrespective of the precision with which they are known. A meaningful histogram ought to only display results with similar uncertainties, and so only results with a relative

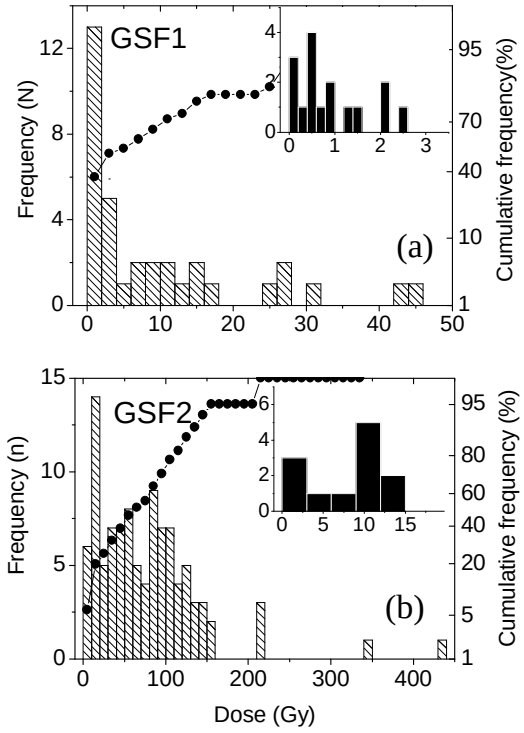

Figure 8.5: Dose histograms and probability plots from small aliquots of samples **a)** GSF1 ($n = 53$) and **b)** GSF2 ($n = 105$). Insets show the lowest dose results.

uncertainty on the estimated dose $< 30\%$ or an absolute uncertainty < 1 Gy were included.

The estimates of dose absorbed since construction calculated using the four approaches are summarised in Table 8.1 and described briefly below.

8.4.3 Small-aliquot dose distributions

Render (GSF1)

Figure 8.5a displays dose histograms obtained from the measurement of small aliquots from the render sample. The dose estimates range from 0.012 ± 0.084 to 45.6 ± 10.8 Gy and the average dose is 7.8 ± 1.5 Gy ($n = 53$). The distribution is skewed suggesting that the sample was incompletely bleached during construction. Nevertheless, the majority of the estimated doses are < 5 Gy. The probability plot and histograms show a dominant ($\sim 50\%$) dose population between 0 to 2 Gy and another population that extends from 2 Gy to about 30 Gy. Both IEU and the lowest 5% approaches gave an equivalent

dose of ~ 0.080 Gy; the difference (dose off-set) from the expected dose (133 mGy) is 0.05 Gy. The probability plot (PP) method gave 0.248 Gy, i.e. 0.11 Gy above the expected dose.

Plaster – Inner Wall (GSF2)

Figure 8.5b presents dose histograms from the inner wall plaster. The dose estimates range from 1.18 ± 0.14 to 430 ± 50 Gy and the average dose was 81 ± 7 Gy ($n = 105$). The dose histograms and the cumulative frequency plot in Figure 8.5b show a polymodal distribution. It appears that the bulk ($\sim 75\%$) of this sample represents a geological dose corresponding to the second slope centred at about 100 Gy, while a small population of the sample was bleached. The minimum dose is overestimated by more than 1 Gy by all the dose estimation methods (Table 8.1).

White Wash (GSF3)

Dose distributions from three different grains sizes ($90-112\,\mu$m, $180-212\,\mu$m and $250-300\,\mu$m) from GSF3 were measured to investigate the grain size dependence of bleaching. The resulting dose distributions are shown in Figure 8.6(a-c). During turbulent mixing coarser grains tend to move to the outer perimeter (Mehta and Barker, 1991; Mehta et al., 1996), which may result in the coarser grains being more completely beached than the smaller grains. The minimum (D_{min}) and average (D_{av}) doses obtained from the three grains sizes are given in Table 8.2.

The dose distributions are significantly skewed, and contain values up to 40 Gy, indicating incomplete bleaching in all three cases. The probability plots indicate the presence of two different dose populations, with the lower dose population (< 1 Gy) comprising about $\sim$12, 44 and 27 % of the grains in the $90-112\,\mu$m, $180-212\,\mu$m and $250-300\,\mu$m grain-size ranges, respectively. The second, higher dose population in the probability plots appears similar in all the cases (Figure 8.6). It seems that the coarser grain sizes ($180-300\mu$m) may be better bleached than the $90-112\,\mu$m fraction.

The dose estimates using the lowest 5% method gave values between 0.20 and 0.48 Gy for the three grains sizes. The IEU method gave values between 0.159 ± 0.030 Gy and 0.765 ± 0.049 Gy and were similar to the values obtained from the PP method (Table 8.1). Despite being relatively less well bleached, $90-112\,\mu$m grain size population gave the closest expected dose estimate; this is caused by the presence of two very well known results at ~ 0.15 Gy (absolute uncertainty of 0.03 and 0.08 Gy) in the $90-112\,\mu$m fraction.

	GSF1		GSF2		GSF3	
	SA	SG	SA	SG	SA	SG
Grain size (μm)	180 – 212	212 – 250	180 – 212	212 – 250	90 – 112 / 180 – 212 / 250 – 300	212 – 250
Average (Gy)	7.78 ± 1.47	5.33 ± 1.33	80.8 ± 6.9	100 ± 13	7.1 ± 1.0 / 4.7 ± 0.8 / 10.1 ± 2.0	13.5 ± 4.3
Lowest 5% (Gy)	0.08 ± 0.04	−0.14 ± 0.17	3.2 ± 1.0	−0.28 ± 0.11	0.25 ± 0.11 / 0.20 ± 0.07 / 0.476 ± 0.007	−0.98 ± 0.42
IEU (Gy)	0.09 ± 0.06	0.15 ± 0.04	1.31 ± 0.11	0.36 ± 0.14	0.16 ± 0.03 / – / 0.77 ± 0.05	0.14 ± 0.05
PP (Gy)	0.25 ± 0.04	0.15 ± 0.04	1.54 ± 0.09	0.36 ± 0.14	0.16 ± 0.03 / 0.68 ± 0.14 / 0.50 ± 0.11	0.14 ± 0.05
Range (Gy)	0.01 to 46	−0.1 to 32	1.2 to 430	−0.5 to 554	0.01 to 46 / 0.1 to 22 / 0.5 to 110	−1.7 to 162
N	53	26	105	71	54 / 38 / 65	55
SG recovery (%)	–	0.33	–	0.55	– / – / –	0.32
Results with D_e < 0.5 Gy (%)	17	31	0	7	9 / 21 / 6	29

Table 8.1: Summary of dose estimates from the samples GSF1, GSF2 and GSF3 using small aliquots **(SA)** and single grains **(SG)**. **Average**: Average of all accepted results. **Lowest 5%**: Average of the lowest 5% of the accepted results. **IEU**: The dose estimation method based on a comparison of internal and external uncertainties. **PP**: Dose estimation based on the probability plot method. **N**: Number of included results. **SG recovery**: Number of accepted single grains compared to the number of measured grains. **Results with $D_e < 0.5$ Gy**: Calculated with respect to N.

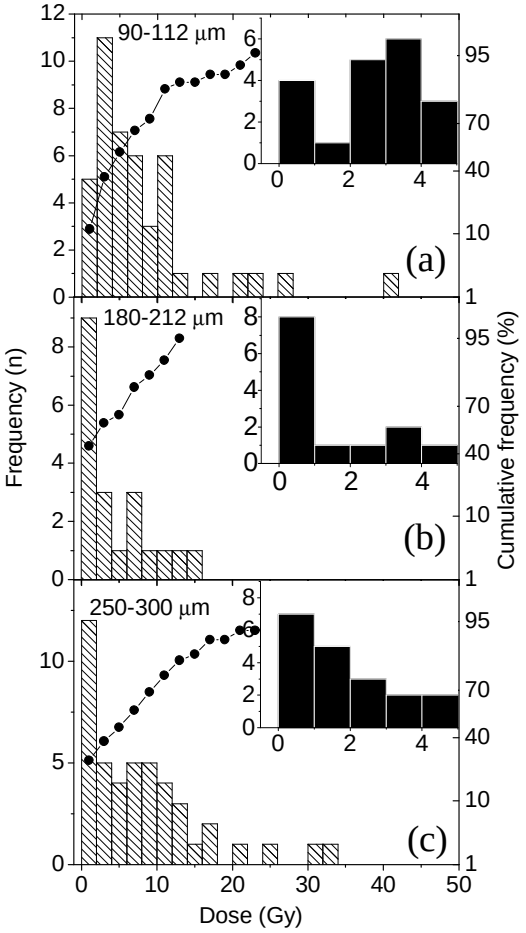

Figure 8.6: Dose histograms and probability plots from small aliquots of the sample GSF3 for the grain size ranges **a)** $90-112\,\mu$m, **b)** $180-212\,\mu$m and **c)** $250-300\,\mu$m. Insets show the lowest dose results.

8.4.4 Single-grain dose distributions

Render (GSF1)

Of the 7,900 grains measured, only 26 grains met the acceptance criteria outlined in section 8.4.1, and 31% of these dose estimates were < 0.5 Gy (see Figure 8.7a). For the small aliquot measurements the corresponding number was 17%. The average dose for single grains was 5.33 ± 1.33 Gy and individual values ranged between -0.14 ± 0.17 and 32 ± 12 Gy. Both the IEU and the PP methods gave a result of 0.145 ± 0.035 Gy (mean dose offset $= 0.012$ Gy), in good agreement with the expected dose. In the lowest 5% method only a single result was included.

Grain size (μm)	D_{min} (Gy)	D_{av} (Gy)
90 – 112	0.14 ± 0.03	7.1 ± 1.0
180 – 212	0.13 ± 0.84	4.7 ± 0.8
250 – 300	0.46 ± 0.15	10.1 ± 2.0

Table 8.2: Minimum and average doses obtained for three different grain sizes for GSF3 using small aliquots.

Plaster–Inner Wall (GSF2)

Of the 12,800 grains measured, only 71 grains met the acceptance criteria. As in the small aliquot distribution, the probability plot indicates the presence of two dose populations. The first is centred at $\sim$ 3 Gy (20% of the results and a relatively narrow-width population) and the second at $\sim$ 70 Gy (80% of the results and a relatively wide population; see Figure 8.7b). The average dose was 100 ± 13 Gy and the results ranged between -0.46 ± 1.12 and 554 ± 130 Gy. The lowest 5% method returned a value of -0.276 ± 0.107 Gy, which is inaccurate as well as imprecise. Both IEU and PP returned a value of 0.355 ± 0.144 Gy (mean dose offset = 0.222 Gy), which is not consistent within 1σ of the expected dose. Poor precision and dose-offset in this sample, as compared to GSF1, is caused by the relatively poor bleaching of this sample, with the bulk of grains still carrying a geological dose (Figures 8.5b and 8.7b).

White Wash (GSF3)

Of the 17,100 grains measured, only 55 grains met the acceptance criteria. The probability plot indicates the presence of two dose populations: a low-dose population (containing 60% of the grains) centred at $\sim$ 0.1 Gy and a wide, high-dose population at $\sim$ 8 Gy (Figure 8.7c). The average dose was 14 ± 4 Gy, and the individual doses ranged between -1.74 ± 1.69 and 162 ± 33 Gy. The 5% method gave a D_e of -0.98 ± 0.42 Gy. Both IEU and PP returned a value of 0.143 ± 0.053 Gy (mean dose offset = 0.01 Gy), in good agreement with the expected dose.

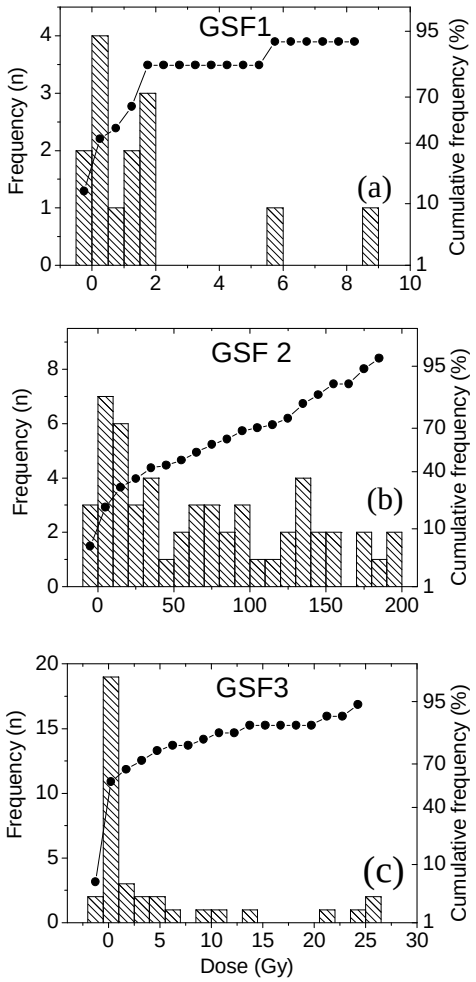

Figure 8.7: Dose histograms and probability plots from single grains of quartz from **a)** GSF1, and **b)** GSF2 (two results > 200 Gy were assigned a value of 200 Gy), and **c)** GSF3 (two results above 25 Gy were assigned a value of 25 Gy).

8.4.5 Comparison of single-grain and small-aliquot results

A comparison of the equivalent doses obtained using single-grains and small-aliquots is shown in Figure 8.8a.

These samples contain few sensitive grains, only 0.3 – 0.5% of the grains gave a relative uncertainty on the first dose < 30% (see Table 8.1 on page 140). It should therefore be expected that the results from single grains and small aliquots ($\sim$ 100 grains) should be similar; only one bright (i.e. detectable) grain is expected in every two to three aliquots. However, there seems to be a

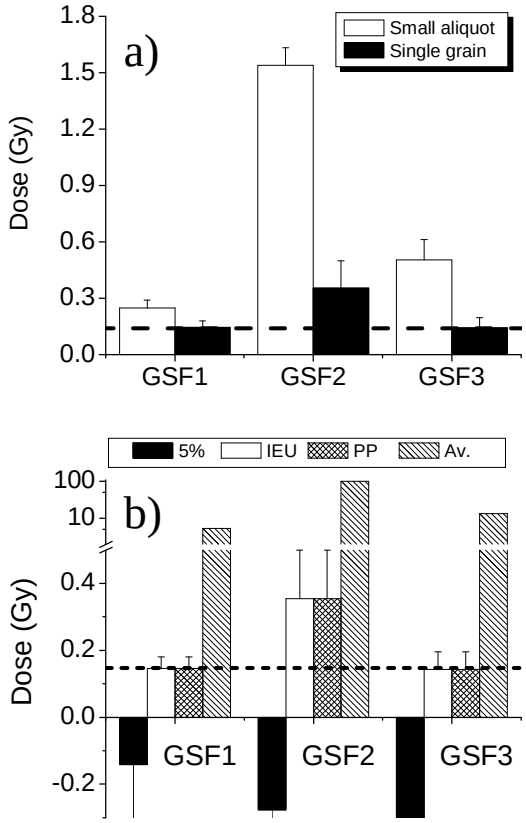

Figure 8.8: Summary of the mortar results. **a)** Comparison of single-grain and small-aliquot results obtained using the PP method. **b)** Comparison of the single-grain results obtained using the four approaches.

discrepancy between the results from small aliquots and single grains, if one compares the percentage of grains/aliquots with doses below 0.5 Gy (Table 8.1). The recovery of these low doses is better using the single grains by a factor of two or three. In GSF2, for example, the minimum dose measured in small aliquots ($n = 107$) was 1.2 Gy, whereas 7% of the total number of single-grain results ($n = 71$) were < 0.5 Gy. Given the very low proportion of bright grains, it seems very unlikely that the overestimation using small aliquots can be attributed to averaging with other bright but poorly bleached grains. Examination of the OSL responses from single grains suggests that there could be two possible explanations for this effect:

1. Grains that have a strong natural signal but no response to laboratory irradiation (e.g. Figure 8.9a); the same observation has been reported by (Thomsen et al., 2003a). These may either be very poorly bleached

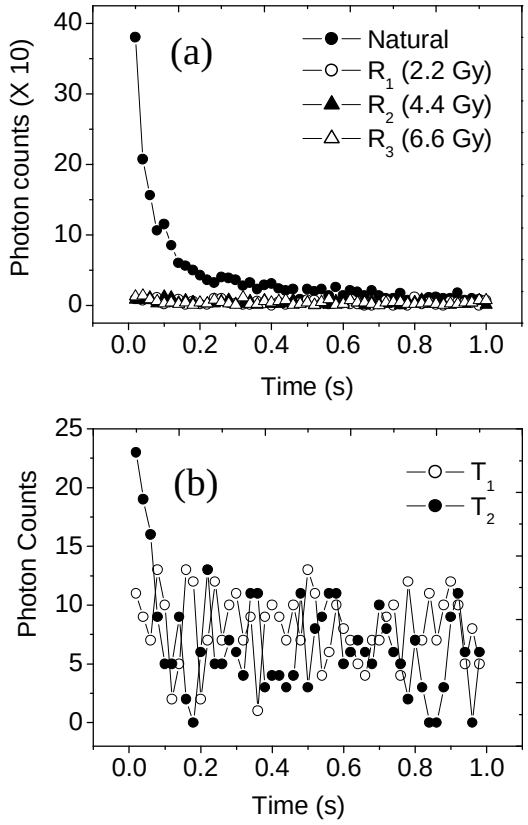

Figure 8.9: Some OSL decay curves from single grains of quartz extracted from GSF2. **a)** Natural and regenerated OSL for laboratory doses of 2.2, 4.4 and 6.6 Gy. This grain had a "high" natural signal but gave no detectable response to laboratory irradiations. **b)** Test dose OSL signals; T_1 after the natural and T_2 after the first regeneration dose OSL measurements. This grain did not give a detectable signal in response to the first test dose T_1, but did give a detectable signal in response to the second test dose T_2.

but insensitive grains, or the OSL characteristics may have changed in a manner not expected in the SAR protocol.

2. Grains that have a low or negligible OSL response (T_1) to the first test dose, but a significant increase in the second test dose OSL response (T_2) (see Figure 8.9b). A possible explanation for this phenomenon could be sensitisation of the fast component from a negligible to a significant level during repeated heating (Jain et al., 2003a). These grains have a natural to test-dose OSL ratio (L_n/T_1) well above the saturation region in the growth curve. Again, such characteristics are not consistent with the behaviour required to meet the SAR assumption.

Such anomalous grains are easily identified and rejected in single grain studies (acceptance criterion of $< 30\%$ relative uncertainty on the natural test dose signal). However, in single aliquot studies, the net OSL is derived from both grains with anomalous behaviour as described above, and from grains with a "normal" dose response. The overall effect of the presence of such anomalous grains in small aliquots would be a significant increase of the L_n/T_1 ratio, and thus an over-estimation of the dose of interest. This would be complicated further by variable thermal transfer on a grain-to-grain basis (see Figures 8.1 and 8.2). It is possible that such problems are common in multiple grain analysis of dim samples.

8.5 Conclusion

1. All three mortar samples, GSF1 (render), GSF2 (inner wall plaster) and GSF3 (white wash) were poorly bleached, but the proportion of grains carrying a geological dose was significantly higher for GSF2. Dose measurements from GSF3 showed that coarser grain sizes ($180-212$ and $250-300\,\mu$m) were probably better bleached than the $90-112\,\mu$m grain size.

2. There was a lack of correlation between thermal transfer and the extent of OSL bleaching. It is inferred that the light insensitive trap structures giving rise to thermal transfer varies from grain to grain and that thermal transfer therefore can be a source of variance in single-grain dose distributions.

3. Despite the poor sensitivity of the samples (implying less than one bright grain per small aliquot), the small aliquot results over-estimated the expected dose. This is thought to arise from a) grains having a high natural signal but no response to the test dose, and/or b) grains having no response to the natural test dose but a significant response to later test doses. In either case, the natural–to–test–dose ratio in multiple-grain analysis is increased and the average dose response curve is not appropriate to the natural signal. It may therefore be desirable to use the single grain approach in dim, poorly bleached samples.

4. Calculation of the equivalent dose using the lowest 5% method gave results with poor precision; the method requires many more measurements which becomes a major drawback for dim samples. The comparison of internal and external uncertainties (IEU) and the probability-plot (PP) methods returned essentially the same values, and these were

generally in good agreement with the expected dose of 0.133 Gy for single grains. The results from the latter two methods are encouraging for D_e estimation from poorly bleached materials.

9 Household and Workplace Chemicals

In the event of an accident involving possible doses of ionising radiation, it is important to provide an assessment of the dose as quickly as possible, to allow appropriate medical treatment of the injured. In the development of luminescence techniques for retrospective assessment of the dose absorbed by communities living and working adjacent to the site of a nuclear accident, attention has concentrated on the use of natural minerals such as quartz and feldspar as dosimeters (e.g. Chapters 5–8). These minerals are widely found in household earthenware and almost all types of bricks and concrete. Their main disadvantages are (i) variable and often low sensitivity, (ii) sample preparation and measurement is often a slow process and (iii) the natural background dose prior to the accident may be significant, depending on the age of the building and the type of building material. However, there are other potential unheated crystalline materials besides natural minerals found in the household, office and industrial environment which may also act as retrospective dosemeters, and may be considerably more sensitive. Göksu et al. (1993) investigated the use of TL signals from the water insoluble fraction of salt to reconstruct the gamma dose distribution in salt mines used for radioactive materials storage. Wieser et al. (1994) successfully used EPR and TL methods to determine accident doses absorbed in a variety of household materials (e.g. cane sugar, egg shells and black board chalk), although the reported detection limits were rather high (> 0.5 Gy). The most obvious of these candidates is probably common salt (NaCl); alkali halides are well known phosphors. Household chemicals are often held in light-tight packaging which is important for TL and OSL signals. Also, these materials are likely to have been manufactured recently, which limits the size of the likely background dose. The work presented in this chapter reports on the results of a preliminary survey of the suitability of a variety of common household and workplace chemicals to act as sensitive OSL dosimeters. The

thermoluminescent and optically stimulated luminescent characteristics of several such chemicals are surveyed and the OSL sensitivity, the size of the residual dose immediately after manufacture, stability and derived minimum detection limits are reported.

9.1 Experimental details

Table 9.1 lists the applications of the seven different materials that have been studied in detail (a further 10 were dismissed early in this study as insensitive or poorly reproducible); all were purchased from a high street supermarket. This list is not exhaustive, and what may be available is likely to depend on region (e.g. the main use for calcium chloride is to protect household drains from frost damage). The OSL and TL signals were measured using an automatic Risø luminescence reader (Bøtter-Jensen et al., 2000a), equipped with a ^{90}Sr/^{90}Y beta source delivering 0.01 Gy/s to quartz. The dose rate has not been explicitly calibrated for the materials studied here, but errors arising from this are very unlikely to affect the conclusions.

9.2 The sources of the OSL signal

Figure 9.1 presents typical OSL data for four of the materials studied (common salt, Glauber salt, washing powder (OMO®) and water softener) all after a preheat of 150 °C for 10 s. OSL data obtained by linearly increasing the stimulation power from 0 to 100% over 500 s (LM-OSL) are shown, with curves measured using constant stimulation power (CW-OSL) given as insets. All materials show a strong and easily stimulated signal, which has decayed to negligible proportions after < 4 s of CW-OSL. The LM-OSL curves demonstrate that a single trap dominates the decay curve, although a weak slow component is also visible (the common salt curves are very similar to those already published for NaCl, Bulur et al., 2001). The initial specific luminescence data (column 4 in Table 9.1) were derived using these and similar data.

Further tests involved the comparison of OSL pulse anneal curves with TL curves. This allows the stability of the OSL signal to be examined as a function of temperature, and thus permits the selection of preheat temperatures likely to improve the stability of the remaining OSL signal. The samples were given a 10 Gy dose, and a preheat at 60 °C for 10 s. The subsequent OSL stimulations were at 0.5% of full power for 0.05 s to reduce the depletion of the OSL signal in each stimulation to a negligible level. Preheat and OSL

Name	Major chemical component	Use	Specific luminescence ($s^{-1}.mg^{-1}.Gy^{-1}$)	Fading		Natural dose (mGy)	Recovery 500 mGy	MDL (mGy)
				24 hr.	2 weeks			
Blue care®	a)	Dish-washing powder	1,600	15%	40%	6 ± 6	1.01 ± 0.01	20
Calcium chloride	$CaCl_2$	Frost protection	4,600	–	–	0.1 ± 0.2	0.94 ± 0.02	1
Common salt	NaCl	Seasoning, defroster	2,000,000	4%	5%	1.3 ± 0.3	0.91 ± 0.02	1
Dynamo colour®	b)	Washing powder	100	–	–	70 ± 30	–	100
Glauber salt	Na_2SO_4	Dyspepsia, dyeing	100	0%	3%	1 ± 4	0.73 ± 0.03	15
OMO Sensitve®	c)	Washing powder	900	6%	7%	-3.0 ± 1.5	0.97 ± 0.02	5
Water softener	$(NaPO_3)_x$	Prevents precipitation	500	2%	25%	1 ± 3	1.02 ± 0.05	10

Table 9.1: Summary of typical application and dosimetry characteristics of materials investigated. **Recovery**: A dose of 500 mGy was given to the material to determine how well a given dose can be recovered. The value listed is the ratio of the average dose recovered compared to the given 500 mGy. **MDL** is the minimum detection limit. a) 15–30% phosphates, sodium carbonate, sodium disilicate, magnesium silicate. b) 15-30% phosphates, sodium sulphate, bentonite, silicates and carbonates. c) Sodium aluminium silicate, sodium perborate and sodium carbonate.

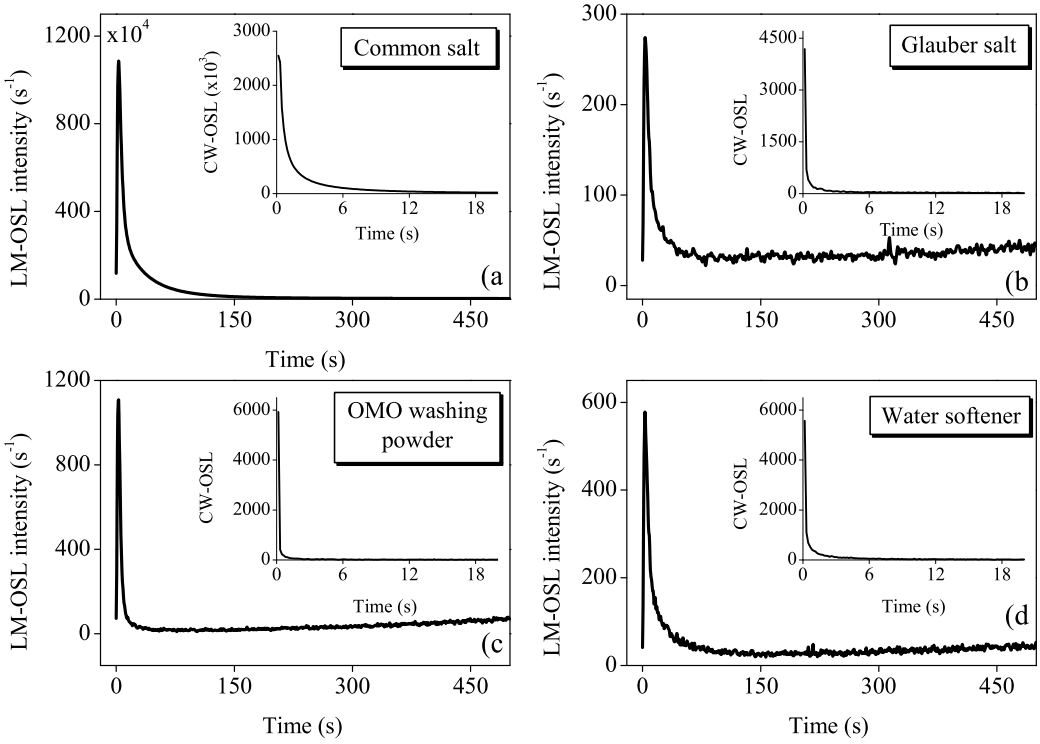

Figure 9.1: LM-OSL curves for four common household chemicals, with stimulation power increased from 0 to 100% in 500 s. The inserts show CW-OSL decay curves, measured at a constant 100% of stimulation power. The samples were given a dose of approximately 2 Gy and preheated to 150 °C before stimulation

stimulation was repeated 18 times, each time increasing the preheat temperature by 20 °C (i.e. 60 – 400 °C). Before and after the pulse anneal sequence, the response to a 1 Gy test dose (preheat 60 °C for 10 s) was measured to allow correction for sensitivity change (see also Figure 9.4). The data were also corrected for signal depletion during the pulse anneal sequence (using a pulse anneal sequence with all preheats at 60 °C). The same four materials are used to illustrate this process in Figure 9.2. The OSL signal from both common salt (Figure 9.2a) and Glauber salt (Figure 9.2b) increases significantly with heating immediately before emptying of a TL peak (at approximately 300 °C) presumably associated with the source of the OSL signal. The increase is most marked for Glauber salt. In contrast, the OSL signals from the washing powder (OMO®, Figure 9.2c) and the water softener (Figure 9.2d) decrease monotonically with temperature. The OMO® OSL decreases smoothly up to about 300 °C, and seems to show a clear association with a strong TL peak at about 300 °C (note that the fine structure in the TL

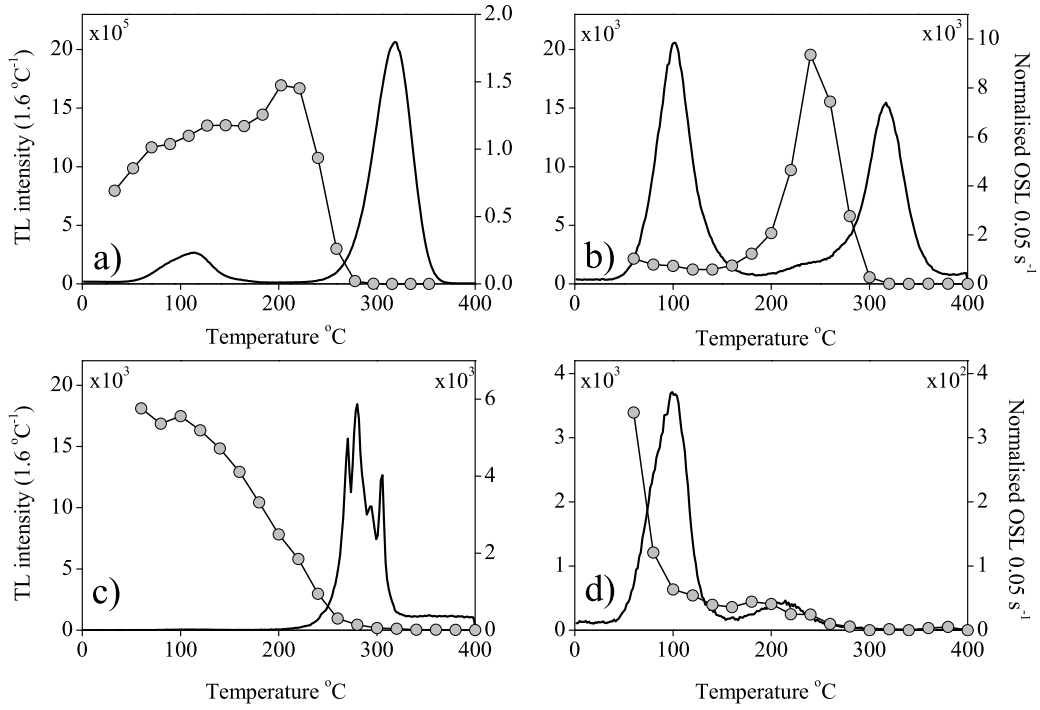

Figure 9.2: OSL pulse anneal curves (filled symbols) and TL curves (no symbols) for **a)** common salt, **b)** Glauber salt, **c)** washing powder (OMO) and **d)** water softener. The OSL signal from common salt and Glauber salt increases significantly with heating immediately before emptying a major TL peak. The OSL signal from both OMO® and the water softener decay monotonically with temperature. From these data and from measurements of reproducibility a preheat temperature of 150 °C for 10 s was adopted for further work.

curve may arise from oxidation of organic components in this complex mixture, rather than TL). The water softener looses $> 80\%$ of its OSL signal at 100 °C, again at the same time as a strong TL peak is emptied. Nevertheless, a significant OSL signal remains. From these data, and from investigations of reproducibility, a preheat of 150 °C for 10 s was adopted for all samples in further work.

9.3 Fading

The stability of the signals from these materials was tested by giving a known dose of about 1 Gy, and storing for periods of 24 hours and two weeks. Sensitivity changes before and after storage were monitored using the OSL response to a smaller test dose, to ensure that any signal loss during storage

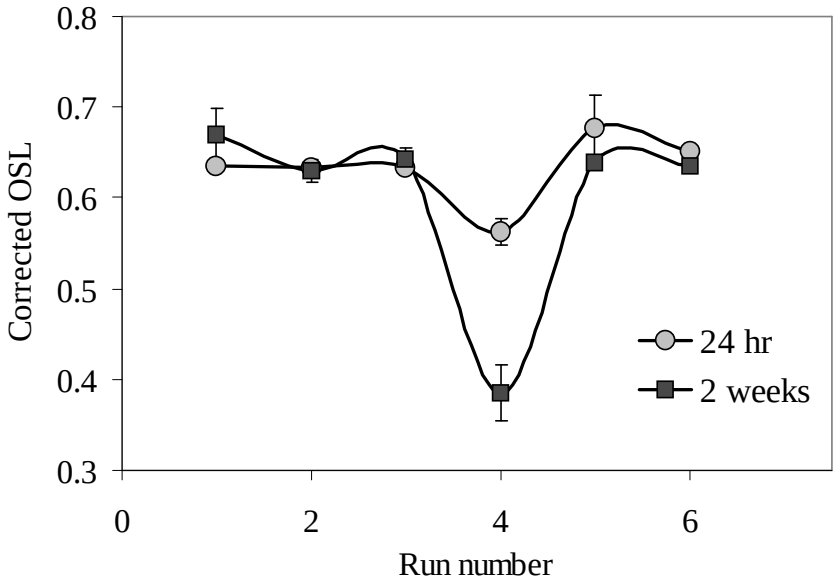

Figure 9.3: Fading data for Blue care®. Each point is an average of two aliquots. The samples were dosed and stored for either 24 hr or 2 weeks at ambient temperature. Prior to storage, three SAR measurement cycles were carried out (run 1, 2 and 3), each time giving the same dose (regeneration dose: 1 Gy, preheat temperature: 150 °C for 10 s, test dose: 0.5 Gy, no cutheat). After storage the same three measurement cycles were carried out (run 4, 5 and 6).

was not an artifact of sensitivity change (Wallinga et al., 2000). The results are summarised in columns 5 and 6 of Table 9.1. Glauber salt, common salt and OMO® showed negligible to small fading over the two week period. Blue care® dish washing powder and the water softener showed a more marked effect, with fading of up to 40%. The fading data for Blue care® are shown in Figure 9.3.

9.4 Growth curves and detection limits

The single-aliquot regenerative-dose protocol (Murray and Wintle, 2000) has been applied to determine the growth curves and natural doses. Only common salt showed no significant sensitivity changes during the generation of the growth curve (Figure 9.4a). The other three samples all showed overall sensitivity changes of about 20%; this effect is completely compensated for by using the SAR protocol (see the repeated points at 0.25 and 4 Gy, the latter measured after the highest dose point). The growth curve for common salt (Figure 9.4a) has been fitted using two saturating exponentials. Saturation of

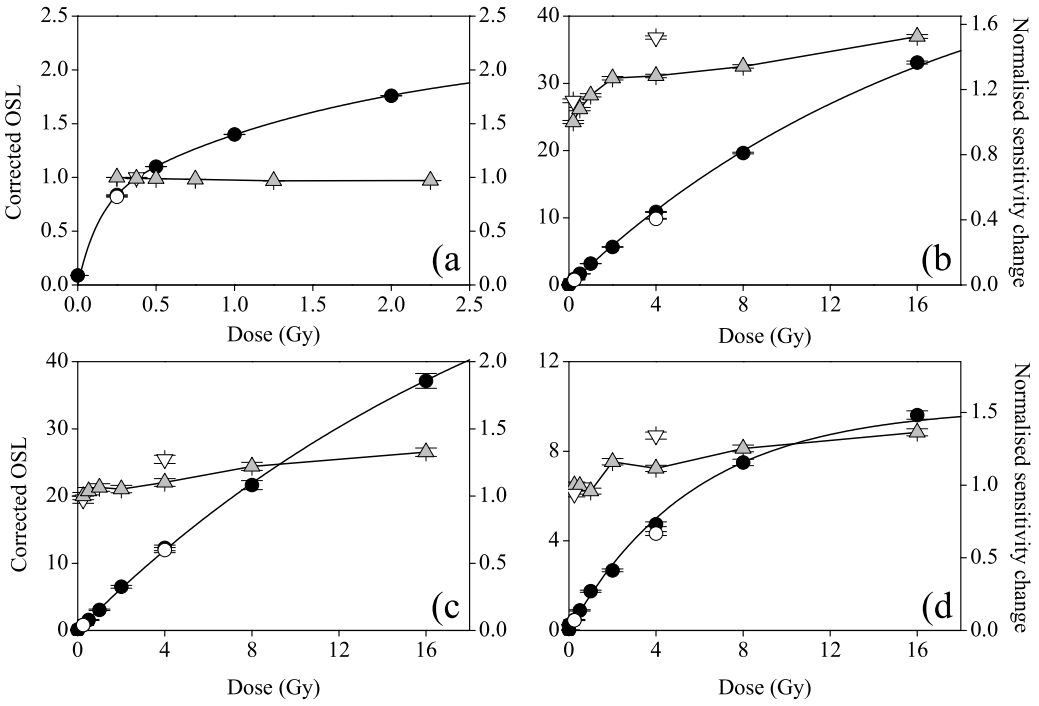

Figure 9.4: Growth curves and sensitivity change during the SAR cycle. The response to a fixed test dose (no cutheat) after each regeneration dose is shown by filled triangles (right hand axis). The sensitivity during re-measurement of a low dose point after completion of the growth curve is shown as an inverted triangle. The OSL signals after correction for sensitivity change are shown as filled circles and the recycling points as unfilled circles. **a)** Common salt, **b)** Glauber salt, **c)** washing powder (OMO) and **d)** water softener.

the PMT occurred at about 4 Gy because of the large specific luminescence for the sample. The other three curves can be adequately represented by a single saturating exponential, at least over the dose range investigated here.

The natural dose in the samples was measured by interpolating the sensitivity corrected natural OSL signal onto the growth curve. With the exception of Dynamo® (for which the reproducibility was atypically poor), the dose in the material at the time of purchase was very small (< 10 mGy); the individual values are summarised in column 7 of Table 9.1, and almost all are consistent with zero. These values are also very similar to those measured after laboratory optical bleaching of the samples (data not shown). In Figure 9.5 the measured natural signal for Blue care® dish washing powder is compared to the regeneration signal measured after administering a dose of 300 mGy to the sample. The average natural dose for Blue care® was found to be 6 ± 6 mGy ($n = 6$).

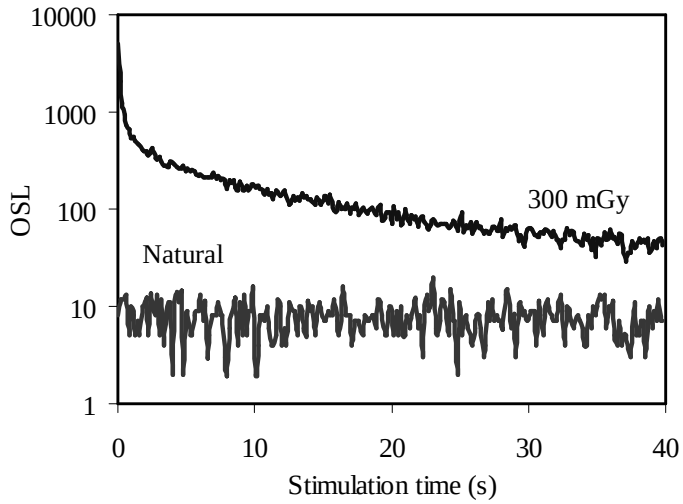

Figure 9.5: The measured natural OSL signal for Blue care® dish washing powder compared to that obtained by giving the sample a dose of 300 mGy in the laboratory.

To determine whether the SAR protocol was able to measure a potential accident dose accurately, a dose recovery test was performed. The performance of the SAR protocol with respect to the regeneration doses is checked by the recuperation and the recycling cycles, but there is no guarantee that the natural dose is estimated correctly. One way to investigate this is to optically zero the sample without any heating, and then administer a known dose in the laboratory. This known dose is then measured using the SAR protocol. In these experiments a dose of 500 mGy was given to the untreated samples (i.e. before the first preheat). The resulting sensitivity corrected OSL signal was interpolated onto the growth curve, to give an estimate of the given dose. This is illustrated in Figure 9.6 for Blue care®. Here the measured dose is estimated to be 503 ± 20 mGy. The average ratio of measured and given dose is 1.01 ± 0.01 ($n = 7$). The average ratio (> 6 aliquots) of measured/given dose for all surveyed materials is listed in column 8 of Table 9.1; only Glauber salt significantly underestimates the known dose. It is clear that an accident dose of a few hundred mGy could be accurately measured by the majority of these materials, at least for several days after the accident, and in some cases much longer.

A practical minimum detection limit can be estimated from the measurement uncertainties on the natural doses. It is likely that a signal more than 3σ above the natural dose could be detected, and this value is listed in column 9 in Table 9.1.

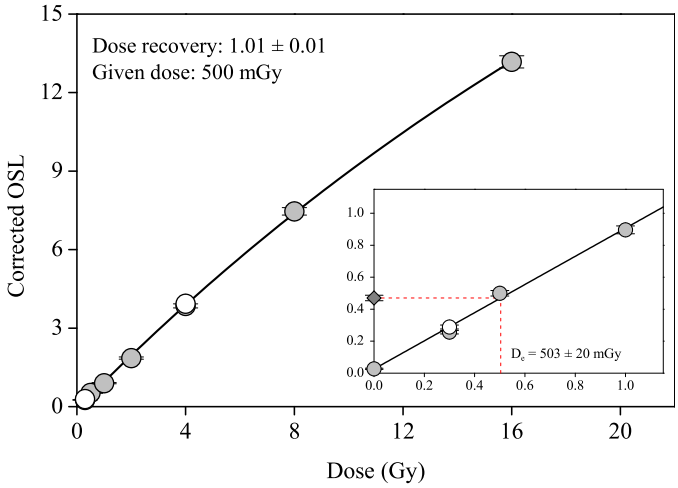

Figure 9.6: Dose recovery experiment for Blue care® dish washing powder. The sample was optically bleached without any heating above room temperature and given a dose of 500 mGy. This known dose was treated an "unknown" and measured using the SAR protocol. The sensitivity corrected "natural" signal was interpolated onto the resulting growth curve to give an estimate of 503 ± 20 mGy, consistent with the given dose. Filled circles represent the regeneration doses and unfilled circles the recycling doses (at 0.25 and 4 Gy).

9.5 Conclusion

It has been found that several materials commonly found in household and workplace environments have strong OSL sensitivity. These include common salt, washing powder, dish-washing powder and water softener. Fading was detected in some of these materials over a period of 14 days, but not in all. This does not significantly reduce the usefulness of a phosphor in accident dosimetry, if it is measured soon after the accident – as would be likely for this class of materials. The SAR protocol has been shown to measure a 500 mGy known dose administered before any other laboratory treatment, to within 20%. Based on analysis of the dose in these samples at the time of purchase, a minimum detection limit of < 20 mGy is derived. It is concluded that household and workplace chemicals should be seriously considered as potential retrospective dosimeters in the event of a radiation accident.

10 Conclusion

In this work the possibility of applying OSL in retrospective dose determinations using unheated materials has been investigated. The research has primarily focused on using single grains of quartz extracted from concrete and mortar. These studies have shown the great potential of using single grains of unheated quartz in retrospective dosimetry.

To investigate the potential of these materials in determining an accident dose superimposed on the natural dose distributions, two concrete samples were irradiated in the laboratory using a ^{137}Cs point source. Both small aliquot and single grain measurements on quartz extracted from the premix concrete were made for different depths into the brick. The small aliquot distributions contained a "continuum" of doses with the leading edge coinciding with the added dose, whereas the single grain dose distributions contained a well-defined sub-population centred on the added dose. Paradoxically, the single grain measurements showed that only 2.5% of the measured grains gave detectable test dose signals, implying that the small aliquots only contained one to two detectable grains, which ought to make the small aliquot distributions close to indistinguishable from the single grain dose distributions. In the study using the industrially produced concrete block, the single grain measurements showed that (again) only 2.5% of the grains gave detectable test dose signals and that there was a large variability in the intensities of the OSL signals on a grain to grain basis. Thus, an aliquot consisting of 100 grains would be expected to contain two to three detectable grains. About 0.3% of the total number of measured grains gave a dose consistent with zero, implying that there would be one well-bleached grain in every three aliquots. Thus, averaging effects would take place in small aliquots, but the resulting overestimate of the added dose might be small given the large variability in the individual OSL intensities. This study focused entirely on single grain measurements, but "synthetic" aliquots consisting of 100 grains each were generated by combining OSL signals from individual single grain measurements, and it was shown that deriving dose estimates

from the resulting dose distributions would have led to a significant overestimate of the added dose. This is assumed to be caused by the presence of a significant number of grains giving a detectable natural signal but no detectable test dose signal. These grains were automatically excluded from the single grain analysis, but would inevitably have been included in small aliquot analysis. Thus, the small aliquots would average over a larger suite of grains than the single grains and would overestimate the smallest possible dose. The validity of summing individual OSL intensities to generate synthetic aliquots remains to be investigated, but the presence of grains with a large natural signal and no response to laboratory irradiation is bound to influence small aliquot distributions. The difference between small aliquot and single grain dose distributions was also observed in the measurements of quartz extracted from the mortar samples. The luminescence sensitivity of these samples was very poor (i.e. only one detectable grain in every two to three aliquots) making it unlikely that the overestimation observed using small aliquots could be attributed to averaging of well-bleached and poorly-bleached grains. The overestimation was attributed to the presence of grains giving a high natural signal but no response to the natural test dose and/or to the presence of grains giving low or negligible natural test dose signals, but a significant response to later test doses. These effects might also explain the occurrence (found in other studies) of aliquots giving natural signals well above the saturation level of the laboratory generated growth curve. It remains to be understood if these large natural signals are genuine and hence an indication of poor-bleaching or if they are caused by sensitivity change occurring between the measurement of the natural and the natural test dose signal and hence an artifact of the measurement protocol. It appears that it is difficult to measure the dose of interest in these sample using small aliquots and that single grain measurements is the better approach.

Despite incomplete zeroing and poor luminescence sensitivity, dose-depth profiles were successfully measured in two concrete samples and a known background dose of 133 mGy was determined in three poorly-bleached mortar samples. Two methods (IEU and PP) for determining the dose of interest in incompletely bleached samples have been suggested. Both methods aim to identify the lowest normal sub-population in a dose distribution and have been applied successfully to most of the measured samples. In retrospect, it is now clear that the samples measured here all contained a relatively large sub-population of well-zeroed grains. It may be that these methods are not applicable to samples with less well-defined sub-populations of well-bleached grains. Future work will concentrate on demonstrating the generality of these methods. Minimum detection limits were derived to be less than 100 mGy

for the concrete samples.

All single grain measurements on quartz extracted from both the concrete and mortar samples showed overall poor luminescence sensitivity. Most grains were dim but a few grains were very bright. This variability within samples has been reported in several single grain studies, but it is not understood what causes this large variation in sensitivity. It would be valuable to investigate the cause of this variability. The single grain work presented in this thesis used considerable instrument time and was only feasible because of the availability of several single grain instruments. It is important to devise methods to separate sensitive grains from insensitive grains and thus reduce the requirement for instrument time. Characterisation of bright grains may also enhance the understanding of luminescence behaviour in general.

Thermal transfer measured in single grains of quartz extracted from a poorly-bleached mortar sample showed that thermal transfer is variable on a grain-to-grain basis. Thus, thermal transfer might contribute to the observed variance in single grain dose distributions. The observed variance in dose distributions is generally attributed to fluctuations in the number of photons detected, incomplete zeroing, heterogeneity in external beta dose dosimetry and instrument reproducibility. The observed variance in single grain dose distributions obtained from a laboratory heated and gamma irradiated sample was examined and it was concluded that approximately 6% of the variance was unaccounted for. Future work will concentrate on determining the origin of this additional contribution to the variance, which could be caused by a non-uniform distribution of luminescence centres within individual grains. This could for instance be investigated by using a more penetrating type of radiation (e.g. gamma radiation) instead of the beta radiation from the ^{90}Sr/^{90}Y source used in this work. Monte Carlo modelling of the dose distribution within a grain in the single grain disc might also help to identify the additional source of variance. Understanding dose distributions containing grains with well-defined but different doses is important. This could be investigated by mixing heated grains given well-known gamma doses. The next step could be to determine the characteristics of unheated single grain dose distributions.

The preliminary investigation of seven materials commonly found in household and workplace environments showed that these types of materials have potential to be used as retrospective dosimeters in the event of a radiation accident. These types of materials had negligible background doses and derived minimum detection limits were less than 20 mGy. Some of these materials do show fading over a period of 14 days, but this is not considered to reduce the usefulness of these materials, if measurements are made soon after the

accident.

This work has mainly focused on using single grains of quartz as retrospective accident dosimeters. However, feldspar minerals are nearly as abundant as quartz and could be used in retrospective dose determinations. Generally, the luminescence sensitivity of feldspars is much improved compared to that of quartz. However, a disadvantage of using feldspars in retrospective dose assessment is that they often suffer from anomalous fading (Wintle, 1973). Future work concentrating on feldspars would be of great value to the luminescence community as a whole.

Acknowledgements

Acknowledging and thanking everybody that has helped and supported me during the last three years (+ a bit) would be a task for Sisyphus himself, so I would like to start by apologising for my briefness and the inevitable omissions.

First and foremost, I would like to thank my external supervisor Lars Bøtter-Jensen, Risø National Laboratory, who has been a tremendous support, since the beginning of this project. Despite Lars's extremely busy and hectic work life, he has always prioritised finding the time to talk to me; regardless of the importance of the issue at hand. I owe a debt of gratitude to Lars for reading this thesis (as well as anything else I have written) meticulously and for his insightful comments.

I would also like to thank my internal supervisor Stig Steenstrup, University of Copenhagen, for all the help I have received over the years; particularly with respect to making administrative problems vanish into thin air.

Andrew Murray, the Nordic Laboratory for Luminescence dating (Aarhus University) has with his ever continuing flow of ideas been a great source of inspiration. Speaking "foreign" as a first language, I have taken every possible advantage of Andrew's generosity with red ink, which has improved numerous scribblings in English from my hand.

I want to thank Mette Adrian and Anne Sørensen for giving me additional reader time when it was most needed and for doing chemistry on some of my samples.

Without the incredible technical staff at Risø, none of this work would have been possible. Special thanks to Henrik E. Christiansen, Jørgen Jakobsen, Finn Jørgensen, Jacob R. Madsen and Finn Willumsen, who all have patiently helped me, whenever I needed it (which was often). The next time something isn't working, I promise to check if I remembered to switch on the power before I come crying for help.

I am grateful to Bente Lauridsen, Risø National Laboratory, who produced all Monte Carlo calculations presented in this work. Bente was willing to step in at the last minute and with her expertise save the day(s).

During these three years I was fortunate enough to spend three weeks at the University of Wales Aberystwyth and nearly three months at the University of Wollongong, NSW. I would like to thank both Geoff Duller and Richard Roberts for inviting me and allowing me to use their laboratory facilities.

Without the support of my two fantastic office mates Mayank Jain and Marianne Aznar, I would never have managed to finish. Thank you ever so much for all the discussions (a few of them even science related), waves, vibes and rafts. You have both earned permanent positions as my proof readers.

Last but not least I want to thank my family for successfully acting as pressure valves. I am particularly grateful to my father Klaus K. Thomsen, who has struggled his way through most of these pages.

References

Aitken, M. J. (1985). *Thermoluminescence Dating*. Academic Press, London.

Aitken, M. J. (1998). *An Introduction to Optical Dating*. Oxford University Press, Oxford.

Aitken, M. J. and Smith, B. W. (1988). Optical dating: recuperation after bleaching. *Quaternary Science Reviews*, 7:387–393.

Andersen, C. E., Aznar, M. C., Bøtter-Jensen, L., Bäck, S. J., Mattsson, S., and Medin, J. (2003). Development of optical fibre luminescence techniques for real time in vivo dosimetry in radiotherapy. In *Standards and Codes of Practice in Medical Radiation Dosimetry (Proc. Int. Symp. Vienna, 2002)*, Vienna. IAEA.

Bailey, S. D., Wintle, A. G., Duller, G. A. T., and Bristow, C. S. (2001). Sand deposition during the last millennium at Aberffraw,Anglesey, North Wales as determined by OSL dating of quartz. *Quaternary Science Reviews*, 20:701–704.

Bailiff, I. K. (1997). Retrospective dosimetry with ceramics. *Radiation Measurements*, 27:923–941.

Bailiff, I. K. and Stepanenko, V. (1996). Final report, experimental collaboration project ecp10. in: Retrospective dosimetry and dose reconstruction. EUR 16540EN:p. 115.

Banerjee, D., Bøtter-Jensen, L., and Murray, A. S. (1999). Retrospective dosimetry: Preliminary use of the single-aliquot regeneration SAR protocol for the estimation of the equivalent dose in quartz from young house bricks. *Radiation Protection Dosimetry*, 84:421–427.

Banerjee, D., Bøtter-Jensen, L., and Murray, A. S. (2000). Retrospective dosimetry: Estimation of the dose to quartz using the single-aliquot regenerative-dose protocol. *Applied Radiation Isotopes*, 52:831–844.

Baran, J., Murray, A. S., and Häggström, L. (2003). Estimating the age of stone structures using OSL: the potential of entrapped sediment. *Quaternary Science Reviews*, 22:1265–1271.

Bauchinger, M. (1998). Retrospective dose reconstruction of human radiation exposure by FISH/chromosome painting. *Mutat. Res.*, 404:89–96.

Becker, K. (1973). *Solid State Dosimetry*. CRC Press.

Berger, G. W. (1995). Progress in luminescence dating methods for quaternary sediments. *Dating Methods for Quaternary Deposits*, GEOtext,2, Geological Association of Canada:81–103.

Berger, G. W. and Luternauer, J. J. (1987). Preliminary fieldwork for thermoluminescence dating studies at the Fraser River delta, British Columbia. *Geological Survey of Canada*, Paper 87/IA:901–904.

Bougrov, N. G., Goeksu, H. Y., Haskell, E., Degteva, M. O., Meckbach, R., and Jacob, P. (1998). In the reconstruction of environmental doses on the basis of thermoluminescence measurements in the Techa riverside. *Health Physics*, 75:574–583.

Bray, H. E., Bailey, R. M., and Stokes, S. (2002). Quantification of cross-irradiation and cross-illumination using a Risø TL/OSL DA-15 reader. *Radiation Measurements*, 35:275–280.

Briesmeister, J. F. (1986). MCNP - a general Monte Carlo code for neutron and photon transport.

Bøtter-Jensen, L. (1995). Retrospective radiation dose reconstruction using optically stimulated luminescence on natural materials. In *The international workshop on scientific bases for decision making after a radioactive contamination of an urban environment*, IAEA TECDOC, Rio de Janeiro and Goiania, Brazil. IAEA.

Bøtter-Jensen, L. (1997). Luminescence techniques: instrumentation and methods. *Radiation Measurements*, 17:749–768.

Bøtter-Jensen, L. (2000). Development of optically stimulated luminescence techniques using natural minerals and ceramics, and their application to retrospective dosimetry. *Risø-R-1211 (EN)*, (DSc. Thesis).

Bøtter-Jensen, L., Andersen, C. E., Duller, G. A. T., and Murray, A. S. (2003). Developments in radiation, stimulation and observation facilities in luminescence measurements. *Radiation Measurements*, 37:535–541.

Bøtter-Jensen, L., Banerjee, D., Jungner, H., and Murray, A. S. (1999a). Retrospective assessment of environmental dose rates using optically stimulated luminescence from Al_2O_3: C and quartz. *Radiation Protection Dosimetry*, 84:537–542.

Bøtter-Jensen, L., Bulur, E., Duller, G. A. T., and Murray, A. S. (2000a). Advances in luminescence instrument systems. *Radiation Measurements*, 32:523–528.

Bøtter-Jensen, L. and Duller, G. A. T. (1992). A new system for measuring OSL from quartz samples. *Nuclear Tracks Radiation Measurements*, 20:549–553.

Bøtter-Jensen, L., Duller, G. A. T., Murray, A. S., and Banerjee, D. (1999b). Blue light emitting diodes for optical stimulation of quartz in retrospective dosimetry and dating. *Radiation Protection Dosimetry*, 84:335–340.

Bøtter-Jensen, L., Markey, B. G., Poolton, N. R. J., and Jungner, H. (1996). Luminescence properties of porcelain ceramics relevant to retrospective radiation dosimetry. *Radiation Protection Dosimetry*, 65:369–372.

Bøtter-Jensen, L. and McKeever, S. W. S. (1996). Optically stimulated luminescence using natural and synthetic materials. *Radiation Protection Dosimetry*, 65:273–280.

Bøtter-Jensen, L. and Murray, A. S. (1999). Developements in optically stimulated luminescence techniques for dating and retrospective dosimetry. *Radiation Protection Dosimetry*, 84:307–316.

Bøtter-Jensen, L. and Murray, A. S. (2001). Optically stimulated luminescence techniques in retrospective dosimetry. *Radiation Physics and Chemistry*, 61:181–190.

Bøtter-Jensen, L., Solongo, S., Murray, A. S., Banerjee, D., and Jungner, H. (2000b). Using the OSL single-aliquot regenerative-dose protocol with quartz extracted from building materials in retrospective dosimetry. *Radiation Measurements*, 32:841–845.

Bulur, E. (1996). An alternative technique for optically stimulated luminescence (OSL) experiment. *Radiation Measurements*, 26:701–709.

Bulur, E., Bøtter-Jensen, L., and Murray, A. S. (2001). LM-OSL signals from some insulators: an analysis of the dependency of the detrapping probability on stimulation light intensity. *Radiation Measurements*, 33:715–719.

Clarke, M. L. (1996). IRSL dating of sands: bleaching characteristics at deposition inferred from the use of single aliquots. *Radiation Measurements*, 26:611–620.

Clarke, M. L., Rendell, H. M., and Wintle, A. G. (1999). Quality assurance in luminescence dating. *Geomorphology*, 29:173–185.

Duller, G. A. T. (1994). Luminescence dating of poorly bleached sediments from Scotland. *Quaternary Science Reviews*, 13:521–524.

Duller, G. A. T. (1995). Luminescence dating using single aliquots: methods and applications. *Radiation Measurements*, 24:217–226.

Duller, G. A. T. (1996). Recent developments in luminescence dating of Quaternary sediments. *Prog. Phys. Geogr.*, 20:127–145.

Duller, G. A. T., Bøtter-Jensen, L., and Murray, A. S. (2000). Optical dating of single sand-sized grains of quartz: sources of variability. *Radiation Measurements*, 32:453–457.

Duller, G. A. T., Bøtter-Jensen, L., Murray, A. S., and Truscott, A. J. (1999). Single grain laser luminescence (SGLL) measurement using a novel automated reader. *Nuclear Instruments and Methods B*, 155:506–514.

Duller, G. A. T. and Murray, A. S. (2000). Luminescence dating of sediments using individual mineral grains. *Geologos*, 5:87–106.

Duller, G. A. T., Wintle, A. G., and Hall, A. M. (1995). Luminescence dating and its application to key pre − Late Devensian sites in Scotland. *Quaternary Science Reviews*, 14:495–519.

Edwards, A. A. (1997). The use of chromosomal aberrations in human lymphocytes for biological dosimetry. *Radiat. Res.*, 148:39–44.

Franklin, A. D. and Hornyak, W. F. (1990). Isolation of the rapidly bleaching peak in quartz TL glow curves. *Ancient TL*, 8:29–31.

Franklin, A. D., Prescott, J. R., and Scholefield, R. B. (1995). The mechanism of thermoluminescence in an Australian sedimentary quartz. *Journal of Luminescence*, 63:317–326.

Fuchs, M. and Lang, A. (2000). OSL dating of coarse-grain fluvial quartz using single-aliquot protocols on sediment from NE Peloponnese Greece. *Quaternary Science Reviews*, 20:783–787.

Galbraith, R. F. (1988). Graphical display of estimates having differing standard errors. *Technometrics*, 30:271–282.

Galbraith, R. F. (1990). The radial plot: graphical assessment of spread in ages. *Nuclear Tracks Radiation Measurements*, 17:207–214.

Galbraith, R. F. (2002). A note on the variance of a background corrected OSL count. *Ancient TL*, 20, No.2:49–51.

Galloway, R. B. (1993). Stimulation of luminescence using green light emitting diodes. *Radiation Protection Dosimetry*, 47:679–682.

Galloway, R. B. (1994). On the stimulation of luminescence with green light emitting diodes. *Radiation Measurements*, 23:547–550.

Göksu, H. Y. (2002). *Personal communication.*

Göksu, H. Y., Regulla, D. F., and Vogenauer, A. (1993). Reconstruction of gamma dose distribution in salt at radioactive waste disposal sites by the water insoluble fraction. *Radiation Protection Dosimetry*, 47:331–333.

Godfrey-Smith, D. I. (1994). Thermal effects in the optically stimulated luminescence of quartz and mixed feldspars from sediments. *Journal of Physics D: Applied Physics*, 27:1737–1746.

Godfrey-Smith, D. L., Huntley, D. J., and Chen, W. H. (1988). Optically dating studies of quartz and feldspar sediment extracts. *Quaternary Science Reviews*, 7:373–380.

Goedicke, C. (2003). Dating historical calcite mortar by blue OSL: results from known age samples. *Radiation Measurements*, 37:409–415.

Haskell, E. H. (1993). Retrospective accident dosimetry using environmental materials: the role of thermoluminescence. *Nuclear Tracks Radiation Measurements*, 24:87–93.

Haskell, E. H., Bailiff, I. K., Kenner, G. H., Kaipa, P. L., and Wrenn, M. E. (1994). Thermoluminescence measurements of gamma-ray doses attributable to fallout from the Nevada Test Site using building bricks as natural dosemeters. *Health Physics*, 66:380–391.

Henshilwood, C. S., d'Errico, F., Yates, R., Jacobs, Z., Tribolo, C., Duller, G. A. T., Mercier, N., Sealy, J. C., Valladas, H., Watts, I., and Wintle, A. G. (2002). Emergence of modern human behaviour: Middle Stone Age engravings from South Africa. *Science*, 295:1278–1280.

Higashimura, T., Ichikawa, Y., and Sidei, T. (1963). Dosimetry of atomic bomb radiation in Hiroshima by thermoluminescence of roof tiles. *Science*, 139:1284–1285.

Hong, D. G., Galloway, R. B., Takano, M., and Hashimoto, T. (2001). Evaluation of environmental dose at jco using luminescence from quartz stimulated by blue light. *Radiation Protection Dosimetry*, 94 (4):329–333.

Horowitz, Y. S. (1984). *Thermoluminescence and Thermoluminescent dosimetry*, volume Vol.1. CRC Press.

Hütt, G., Brodski, L., Bailiff, I. K., Göksu, Y., Haskell, E. H., Junger, H., and Stoneham, D. (1993). Accident dosimetry using environmental materials collected from regions downwind of Chernobyl: a preliminary evaluation. *Radiation Protection Dosimetry*, 47:307–313.

Hütt, G., Jaek, I., and Tchonka, J. (1988). Optical dating: K − feldspars optical response stimulation spectra. *Quaternary Science Reviews*, 7:381–385.

Huntley, D. J., Godfrey-Smith, D. I., and Haskell, E. H. (1991). Light-induced emission spectra from some quartz and feldspars. *Nuclear Tracks and Radiation Measurements*, 18:127–131.

Huntley, D. J., Godfrey-Smith, D. I., and Thewalt, M. L. W. (1985). Optical dating of sediments. *Nature*, 313:105–107.

Huston, A. L., Justus, B. L., Falkenstein, P. L., Miller, R., Ning, H., and Altemus, R. (2002). Optically stimulated luminescent glass optical fibre dosemeter. *Radiation Protection Dosimetry*, 101:23–26.

IAEA (1999). *Generic procedures for monitoring in a nuclear or radiological emergency.* International Atomic Energy Agency, Vienna. IAEA-TECTOC-1092.

IAEA and WHO (1998). *Planning the medical response to radiological accidents.* International Atomic Energy Agency, Vienna. Safety Reports Series No.4.

ICRU Report 33 (1980). *Radiation quantities and units.* International Commission on radiation units and measurements, Washington DC.

ICRU Report 68 (2002). Retrospective assessment of exposures to ionising radiation. *Journal of the ICRU*, Vol 2(2):144.

Jain, M., Bøtter-Jensen, L., Murray, A. S., and Jungner, H. (2002). Retrospective dosimetry: Dose evaluation using unheated and heated quartz from a radioactive waste storage building. *Radiation Protection Dosimetry*, 101:525–530.

Jain, M., Murray, A. S., and Bøtter-Jensen, L. (2003a). Characterisation of blue-light stimulated luminescence components in different quartz samples: Implications for dose measurement. *Radiation Measurements*, 37:441–449.

Jain, M., Thomsen, K. J., Bøtter-Jensen, L., and Murray, A. S. (2003b). Thermal transfer and apparent dose distributions in poorly-bleached mortar samples: results from OSL measurements of single grains and small aliquots of quartz. *Radiation Measurements*, 38:101–109.

Karaoglou, A. and Chadwick, K. H. (1998). Health consequences of Chernobyl and other radiation accidents. *Radiat. Environ. Biophys.*, 37:1–9.

Lamothe, M., Balescu, S., and Auclair, M. (1994). Natural IRSL intensities and apparent luminescence ages of single feldspar grains extracted from partially bleached sediments. *Radiation Measurements*, 23:555–561.

Larsen, N. A. (1999). *Dosimetry based on thermally and optically stimulated luminescence*. PhD. thesis, Risø-R-1090(EN), Niels Bohr Institute, University of Copenhagen.

Lauridsen, B. (2000). *Private communication*.

Lauridsen, B. (2002). *Private communication*.

Lepper, K., Larsen, N. A., and McKeever, S. W. S. (2000). Equivalent dose distribution analysis of Holocene aeolian and fluvial quartz sands from Central Oklahoma. *Radiation Measurements*, 32:603–608.

Levy, P. W. (1985). Thermoluminescence kinetics in materials exposed to the low doses applicable to dating and dosimetry. *Nuclear Tracks Radiation Measurements*, 10:547–556.

Li, S.-H. (1994). Optical dating: insufficiently bleached sediments. *Radiation Measurements*, 23:563–567.

Markey, B. G., Bøtter-Jensen, L., and Duller, G. A. T. (1997). A new flexible system for measuring thermally and optically stimulated luminescence. *Radiation Measurements*, 27, No. 2:83–89.

McFee, C. J. (1998). The measurement of single grain IRSL EDs using an imaging photon detector. *Quaternary Science Reviews*, 17:1001–1008.

McFee, C. J. and Tite, M. S. (1994). Investigations into the thermoluminescence properties of single quartz grains using an imaging photon detector. *Radiation Measurements*, 23:355–360.

McKeever, S. W. S. (2001). Optically stimulated luminescence dosimetry. *Nuclear Instruments and Methods in Physics Research B*, 184:29–54.

McKeever, S. W. S., Markey, B. G., and Akselrod, M. S. (1996). Pulsed optically stimulated luminescence dosimetry using $\alpha-Al_2O_3$:C. *Radiation Protection Dosimetry*, 65:267–272.

McKinlay, A. F. (1981). *Thermoluminescence dosimetry*. Adam Hilger Ltd.

Meckbach, R. and Chumak, V. (1996). Reconstruction of the external dose of evacuees from contaminated areas based on simulation modelling. In proceedings of the EU conference on *the Radiological Consequences of the Chernobyl accident*, (EUR 16544EN):965–974.

Mehta, A. and Barker, G. C. (1991). Vibrated powders: A microscopic approach. *Physical Review Letters*, 67:394–397.

Mehta, A., Luck, J. M., and Needs, R. J. (1996). Dynamics of sand piles: Physical mechanisms, coupled stochastic equations and alternative universality classes. *Physical Reviews*, E 53:92–102.

Mott, N. F. and Gurney, R. W. (1948). *Electronic Processes in Ionic Crystals*. Oxford University Press, London, 2nd edition.

Murray, A. S. and Clemmensen, L. B. (2001). Luminescence dating of Holocene aeolian sand movement, Thy, Denmark. *Quaternary Science Reviews*, 20:751–754.

Murray, A. S. and Olley, J. M. (1999). Determining sedimentation rates using luminescence dating. *Georesearch Forum*, 5:121–144.

Murray, A. S. and Olley, J. M. (2002). Precision and accuracy in the optically stimulated luminescence dating of sedimentary quartz: a status review. *Geochronometria*, 21:1–16.

Murray, A. S., Olley, J. M., and Caitcheon, G. G. (1995). Measurement of equivalent doses in quartz from contemporary water-lain sediments using optically stimulated luminescence. *Quaternary Science Reviews*, 14:365–371.

Murray, A. S. and Roberts, R. G. (1997). Determining the burial time of single grains of quartz using optically stimulated luminescence. *Earth and Planetary Science Letters*, 152:163–180.

Murray, A. S. and Roberts, R. G. (1998). Measurement of the equivalent dose in quartz using a regenerative-dose single aliquot protocol. *Radiation Measurements*, 29:503–515.

Murray, A. S., Roberts, R. G., and Wintle, A. G. (1997). Equivalent dose measurement using a single aliquot of quartz. *Radiation Measurements*, 27:171–184.

Murray, A. S. and Wintle, A. G. (1998). Factors controlling the shape of the OSL decay curve in quartz. *Radiation Measurements*, 29:65–79.

Murray, A. S. and Wintle, A. G. (1999). Isothermal decay of optically stimulated luminescence in quartz. *Radiation Measurements*, 30:119–125.

Murray, A. S. and Wintle, A. G. (2000). Luminescence dating of quartz using an improved single-aliquot regenerative-dose protocol. *Radiation Measurements*, 32:57–73.

Nakamura, N. and Miyazawa, C. (1997). Alkaline denaturation of dentin - a simple way to isolate human tooth enamel for electron spin resonance dosimetry. *J. Radiat. Res. (Tokyo)*, 38(3):173–177.

Olley, J., Caitcheon, G., and Roberts, R. G. (1999). The origin of dose distributions in fluvial sediments, and the prospect of dating single grains from fluvial deposits using optically stimulated luminescence. *Radiation Measurements*, 30:207–217.

Olley, J. M., Caitcheon, G. G., and Murray, A. S. (1998). The distribution of apparent doses as determined by optically stimulated luminescence in small aliquots of fluvial quartz: implications of dating young sediments. *Quaternary Science Reviews*, 17:1033–1040.

Orise (2000). *Radiation accident registries*. Oak Ridge, USA. ORISE-EHSD-REAC/TS.

Pierce, D. A., Shimizy, Y., Preston, D. L., Vaeth, M., and Mabuchi, K. (1996). Studies of the mortality of a-bomb survivors. report 12, part i. cancer: 1950-1990. *Radiat. Res.*, 146:1–27.

Polf, J. C. (2002). *A study of optically stimulated luminescence in Al_2O_3 fibers for the development of a real-time, fiber optic dosimetry system.* Unpublished Ph.D thesis, Oklahoma State University.

Poolton, N. R. J., Bøtter-Jensen, L., and Jungner, H. (1995). An optically stimulated luminescence study of porcelain related to radiation dosimetry. *Radiation Measurements*, 24:543–549.

Rhodes, E. J. (2000). Observation of thermal transfer OSL signals in glacigenic quartz. *Radiation Measurements*, 32:595–602.

Rhodes, E. J. and Pownall, L. (1994). Zeroing of the OSL signal in quartz from young glaciofluvial sediments. *Radiation Measurements*, 23:581–585.

Roberts, R. G. (1997). Luminescence dating in archaeology: from origins to optical. *Radiation Measurements*, 27:819–892.

Roberts, R. G., Bird, M., Olley, J., Galbraith, R. F., Lawsen, E., Laslett, G., Yoshida, H., Jones, R., Fullagar, R., Jacobsen, G., and Hua, Q. (1998). Optical and radiocarbon dating at Jinmium rock shelter in Northern Australia. *Nature*, 393:358–362.

Roberts, R. G., Galbraith, R. F., Olley, J. M., Yoshida, H., and Laslett, G. M. (1999). Optical dating of single and multiple grains of quartz from Jinmium rock shelter, Northern Australia: Part II, results and implications. *Archaeometry*, 41, 2:365–395.

Roesch, W. C. (1987). *US-Japan joint reassessment of atomic bomb radiation dosimetry in Hiroshima and Nagasaki.* The Radiation Effects Research Foundation, Hiroshima, Japan. In final report (Ed. W.C. Roesch) Vols. 1 and 2.

Sanderson, D. C. W., Carmichael, L. A., and Fisk, S. (1998). Establishing luminescence methods to detect irradiated foods. *Food science and Technology Today*, 12(2):97–102.

Spooner, N. A. and Allsop, A. (2000). The spatial variation of dose rate from ^{90}Sr/^{90}Y beta sources for use in luminescence dating. *Radiation Measurements*, 32:49–56.

Stokes, S., Bray, H. E., and Blum, M. D. (2001). Optical resetting in large drainage basins: tests of zeroing assumptions using single-aliquot procedures. *Quaternary Science Reviews*, 20:880–885.

Stokes, S. and Rhodes, E. J. (1989). Limiting factors in the optical dating of quartz from young sediments. *Long and Short range Limits in Luminescence dating*, Research Laboratory for Archaeological and the History of Art, Oxford, Occasional publication.

Takada, J., Hoshi, M., Rozenson, R. I., Endo, S., Yamamoto, M., Nagatomo, T., Imanaka, T., Gusev, B. I., Apsalikov, K. N., and Tachaijunusova, N. J. (1997). Environmental radiation dose in Semipalatinsk area near nuclear test site. *Health Physics*, 73:524–527.

Thomsen, K. J., Bøtter-Jensen, L., and Murray, A. S. (2002a). Household and workplace chemicals as retrospective luminescence dosemeters. *Radiation Protection Dosimetry*, 101:515–518.

Thomsen, K. J., Bøtter-Jensen, L., Murray, A. S., and Solongo, S. (2002b). Retrospective dosimetry using unheated quartz: a feasibility study. *Radiation Protection Dosimetry*, 101:345–348.

Thomsen, K. J., Jain, M., Bøtter-Jensen, L., Murray, A. S., and Jungner, H. (2003a). Variation with depth of dose distributions in single grains of quartz extracted from an irradiated concrete block. *Radiation Measurements*, 37:315–321.

Thomsen, K. J., Murray, A. S., and Bøtter-Jensen, L. (2003b). Sources of variability in OSL dose measurements using single grains of quartz. *Radiation Measurements*, (in press).

Topping, J. (1955). *Errors of Observation and their Treatment*. The Institute of Physics and the Physical Society, London.

Turai, I. and Veress, K. (2001). Radiation accidents: Occurrence, types, consequences, medical management, and the lessons to be learned. *DEJOEM*, Vol 7 No.1:3–14.

Wallinga, J. (2001). *The Rhine-Meuse system in a new light: optically stimulated luminescence dating and its application to fluvial deposits*. Ph.D thesis, Faculty of Geographical Sciences, Utrecht University.

Wallinga, J., Murray, A. S., Duller, G. A. T., and Törnqvist, T. E. (2001). Testing optically stimulated luminescence dating of sand-sized quartz and feldspar from fluvial deposits. *Earth and Planetary Science Letters*, 193:617–630.

Wallinga, J., Murray, A. S., and Wintle, A. G. (2000). The single-aliquot regenerative-dose (SAR) protocol applied to coarse grain feldspar. *Radiation Measurements*, 32:529–533.

Wieser, A., Göksu, H. Y., Regulla, D. F., and Vogenauer, A. (1994). Limits of retrospective accident dosimetry by EPR and TL with natural materials. *Radiation Measurements*, 23:509–514.

Wieser, A., Onori, S., Aragno, D., Fattibene, P., Romanyukha, A., Ignatiev, E., Koshta, A., Skvortzov, V., Ivannikov, A., Stepanenko, V., Chumak, V., Sholom, S., Haskell, E., Hayes, R., and Kenner, G. (2000). Comparison of sample preparation and signal evaluation methods for EPR analysis of tooth enamel. *Appl. Radiat. Isotopes*, 52:1059–1064.

Wintle, A. G. (1973). Anomalous fading of thermoluminescence in mineral samples. *Nature*, 245:143–144.

Wintle, A. G. (1975). Thermal quenching of thermoluminescence in quartz. *Geophysics J.R. Astr. Soc.*, 41:107–113.

Wintle, A. G. (1997). Luminescence dating: laboratory procedures and protocols. *Radiation Measurements*, 27:769–817.

Wintle, A. G. and Murray, A. S. (1977). Thermoluminescence dating: Reassessment of the fine grain dose-rate. *Archaeometry*, 19, 1:95–98.